II RESULTS AND DISCUSSION

2.1 The reaction of $[CpCr(CO)_3]_2$ (1) with elemental Phosphorus

2.1.1 Isolation of $[CpCr(CO)_2]_5P_{10}$

From the experimental results obtained, the reaction of **1** with P_4 was shown to produce a mixture of $[CpCr(CO)_2]_2$ (**4**), $[CpCr(CO)_2]_5P_{10}$ (**8**), $CpCr(CO)_2P_3$ (**14**) and $[CpCr(CO)_2]_2P_2$ (**15**) Spectral detection and isolation of products showed that the relative composition of the product mixture varies with both the Cr:P mole ratio and the duration of reaction, as shown in Table 1.

Generally, complexes **14** and **15** account for more than 70% of the total product yield after 3.5 h. The Cr≡Cr complex (**4**) was spectrally detected or isolated (a) at low P:Cr ratios, e.g. 1:1, despite a higher reaction temperature of 110°C, or (b) before completion of reaction, e.g. 1.25 h at 90°C or 4 h at 80-85°C for P:Cr ratios of 2:1 and 3:1, respectively. At the higher P:Cr ratio of 4:1, **4** was not detected at all. Instead, the polyphosphane complex, **8**, was formed in substantial yield (*ca.* 20%). In addition, monitoring this reaction up to 15 h indicated that **8** was thermally stable, as was **14**, while **15** completely degraded to $Cp_2Cr_2P_5$ (**16**) [^{1}H NMR (benzene-d_6) : δ 18.8 ($\nu_{½}$ *ca.* 100 Hz)].

The detection and isolation of $[Cp(CO)_2Cr{\equiv}Cr(CO)_2Cp]$ (**4**) necessitated control experiments involving the thermal decarbonylation of **1** as well as the cothermolysis of **4** with P_4 under similar reaction conditions, in order to diagnose the reaction pathways (Scheme I). Although Manning[61] had reported a facile thermal conversion (90%) of $[CpCr(CO)_3]_2$ to **4** after 2.5 h in refluxing toluene, NMR spectral monitoring showed that the decarbonylation process, route (iii), was only 26% complete after 4 h at 80-85°C. Considering that the reaction of $[CpCr(CO)_3]_2$ with P_4 required only 4 h to reach completion under these conditions, these findings indicate that route (iv), via **4**, that Scherer had established for the (C_5Me_5) analogs of Cr, Mo, and W complexes,[62-64] can only constitute a subsidiary pathway. This indicates that

Table 1. Product Composition from the reaction of $[CpCr(CO)_3]_2$ (**1**) with Various Mole Equivalents of P_4[a]

				Products (% yields)		
Cr:P (mole)	reaction time (h)	$Cp_2Cr_2(CO)_4P_2$ (**2**)	$CpCr(CO)_2P_3$ (**3**)	$Cp_2Cr_2(CO)_4$ (**4**)	$[CpCr(CO)_2]_5P_{10}$ (**5**)	Others
1:1	3.5[b]	36	42	12	0	10 (unidentified δ 4.03)
	3.5[c,d]	19	14	16	6	
1:2	3.5[d,e]	53	40	0	0	24 (unidentified δ 4.48 br)[i]
	2.25[b]	37	23	17	0	
1:3	4[f,d]	34	34	17	13	
1:4	3.5[b,g]	37	45	0	18	
	10[b,g]	12	50	0	14	24 ($Cp_2Cr_2P_5$)
	15[b,g]	2	33	0	22	43 ($Cp_2Cr_2P_5$)

a - In toluene, at 90 °C, unless otherwise stated.
b - Product yields by integration of Cp resonances in ^1H NMR spectrum of product mixture.
c - At 110 °C. d Product yields of isolated complexes.
e - From ref.15. f - At 80-85 °C.
g - Aliquots of the same reaction mixture. i br = broad.

Scheme I

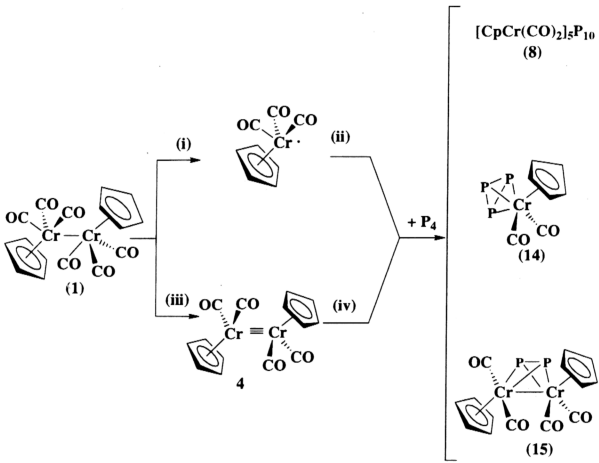

our earlier proposed radical route,[15] shown as pathway (ii), must be the predominant pathway, in agreement with the observed facile Cr-Cr bond dissociation **1**[65-69] and accumulating evidence suggesting that reactions of **1** generally proceed via its 17-electron monomeric derivative.[65, 66]

As shown in Table 1, the polyphosphorus complex **8** is only formed with P:Cr equivalents greater than or equal to 3:1 at 90°C, though at 110°C, a small amount (6%) is formed in a reaction using a P:Cr mole ratio of 1:1. The small scale reaction of **4** at 85°C, using a P:Cr mole equivalent of 3:1, also produces **8** (11%). These findings, together with earlier reports,[62-64] indicate that the quantitative product distribution depends on detailed thermolysis conditions. A similar dependence was observed in the synthesis of polycyclic organophosphanes via the thermolysis of corresponding phosphorus-poorer smaller cyclic compounds.[70, 71]

2.1.2 Spectral characteristics

2.1.2.1 N.M.R. spectra

The proton NMR spectrum in benzene-d_6 shows five Cp resonances - two sharp peaks at δ 5.07 and 4.90 ($\nu_{1/2}$ = 3Hz) and three broader peaks at δ 4.51($\nu_{1/2}$ = 6 Hz), 4.43 ($\nu_{1/2}$ = 12 Hz) and 4.35 ($\nu_{1/2}$ = 12 Hz) at ambient temperature. Spectra have been measured between -50 C and +90 C in toluene-d_8 (Figure 24) within the temperature range -50 to +90 C, the two sharp peaks exhibit little change in their line widths or chemical shifts, which vary from δ 5.00 to 5.05 (i.e. Δδ = 0.05) and δ 4.84 to 4.87 (i.e. Δδ = 0.03), respectively. The three broader resonances show greater VT behavior, their temperature-dependent shifts being more pronounced than for the above. Thus their chemical shifts for the temperature range -50 to +90°C are (i) δ = 4.38-4.54 (i.e. Δδ = 0.16) (ii) δ = 4.28-4.46 (i.e. Δδ = 0.18), and (iii) δ = 4.18-4.44 (i.e. Δδ = 0.26), respectively. Of these the two higher field resonances almost coalesce at 0°C to give a broad peak centered at δ 4.34. At -50 and +90°C, their line widths are all similar to those of the two sharp peaks at δ 5.00-5.05 and δ 4.84-4.87, respectively.

Figure 24. Temperature-dependent ^{1}H NMR spectra of a solution of $[CpCr(CO)_2]_3P_{10}$ (**8**) in d_8-toluene.

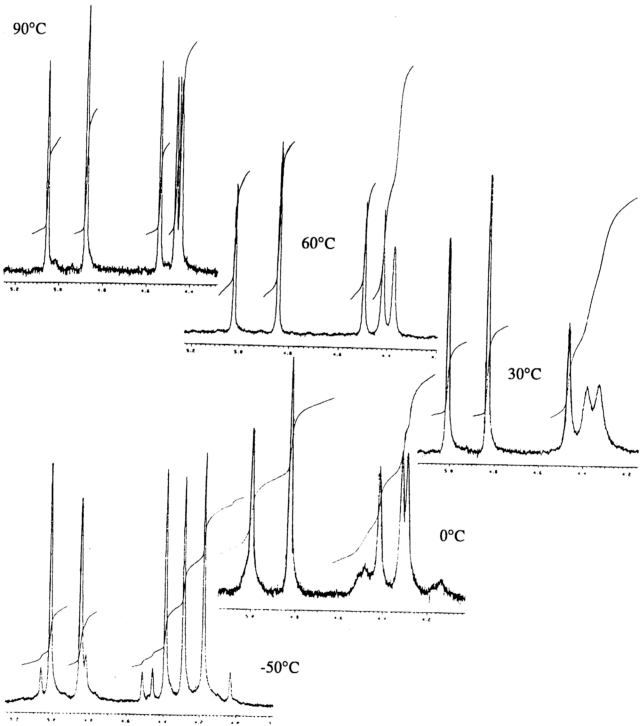

The ^{13}C NMR spectrum showed an unresolved cluster of 4-5 peaks at δ 89.72-89.82. The ^{31}P NMR spectrum is illustrated in Figure 25. Owing to a lack of symmetry, 10 clusters of resonances are observed for the P_{10} core, with chemical shifts ranging between -170.5 and +232.8 ppm, as detailed in Table 2. This span of chemical shifts is greater than any observed for Baudler's cyclic and polycyclic organophosphanes, of which P_9tBu_3 and P_{16}^{2-} had been found to possess P resonances between -180 and +150 ppm[70] and between -180 and +60 ppm,[71] respectively. Indeed, the resonances at 232.8 ppm occurs at lower field than any observed for polycyclic phosphanes. This could arise from the large variation in ring size : from three-membered to six membered rings in **8**. It has been observed that the more the rings of a cyclophosphane differ in size the larger is the difference of the observed chemical shifts, with P resonances in three- or four-membered rings shifted to higher field.[72] Fortunately, under such circumstances, higher-order effects become negligible and this makes it possible to make some empirical assignments. On the basis of the first-order P-P coupling effects and the observed multiplicity of the resonances, the P-P connectivities pertaining to each set of resonances can be worked out to give the assignments as illustrated in Table 2. The highest field chemical shift thus assigned to P5 agrees with what is expected for a P atom in a three-membered ring.

2.1.2.2 Mass spectrum

The FAB mass spectrum shows the parent ion *m/z* = 1175.6 $[Cp_5Cr_5(CO)_{10}P_{10}]$ and two other P_{10}-containing ions, vis. *m/z* 1119.6 $[Cp_5Cr_5(CO)_8P_{10}]$ and 1063 $[Cp_5Cr_5(CO)_6P_{10}]$ (refer to Table 3). In the EI mass spectrum, only mass fragments arising from $Cp_2Cr_2P_5$ and $CpCr(CO)_2P_3$[15] were observed.

Figure 25. $^{31}P\{^{1}H\}$ NMR spectrum of $[CpCr(CO)_2]_5P_{10}$ (**8**).

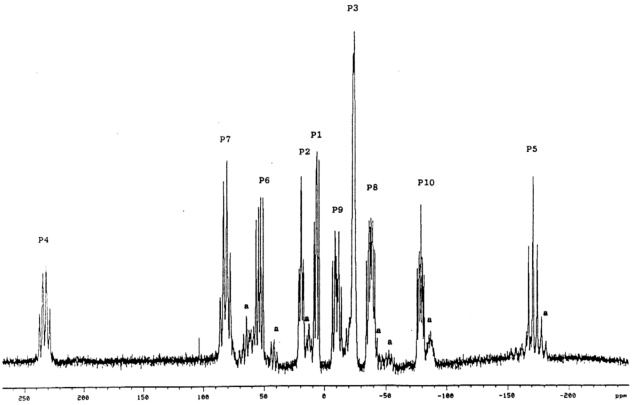

[a] - From unknown impurities.

Table 2. $^{31}P\{^{1}H\}$ NMR Resonances of $[CpCr(CO)_2]_5P_{10}$ (**8**)

chemical shift (±0.2 ppm)	assgnt	multiplicity [J (±20 Hz)]	connectivities
+232.8	P4	ddd (430, 310,[a] 370[a])	P5P7P9Cr4
+82.0	P7	ddd (310, 370,[a] 340[a])	P4P8P10
+53.8	P6	dd (450, 260)	P5P8Cr1Cr5
+19.3	P2	dd (220,[a] 205)	P9P10Cr2Cr3
+6.5	P1	dd (270, 215)	P8P9Cr1Cr2
-10.3	P9	ddd (220, 270, 370)	P1P2P4
-23.9	P3	d (140)	P10Cr3Cr4
-37.8	P8	ddd (215, 260, 370)	P1P6P7
-78.7	P10	ddd (205, 140, 340)	P2P3P7
-170.4	P5	dd (430, 450[a])	P4P6Cr5

[a] Estimated from broad fine structure.

Table 3. Fast atom bombardment and Electron impact mass spectrum of $[CpCr(CO)_2]_5P_{10}$ (**8**)

m/e	Assignments
1176	$[Cp_5Cr_5(CO)_{10}P_{10}]$
1120	$[Cp_5Cr_5(CO)_8P_{10}]$
1063	$[Cp_5Cr_5(CO)_6P_{10}]$
469	[unassigned]
431	[unassigned]
389	$[Cp_2Cr_2P_5]$
358	$[Cp_2Cr_2P_4]$
327	$[Cp_2Cr_2P_3]$
296	$[CpCr_2P_2]$
266	$[CpCr(CO)_2P_3]$
262	$[CpCr_2P_3]$
238	$[CpCr(CO)P_3]$
213	$[Cp_2CrP]$
210	$[CpCrP_3]$
200	$[CpCr_2P]$
182	$[Cp_2Cr]$
169	$[CpCr_2]$

2.1.2.3 EPR spectrum

A frozen glass of the complex at 4.9 K showed a broad featureless X-band signal in the g = 4 region. The 35-GHz EPR spectrum of an arbitrarily oriented single crystal at 6.1 K is complex (Figure 26). It comprises about 30 peaks in the 1.68-T range of the magnet, the narrowest having a peak to peak derivative line width of 1.5 x 10^{-3} T. The pattern is highly dependent on crystal orientation in the field, shows significant broadening at 20 K, and has all but disappeared at 50 K. The multiplicity of peaks probably arises from a set of S = 1/2 centers which are exchange coupled. The multiplicity does not arise from magnetic inequivalence since the space group is $P\bar{1}$ and there are two equivalent molecules in the cell (related by inversion). The relative temperature independence of intensities between 6 and 20 K suggests that any exchange couplings are small (less than or equal to 1 cm^{-1}). It has not been feasible to further examine the spectrum. The magnetic moment of 1.75 μB (8K) for the solid confirms the presence of an unpaired electron. However, the solution magnetic moment could not be determined by Evan's method[73] on account of the low limiting solubility of the complex.

2.1.3 Electrochemical studies

Complex **8** undergoes three one-electron processes at 200 K : a quasi-reversible reduction at -1.29 V (observable by ac voltametry) and two reversible oxidations at 0.61 and 1.03 V, respectively. A sample oxidized with $AgPF_6$ in CD_2Cl_2 gave a red-brown solution which exhibited a broad featureless peak in the ^1H NMR at δ 5.2-4.8. This reverted to the starting material within 1-2 h at ambient temperature [δ (Cp) at 5.25, 5.04, 4.97, 4.82, and 4.76 in CD_2Cl_2].

2.1.4 Molecular structure

The structure of **8** is shown in Figure 27. It contains a central P_{10} unit with each metal atom joined to two P atoms, of which four bond to two metals, two bond

Figure 26. 35-Ghz EPR spectrum of an arbitrarily oriented crystal of $[CpCr(CO)_2]_5P_{10}$ (**8**) at 6.1 K.

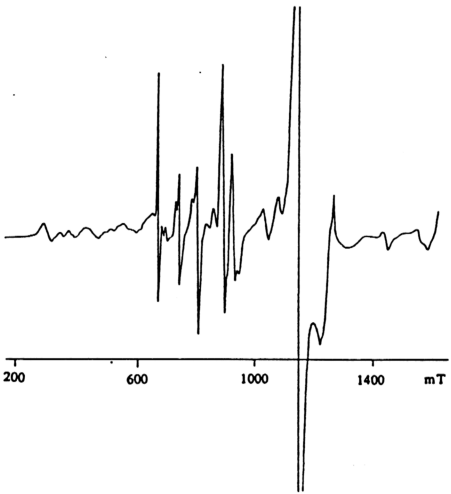

Figure 27. Structure of $[CpCr(CO)_2]_5P_{10}$ (**8**)

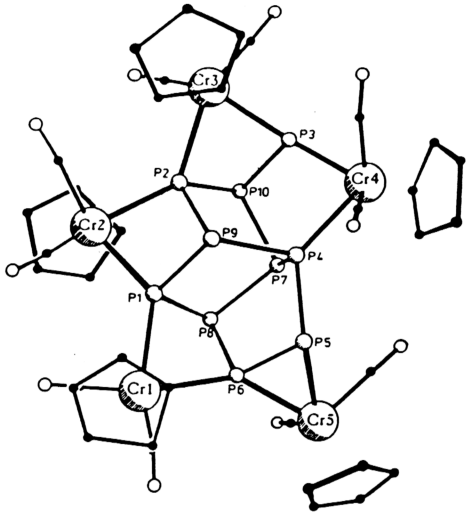

Figure 28. Stereoview of the Cr_5P_{10} unit of $[CpCr(CO)_2]_5P_{10}$ (**8**). CO and Cp groups are removed for clarity

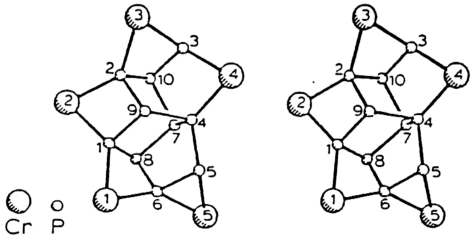

to a single metal atom, and the remaining four bond only to other P atoms. Figure 28 shows a stereoview of Cr_5P_{10}. The atoms are numbered according to the chromium atoms such that Cr1 through Cr5 lie in a rough plane with Cr1, Cr3, and Cr4 above and Cr2 and Cr5 slightly below the plane. Atomic and thermal parameters are given in Table 4. Bond lengths and angles are given in Table 5.

The P_{10} unit makes up a unique polyphosphorus structure. Two boat-configued six-membered rings of distorted sp^3 trigonal P atoms share the P8-P1-P9 fragment, with an external link P4-P7 and a single external ring substituent P3. The ring system can also be described in terms of the three cyclopentane-type rings with P4-P9 and P7-P8 each shared by two rings and P4-P7 shared by all three.

The three chromium atoms (Cr1, Cr2, Cr3), which formed corner-sharing CrP_3 rings, produce a short P-P distance across the rings (2.80-2.85 Å) and a dramatically reduced P-P-P angle (79°) opposite the metal. Cr4 links a larger P-P gap (3.042 Å) to make CrP_4 the smallest new ring. Cr5 bonds across the P5-P6 bond to form a three-membered ring.

The three four-membered CrP_3 rings are unique. In each case the metal is at a nonbonding distance from the P atom on the opposite side. This distance is shortest for Cr3 (Cr3-P10 = 3.348 Å) and Cr1 (Cr1-P8 = 3.363 Å) and longest for Cr2 (Cr2-P9 = 3.522 Å). For the five-membered ring, the nonbonding M-P distances are greater (Cr4-P7 = 3.755 Å, Cr4-P10 = 4.002 Å), as expected.

The average P-P bond length is 2.22 Å, throughout the P_{10} core, indicating that the P-P bonds are single, close to the interatomic distance (2.21 Å) in P_4 vapour.[74] The average Cr-P distance, 2.43 Å, falls within the range observed for other $CpCr(CO)_2$ complexes, viz. 2.342-2.474 Å for $[CpCr(CO)_2]_2(\mu\text{-}\eta^2\text{-}P_2)]$ and 2.427-2.494 Å for $[CpCr(CO)_2(\eta^3\text{-}P_3)]$.[15]

Despite the syntheses of many polycyclophosphanes in the last two decades,[71, 75] the bonding of such homocyclic annelated ring systems to organometallic fragments was previous unkown. The structure of **8** contains three homocyclic P_5 rings

Table 4. Positional parameters for $[CpCr(CO)_2]_5P_{10}$ (8)

atom	x	y	z	atom	x	y	z
Cr1	0.8499 (2)	0.1023 (2)	0.0824 (1)	C2Cr4	0.530 (2)	0.355 (1)	0.495 (1)
Cr2	1.0951 (2)	0.4270 (1)	0.2028 (1)	C3Cr4	0.435 (1)	0.316 (1)	0.451 (1)
Cr3	0.9040 (2)	0.6069 (1)	0.3224 (1)	C4Cr4	0.408 (2)	0.210 (1)	0.412 (1)
Cr4	0.5701 (2)	0.3310 (2)	0.3676 (1)	C5Cr4	0.520 (2)	0.197 (1)	0.447 (1)
Cr5	0.5948 (2)	−0.0747 (1)	0.2613 (1)	C41	0.559 (1)	0.452 (1)	0.345 (1)
P1	0.9155 (3)	0.2621 (2)	0.1836 (2)	O42	0.426 (1)	0.2625 (9)	0.1997 (8)
P2	0.9396 (3)	0.4527 (2)	0.2765 (2)	O41	0.539 (1)	0.526 (1)	0.3328 (8)
P3	0.7787 (3)	0.4606 (2)	0.3949 (2)	C42	0.485 (1)	0.288 (1)	0.268 (1)
P4	0.6731 (3)	0.2428 (2)	0.2969 (2)	C1Cr5	0.426 (2)	−0.158 (1)	0.181 (1)
P5	0.5856 (3)	0.0895 (2)	0.2170 (2)	C2Cr5	0.415 (1)	−0.208 (1)	0.255 (1)
P6	0.7424 (3)	0.0615 (2)	0.2045 (2)	C3Cr5	0.501 (2)	−0.246 (1)	0.258 (1)
P7	0.8060 (3)	0.2273 (2)	0.3845 (2)	C4Cr5	0.563 (2)	−0.221 (2)	0.187 (1)
P8	0.8945 (3)	0.1693 (2)	0.2904 (2)	C5Cr5	0.517 (2)	−0.170 (2)	0.142 (1)
P9	0.7824 (3)	0.3289 (2)	0.1998 (2)	C51	0.729 (1)	−0.073 (1)	0.3194 (9)
P10	0.9183 (3)	0.3983 (2)	0.4025 (2)	O51	0.803 (1)	−0.0838 (8)	0.3564 (8)
C1Cr1	0.697 (2)	0.100 (2)	0.014 (1)	C52	0.570 (1)	−0.035 (1)	0.364 (1)
C2Cr1	0.709 (2)	0.013 (2)	−0.016 (1)	O52	0.566 (1)	−0.011 (1)	0.439 (1)
C3Cr1	0.836 (2)	0.067 (2)	−0.053 (1)	H1Cr1	0.6310	0.1016	0.0373
C4Cr1	0.857 (2)	0.158 (1)	−0.042 (1)	H2Cr1	0.6519	−0.0576	−0.0105
C5Cr1	0.785 (2)	0.177 (2)	−0.007 (1)	H3Cr1	0.8801	0.0325	−0.0682
C11	1.015 (1)	0.143 (1)	0.089 (1)	H4Cr1	0.9225	0.2086	−0.0672
O11	1.116 (1)	0.165 (1)	0.0933 (8)	H5Cr1	0.7976	0.2504	0.0127
C12	0.863 (1)	−0.015 (1)	0.109 (1)	H1Cr2	1.1461	0.2568	0.2516
O12	0.862 (1)	−0.098 (1)	0.122 (1)	H2Cr2	1.2607	0.3499	0.1489
C1Cr2	1.183 (1)	0.330 (1)	0.252 (1)	H3Cr2	1.3411	0.5523	0.1900
C2Cr2	1.246 (1)	0.380 (1)	0.196 (1)	H4Cr2	1.2540	0.5711	0.3242
C3Cr2	1.294 (2)	0.497 (1)	0.220 (1)	H5Cr2	1.1424	0.3926	0.3700
C4Cr2	1.244 (1)	0.507 (1)	0.293 (1)	H1Cr3	0.8836	0.5654	0.1441
C5Cr2	1.181 (1)	0.408 (1)	0.324 (1)	H2Cr3	0.6924	0.5211	0.2112
C21	1.076 (1)	0.404 (1)	0.093 (1)	H3Cr3	0.7214	0.6799	0.3163
O21	1.075 (1)	0.392 (1)	0.020 (1)	H4Cr3	0.9456	0.8166	0.3143
C22	1.113 (1)	0.551 (1)	0.167 (1)	H5Cr3	1.0364	0.7410	0.2059
O22	1.130 (1)	0.6334 (9)	0.1456 (8)	H1Cr4	0.6594	0.2983	0.5197
C1Cr3	0.873 (2)	0.612 (1)	0.188 (1)	H2Cr4	0.5759	0.4283	0.5237
C2Cr3	0.762 (1)	0.586 (1)	0.225 (1)	H3Cr4	0.3728	0.3434	0.4419
C3Cr3	0.780 (1)	0.673 (1)	0.282 (1)	H4Cr4	0.3429	0.1697	0.3804
C4Cr3	0.908 (1)	0.751 (1)	0.282 (1)	H5Cr4	0.5338	0.1370	0.4357
C5Cr3	0.959 (1)	0.710 (1)	0.223 (1)	H1Cr5	0.3756	−0.1292	0.1599
C31	1.062 (1)	0.650 (1)	0.3599 (9)	H2Cr5	0.3585	−0.2143	0.2925
O31	1.161 (1)	0.6840 (8)	0.3800 (7)	H3Cr5	0.5136	−0.2856	0.2994
C32	0.908 (1)	0.668 (1)	0.422 (1)	H4Cr5	0.6372	−0.2274	0.1759
O32	0.915 (1)	0.7111 (9)	0.4952 (8)	H5Cr5	0.5394	−0.1430	0.0925
C1Cr4	0.583 (1)	0.282 (1)	0.492 (1)				

Table 5. Selected bond lengths and angles for $[CpCr(CO)_2]_5P_{10}$ (**8**)

(a) Distances (Å)

Cr1–C12	1.80 (2)	Cr4–C3Cr4	2.15 (2)
Cr1–C11	1.87 (2)	Cr4–C2Cr4	2.16 (2)
Cr1–C1Cr1	2.12 (2)	Cr4–C1Cr4	2.19 (2)
Cr1–C5Cr1	2.15 (2)	Cr4–C4Cr4	2.22 (2)
Cr1–C2Cr1	2.17 (2)	Cr4–C5Cr4	2.25 (2)
Cr1–C3Cr1	2.18 (2)	Cr4–P4	2.376 (4)
Cr1–C4Cr1	2.21 (2)	Cr4–P3	2.457 (4)
Cr1–P6	2.404 (4)	Cr5–C52	1.78 (1)
Cr1–P1	2.474 (4)	Cr5–C51	1.85 (1)
Cr2–C21	1.76 (2)	Cr5–C4Cr5	2.17 (2)
Cr2–C22	1.80 (2)	Cr5–C5Cr5	2.19 (2)
Cr2–C4Cr2	2.13 (2)	Cr5–C3Cr5	2.19 (2)
Cr2–C1Cr2	2.22 (2)	Cr5–C1Cr5	2.20 (2)
Cr2–C2Cr2	2.23 (2)	Cr5–C2Cr5	2.22 (2)
Cr2–C3Cr2	2.23 (2)	Cr5–P6	2.321 (4)
Cr2–C5Cr2	2.26 (2)	Cr5–P5	2.504 (4)
Cr2–P2	2.440 (4)	P1–P8	2.200 (5)
Cr2–P1	2.440 (4)	P1–P9	2.216 (5)
Cr3–C32	1.75 (2)	P2–P10	2.215 (5)
Cr3–C31	1.84 (1)	P2–P9	2.227 (4)
Cr3–C4Cr3	2.16 (1)	P3–P10	2.229 (5)
Cr3–C3Cr3	2.18 (2)	P4–P7	2.198 (5)
Cr3–C1Cr3	2.19 (2)	P4–P9	2.213 (5)
Cr3–C5Cr3	2.19 (2)	P4–P5	2.224 (4)
Cr3–C2Cr3	2.20 (2)	P5–P6	2.142 (5)
Cr3–P3	2.431 (4)	P6–P8	2.190 (5)
Cr3–P2	2.441 (4)	P7–P8	2.203 (5)
Cr4–C42	1.79 (2)	P7–P10	2.205 (4)
Cr4–C41	1.81 (2)		

(b) Angles (deg)

P6–Cr1–P1	70.1 (1)	P10–P3–Cr3	91.7 (2)
P2–Cr2–P1	71.5 (1)	P10–P3–Cr4	117.2 (2)
P3–Cr3–P2	71.6 (1)	Cr3–P3–Cr4	133.1 (2)
P4–Cr4–P3	78.0 (1)	P7–P4–P9	102.8 (2)
P6–Cr5–P5	52.5 (1)	P7–P4–P5	106.3 (2)
P8–P1–P9	102.6 (2)	P7–P4–Cr4	110.2 (2)
P8–P1–Cr2	112.9 (2)	P9–P4–P5	95.2 (2)
P8–P6–Cr1	94.0 (2)	P9–P4–Cr4	114.7 (2)
Cr5–P6–Cr1	142.4 (2)	P5–P4–Cr4	124.8 (2)
P4–P7–P8	96.9 (2)	P6–P5–P4	97.0 (2)
P4–P7–P10	93.4 (2)	P6–P5–Cr5	59.3 (1)
P8–P7–P10	102.9 (2)	P4–P5–Cr5	121.5 (2)
P6–P8–P1	79.4 (2)	P5–P6–P8	112.8 (2)
P6–P8–P7	101.8 (2)	P5–P6–Cr5	68.1 (1)
P1–P8–P7	108.1 (2)	P5–P6–Cr1	121.0 (2)
P4–P9–P1	104.9 (2)	P8–P6–Cr5	116.8 (2)
P4–P9–P2	101.9 (2)	P8–P6–Cr1	94.0 (2)
P1–P9–P2	79.8 (2)	Cr5–P6–Cr1	142.4 (2)
P7–P10–P2	106.8 (2)	P4–P7–P8	96.9 (2)
P7–P10–P3	100.5 (2)	P4–P7–P10	93.4 (2)
P2–P10–P3	79.8 (2)	P8–P7–P10	102.9 (2)
P8–P1–Cr1	91.9 (1)	P6–P8–P1	79.4 (2)
P9–P1–Cr2	98.2 (1)	P6–P8–P7	101.8 (2)
P9–P1–Cr1	115.3 (2)	P1–P8–P7	108.1 (2)
Cr2–P1–Cr1	132.9 (2)	P4–P9–P1	104.9 (2)
P10–P2–P9	102.7 (2)	P4–P9–P2	101.9 (2)
P10–P2–Cr2	115.4 (2)	P1–P9–P2	79.8 (2)
P10–P2–Cr3	91.9 (2)	P7–P10–P2	106.8 (2)
P9–P2–Cr2	97.9 (2)	P7–P10–P3	100.5 (2)
P9–P2–Cr3	112.0 (2)	P2–P10–P3	79.8 (2)
Cr2–P2–Cr3	134.0 (1)		

(c) Nearest Nonbonding Cr–P Distances (Å)

Cr1–P5	3.960 (4)	Cr3–P9	3.871 (4)
Cr1–P8	3.363 (4)	Cr3–P10	3.348 (4)
Cr1–P9	3.963 (4)	Cr4–P7	3.755 (4)
Cr2–P8	3.868 (4)	Cr4–P9	3.867 (4)
Cr2–P9	3.522 (4)	Cr4–P10	4.002 (4)
Cr2–P10	3.934 (4)	Cr5–P8	3.843 (4)

annelated like in the polyanion P_{16}^{2-} [75] and heterocyclic rings, which include one three-membered CrP_2, three four-membered CrP_3, one five-memebred CrP_4, four six-membered CrP_5, and one six-membered Cr_2P_4, with each of the five $CpCr(CO)_2$ fragments bridging across two P atoms. The closest examples are the iron complexes $Cp'_4Fe_4(CO)_6P_8$ and $Cp'_4Fe_6(CO)_{13}P_8$ ($Cp' = \eta^5\text{-}C_5H_4Me$) containing a regular-type $\alpha\text{-}P_8$ core, wherein the coordination of the four bridgehead P atoms of the P_8 subunit of Hittorf's monoclinic phosphorus to $Cp'Fe(CO)_n$ fragments produces two four-membered FeP_3 rings in both complexes and an additional five-memebred FeP ring in the second case.[76] The next nearest example involves the coordination of the P atoms of the cyclotriphosphane ring in theheptahetero-norticyclene, $P_4[SiMe_2]_3$ to ML_n fragments ,[77, 78] and other known metal polyphosphides have been reported to contain only a simple monocyclic phosphanes, e.g. cyclic P_6 in Ti_2P_6[79] and Th_2P_{11}.[80]

Cu_4SnP_{10} is the only other known M_5P_{10} complex but, again, does not present an instance of coordination of organometallic metal groups to a polycyclic phosphane, and there is no similarity with $[CpCr(CO)_2]_5P_{10}$. Cu_4SnP_{10} contains a quasi-tetrahedral $[SnCu_3]$ cluster which interlinks four adamantane P_{10}^{6-} groups, thereby forming an extended structure containing six trimetallic six-membered rings as well as six bimetallic five-membered rings, all centered at Sn.[81] It is apparent there exists no similarity with the structure of **5**, wherein five $[(\eta^5\text{-}C_5H_5)Cr(CO)_2]$ fragments on the periphery of a P_{10} core form a discrete entity.

Considering a neutral core, the formal oxidation state of each Cr is +1. The moelcule possesses a valence electron count of 125, 15 e per $CpCr(CO)_2$ fragment and 5 e per P atom. The magnetic moment and EPR spectrum are both in support of the presence of an unpaired electron, though a full interpretation of the complex EPR spectrum will require much more work than possible at this stage. It is apparent from the sharp resonances observed in the ^1H and ^{31}P NMR spectra that the effect of the odd electron on the Cp rings and the P atoms is negligible. This osbervation resembles those in biological molecules like HiPIP, where the presence of Fe(III) in its d^5 high-

spin state does not affect the proton resonance.[82] In this case, although the Cp ring signals appear in the normal region for diamagnetic Cp resonances, the variation in their line width from 3 to 12 Hz at ambient temperature may indicate a variation in proximity to the odd electron or different unpaired spin density environments.

2.2 Studies with elemental Arsenic

2.2.1 The reaction of $[CpCr(CO)_3]_2$ with elemental Arsenic

A deep green solution of $[CpCr(CO)_3]_2$ (**1**) underwent complete reaction under rigorous stirring with excess gray arsenic powder in refluxing toluene for 1-1.5 h. Column chromatography of the resultant purplish black solution led to the isolation of $Cp_2Cr_2(CO)_4(\mu\text{-}\eta^2\text{-}As_2)$ (**2**) as dark purple crystals (20.4% yield), $CpCr(CO)_2(\eta^3\text{-}As_3)$ (**3**) as yellow crystalline flakes (14.2% yield), the known $Cp_2Cr_2(CO)_4(Cr{\equiv}Cr)$ (**4**) (5.3% yield), and a Prussian blue complex of empirical formula $Cp_2Cr_2AsO_5$ (**6**) (13.6% yield), as well as minor amounts of two uncharacterizable Cp-containing species, showing bonds at δ 14.8 and 15.5 in the ^1H NMR spectrum. Product composition varies with reaction conditions. A prolonged reaction of 16 h under similar condition gave **3**, $Cp_2Cr_2As_5$ (**5**), **6** and $Cp_5Cr_5As_4O_5$ (**7**) in 5, 22, 39 and 8% yields, respectively, apparently at the expense of of **2**, **3** and **4**. The product composition is also altered by the temperature of the reaction. Under elevated temperature in refluxing xylene for 6 h, the reaction produced only **3** and **7** in 3 and 15% yields, respectively. From these observations, it can be deduced that **2**, **3**, **4** and **6** are the primary products of the cothermolysis of **1** with arsenic. This deduction is further substantiated by thermolysis studies, whereby it is observed that the thermal degradation of **2** at 110°C for 16 h gave **5** and **7** in 46.5 and 28% in isolated yields, respectively. Whereby, **3** also thermally degrades to **5** but at a longer time of 21 h to gave 18% yield with remaining 68% of **3** unreacted.

2.2.2 The reaction of $[CpCr(CO)_2]_2$ with elemental Arsenic

The reaction of the Cr≡Cr complex **4** with excess gray arsenic powder in refluxing toluene for 1 h gave **2**, **3** and **4** in 18.5, 31.9 and 38.3% in isolated yields, respectively, in a similar manner comparable to the reaction with **1**. At 5 h, the reaction under similar condition, gave only **2** and **4** in 18.6 and 44.2% in isolated yields, respectively.

2.2.3 Mechanistic pathways : Formation of $[CpCr(CO)_2]_2(\mu\text{-}\eta^2\text{-}As_2)$ (2) and $CpCr(CO)_2(\eta^3\text{-}As_3)$ (3)

The reaction of $[CpCr(CO)_3]_2$ (1) with gray arsenic can be represented by the following Equation (xxi) below :

$$[CpCr(CO)_3]_2 \xrightarrow[1.5\ h/\ 110°C]{As} [CpCr(CO)_2]_2As_2 + CpCr(CO)_2As_3 + [CpCr(CO)_2]_2 + [Cp_2Cr_2AsO_5 + \text{others (very low yields)} \quad \ldots (xxi)$$

This facile reaction with gray As under heterogeneous conditions is unusual. Only a few reactions of organotransition-metal complexes with elemental arsenic have been reported hitherto, and all but one of these invariably involved the use of the reactive yellow As_4 vapor dissolved in solution. Ziegler's reaction of the analogous Mo and W complexes with metallic As required more drastic conditions (24 h in refluxing xylene) to produce the respective $\mu\text{-}\eta^2\text{-}As_2$ and $Cp_3M_3(CO)_6As$ complexes.[17] It is conceivable that the ease of reaction in this case derives from the high propensity of **1** to dissociate into its monomer radicals as shown in Equation (xx).[67, 69]

$$[CpCr(CO)_3]_2 \rightleftharpoons 2[CpCr(CO)_3\cdot] \quad \ldots (xxii)$$

The subsequent radical attack of $CpCr(CO)_3\cdot$ on elemental arsenic would generate the Cr-As complexes **2** and **3**, as postulated for the analogous reaction with P_4.[15] However, as in all reactions of **1** under thermolytic conditions, the intermediatory role of $[CpCr(CO)_2]_2(Cr{\equiv}Cr)$ (**4**) arising from the decarbonylation of **1**[15, 16, 61] always provides an alternative pathway. In this reaction, **4** was indeed isolated (5.3% yield) from the product mixture. Subsequently, it is herein demonstrated that the reaction of a suspension of **4** with a 16-17-fold molar excess of pulverised elemental arsenic reaches completion within 1 h in refluxing toluene, giving

2 (18.5%), **3** (31.9%), and **6** (38.3%). An extended reaction period of 5 h gave **2** (18.6%) and **6** (44.2%).

This finding indicates the route *via* **4** could contribute substantially to the reaction. However, as in the reaction with P_4,[15, 16] this contribution can only be subsidiary, judging from the short reaction time versus the longer time required for complete decarbonylation, which has been reported to exceed 2.5 h in refluxing toluene.[61] It is appropriate to note here that Scherer's reaction of the analogous $[Cp^*Mo(CO)_2]_2(Mo{\equiv}Mo)$ complex ($Cp^* = \eta^5\text{-}C_5Me_5$) with yellow As_4 in refluxing xylene (140°C) gave, after 30 h, $[Cp^*Mo(CO)_2]_2(\mu\text{-}\eta^2\text{-}As_2)$ (1.2%), $Cp^*Cr(CO)_2(\eta^3\text{-}As_3)$ (15%), $[Cp^*Mo(CO)(\mu\text{-}\eta^2\text{-}As_2)]_2$ (1.7%), and cis-$[Cp^*_2Mo_2(\mu\text{-}O)_2O_2]$ (2%).[21]

Compared to the isolation of **2**, **3** and **6** in 20.4%, 14.2%, and 13.6% yields, respectively, from 1 to 1.5 h reaction time in refluxing toluene, the reaction when extended to 16 h gave **3**, **5**, **6**, and **7** in 5, 22, 39, and 8% yields, respectively. Prolonged cothermolysis of **1** with As in refluxing xylene (*ca.* 140°C) for 6 h led to the isolation **3** (3% yield) and a mixture of two Cp-containing species possessing δ(Cp) 14.8 and 15.5 in ^{1}H NMR spectrum. These could be separated to give the former species in 15% yield [δ 14.8, approximate empirical formula $Cp_5Cr_5As_4O_8$ (**7**)]. Indeed, an NMR study of the thermolytic degradation of **2** in toluene-d_8 at *ca.* 110°C indicated a fairly rapid transformation to **4** and $Cp_2Cr_2As_5$ (**5**), which is spectrally detected at 30 mins and is complete in 5 h to give a 1:1 mmolar mixture of **4** and **5**. Further thermolysis to 18 h gave only **5** and the species possessing broad resonances at δ 14.8 and 15.5 mentioned above. A product isolation from the thermolysis of **2** after 16 h in refluxing toluene yielded **5** (46.5%) and **7** (δ 14.8, 28%).

Likewise, **3** also thermally degrades to **5**, though at a much slower rate (*ca.* 30% after 21 h in refluxing toluene). The thermolytic degradation of **2** and **3** to **5** is consistent with Scherer's isolation of only $Cp_2Cr_2As_5$ (**5**) in 37.7% yield from the reaction of **1** with yellow As_4 at 150°C for 2.5-3 h.[83] Similarly, the forcing conditions employed (30 h, 150°C) may be the cause of the low yield of the $\mu\text{-}\eta^2\text{-}As_2$ complex

(1.2%) from the reaction of the $[Cp^*Mo(CO)_2]_2$(Mo≡Mo) complex with yellow As_4.[21]

The reaction pathways involved in the reaction of $[CpCr(CO)_3]_2$ with As_4 are presented in Scheme II. The findings are reminiscent of similar reaction and degradation pathways for the analogous P complexes[15, 16] and indicate that the reaction proceeds via a radical route, as well as *via* the Cr≡Cr triply bonded complex **4** to give $Cp_2Cr_2(CO)_4As_2$, $CpCr(CO)_2As_3$ and $Cp_2Cr_2AsO_5$, as primary products. The formation of $Cp_2Cr_2As_5$ proceeds *via* the thermal degradation of the μ-η^2-As_2 and η^3-As_3 complexes.

2.2.4 Physical properties

$Cp_2Cr_2(CO)_4(\mu$-η^2-$As_2)$ (2)

The complex exists as fine deep purple crystals, air-stable for extended periods at ambient temperature. It is slightly soluble in *n*-hexane and soluble in most organic solvents, giving a purple solution which is fairly stable at room temperature under an inert atmosphere.

$CpCr(CO)_2(\eta^3$-$As_3)$ (3)

The complex exists as orange yellow crystalline platelets which are much less stable compared to **2** and definitely incapable of lasting several days at ambient temperature. It is very soluble in *n*-hexane and in most organic solvents, giving a yellow solution which is fairly stable at room temperature under an inert atmosphere only for a few days.

$Cp_2Cr_2As_5$ (5)

The complex is obtained as an air-stable fine dark crystalline solid, insoluble in *n*-hexane but moderately soluble in benzene, toluene and THF. The orangy yellow solution is very air-sensitive, producing a sparingly soluble green precipitate.

Scheme II

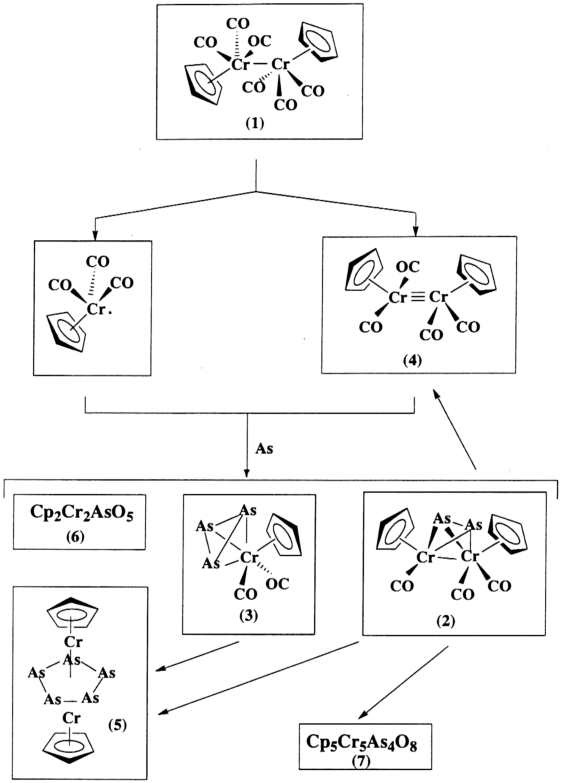
CO
CO
OC
Cr
Cr
CO
CO
CO
(1)
CO
CO
CO
Cr.
OC
Cr≡Cr
CO
CO
CO
(4)
As
Cp2Cr2AsO5
(6)
As
As
As
Cr
CO
OC
(3)
As
As
Cr
Cr
CO
CO
CO
(2)
Cr
As
As
As
As
Cr
(5)
Cp5Cr5As4O8
(7)

2.2.5 Spectral characteristics

2.2.5.1 I.R. spectra

$Cp_2Cr_2(CO)_4(\mu\text{-}\eta^2\text{-}As_2)$ (2)

A toluene solution of **2** exhibits ν_{CO} at 1932 vs and 1875 vs cm^{-1} as illustrated in Figure 29.

$CpCr(CO)_2(\eta^3\text{-}As_3)$ (3)

The ν_{CO} stretching frequencies of **3** in toluene at 1960 vs and 1905 vs cm^{-1} are strikingly similar to those of its analogous *cyclo*-(η^3-P_3) complexes (1975 vs and 1920 vs cm^{-1})[15] and point to a similarity in symmetry and structure (Figure 30).

2.2.5.2 NMR spectra

$Cp_2Cr_2(CO)_4(\mu\text{-}\eta^2\text{-}As_2)$ (2)

The complex is diamagnetic, and the Cp rings and CO ligands appeared as singlets in both the ^1H and ^{13}C NMR spectra. These resonances of **2** [δ (Cp) 4.12 for ^1H and 85.23 for ^{13}C and δ(CO) 239.31] are very close to values obtained for its analogous μ-η^2-P_2 [δ (Cp) 4.15 and 86.4 and δ (CO) 238.6] complex[15].

$CpCr(CO)_2(\eta^3\text{-}As_3)$ (3)

3 is also diamagnetic, and the Cp ring and CO ligands appeared as singlets in both the ^1H and ^{13}C NMR spectra. These resonances of **3** (δ(Cp) 3.94 for ^1H and 83.04 for ^{13}C and δ (CO) 233.93] are also very close compared to values obtained for its analogous η^3-P_3 [δ (Cp) 3.92 and 84.91 and δ (CO) 233.74] complex[15].

$Cp_2Cr_2As_5$ (5)

5 is paramagnetic, and the Cp protons appeared as a broad signal in the ^1H spectrum at δ 23.5 ($\nu_{1/2}$ = 176 Hz). Attempts to measure the ^{13}C resonances of the complex at 30°C failed to detect any signals.

Figure 29. CO stretching frequencies of $Cp_2Cr_2(CO)_4As_2$ (**2**) in toluene

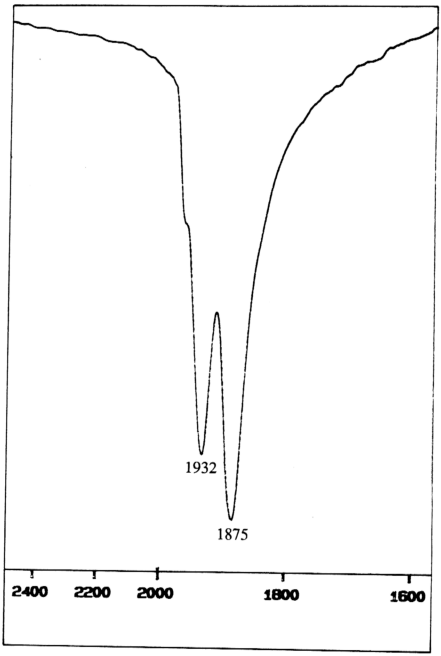

Figure 30. CO stretching frequencies of $CpCr(CO)_2As_3$ (**3**) in toluene

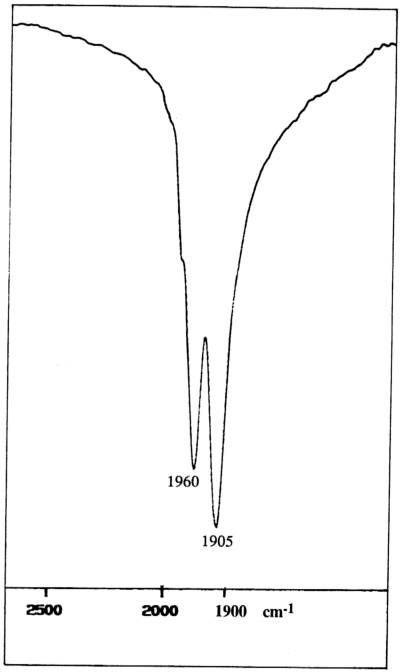

2.2.5.3 Mass spectra

$Cp_2Cr_2(CO)_4(\mu\text{-}\eta^2\text{-}As_2)$ (2)

The mass spectrum of **2** shows the parent ion and its fragmentation ions, as well as those of $Cp_2Cr_2As_5$ (**5**), which is consistent with its facile degradation to **5** observed under thermolytic conditions (Table 6).

$CpCr(CO)_2(\eta^3\text{-}As_3)$ (3)

The mass spectrum of **3** also shows the parent ion and its fragmentation ions, as well as those of $Cp_2Cr_2As_5$ (**5**), which is consistent with its facile degradation to **5** observed under thermolytic conditions (Table 7).

$Cp_2Cr_2As_5$ (5)

The mass spectrum of **5** also shows the parent ion and its fragmentation ions in Table 8.

2.2.6 Molecular structures

$Cp_2Cr_2(CO)_4(\mu\text{-}\eta^2\text{-}As_2)$ (2)

A perspective view of the molecular structure with atom numbering is shown in Figure 31. The molecule is isostructural with the isomorphous Mo and W analogues,[84] having a $\mu\text{-}\eta^2\text{-}As_2$ ligand bridging two Cr atoms, and also with the analogous $\mu\text{-}\eta^2\text{-}P_2$ complex,[15] although the compounds crystallize in different space groups. The unit-cell dimensions of **2** are in fact consistent with those of the Mo and W analogues[15] with interchange of the *a* and *c* axes. Some selected bond lengths and bond angles are presented in Table 9 and compared in Table 10 with those of the Mo and W analogues and two other structurally determined $\mu\text{-}\eta^2\text{-}As_2$ complexes.

The As-As distance (2.276 Å) almost matches the shortest ever observed As-As bond (2.273 Å) in $Co_2(CO)_5(PPh_3)As_2$[19]and is significantly shorter than that in gaseous As_4 (2.44 Å)[74] and in the *cyclo*-polyarsines $[AsCH_3]_5$ (2.428 (8) Å)[85] and $[As(C_6H_5)]_6$ (2.456 (5) Å).[86] Dahl et al. had attributed this bond shortening to a partial charge transfer from the As_2 moiety to the metal fragment 'electron sink',

Table 6. Fast atom bombardment mass spectrum of $[CpCr(CO)_2]_2As_2$ (**2**)

m/e	Assignments
609	$[Cp_2Cr_2As_5]$
534	$[Cp_2Cr_2As_4]$
496	$[Cp_2Cr_2(CO)_4As_2]$
468	$[Cp_2Cr_2(CO)_3As_2]$
459	$[Cp_2Cr_2As_3]$
440	$[Cp_2Cr_2(CO)_2As_2]$
412	$[Cp_2Cr_2(CO)As]$
384	$[Cp_2Cr_2As_2]$
319	$[CpCr_2As_2]$
267	$[CpCrAs_2]$
192	$[CpCr_2As]$
182	$[Cp_2Cr]$
117	[CpCr]

Table 7. Fast atom bombardment mass spectrum of $CpCr(CO)_2As_3$ (**3**)

m/e	Assignments
609	$[Cp_2Cr_2As_5]$
534	$[Cp_2Cr_2As_4]$
496	$[Cp_2Cr_2(CO)_4As_2]$
468	$[Cp_2Cr_2(CO)_3As_2]$
459	$[Cp_2Cr_2As_3]$
440	$[Cp_2Cr_2(CO)_2As_2]$
412	$[Cp_2Cr_2(CO)As]$
384	$[Cp_2Cr_2As_2]$
319	$[CpCr_2As_2]$
267	$[CpCrAs_2]$
192	$[CpCr_2As]$
182	$[Cp_2Cr]$
117	$[CpCr]$

Table 8. Electron impact mass spectrum of $Cp_2Cr_2P_5$ (**5**)

m/e	Assignments
609	$[Cp_2Cr_2As_5]$
459	$[Cp_2Cr_2As_3]$
394	$[Cp_2CrAs_3]$
384	$[Cp_2Cr_2As_2]$
319	$[CpCr_2As_2]$
257	$[Cp_2CrAs]$
182	$[Cp_2Cr]$
104	$[Cr_2]$
52	[Cr]

Figure 31. ORTEP drawing of the molecular structure of $[CpCr(CO)_2]_2As_2$ (**2**).

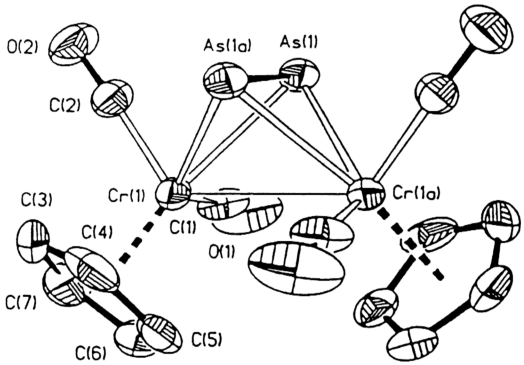

Table 9. Bond Lengths (Å) and Bond Angles (deg) for $[CpCr(CO)_2]_2As_2$ (2).

Cr(1)–Cr(1a)[a]	3.026 (1)	Cr(1)–As(1)	2.597 (1)
Cr(1)–As(1a)	2.452 (1)	As(1)–As(1a)	2.276 (1)
Cr(1)–C(1)	1.829 (7)	Cr(1)–C(2)	1.859 (6)
Cr(1)–X(1a)[b]	1.862 (6)	C(1)–O(1)	1.160 (9)
C(2)–O(2)	1.152 (8)	C(3)–C(4)	1.40 (1)
C(3)–C(7)	1.40 (2)	C(4)–C(5)	1.40 (1)
C(5)–C(6)	1.41 (1)	C(6)–C(7)	1.37 (1)
Cr(1a)–Cr(1)–As(1)	51.0 (1)	Cr(1a)–Cr(1)–As(1a)	55.4 (1)
As(1)–Cr(1)–As(1a)	53.5 (1)	Cr(1a)–Cr(1)–C(1)	89.3 (2)
As(1)–Cr(1)–C(1)	71.8 (2)	As(1a)–Cr(1)–C(1)	125.2 (2)
Cr(1a)–Cr(1)–C(2)	128.3 (2)	As(1)–Cr(1)–C(2)	79.4 (2)
As(1a)–Cr(1)–C(2)	85.6 (2)	C(1)–Cr(1)–C(2)	87.8 (3)
Cr(1a)–Cr(1)–X(1a)	114.0 (2)	AS(1)–Cr(1)–X(1a)	164.6 (2)
As(1a)–Cr(1)–X(1a)	117.3 (2)	C(1)–Cr(1)–X(1a)	115.1 (3)
C(2)–Cr(1)–X(1a)	113.7 (3)	Cr(1)–As(1)–Cr(1a)	73.6 (1)
Cr(1)–As(1)–As(1a)	60.0 (1)	Cr(1a)–As(1)–As(1a)	66.5 (1)
Cr(1)–C(1)–O(1)	175.7 (6)	CR(1)–C(2)–O(2)	177.4 (5)
C(4)–C(3)–C(7)	107.0 (7)	C(3)–C(4)–C(5)	108.5 (8)
C(4)–C(5)–C(6)	107.0 (6)	C(5)–C(6)–C(7)	108.5 (7)
C(3)–C(7)–C(6)	109.0 (8)		

[a] Symmetry transformation for a: $1 - x, y, {}^1/_2 - z$. [b] X(1a) is the center of the ring composed of carbon atoms C(3)–C(7).

Table 10. Comparison of Selected Bond Distances (Å) and Angle (deg) for $[CpM(CO)_2]_2As_2$

	M = Cr[a]	M = Mo[a]	M = W[a]	$Co_2(CO)_6$-$(PPh_3)As_2$[b]	$[(MeC_5H_4)$-$Mo(CO)]_2$-$(As_2)_2$[c]
M–M′	3.026 (1)	3.038 (2)	3.026 (2)	2.594[d]	2.950 (1)
		3.039 (2)	3.013 (2)		
As–As′	2.276 (1)	2.311 (3)	2.326 (5)	2.273 (3)	2.300 (2)
		2.312 (3)	2.319 (5)		2.279 (2)
M–As	2.597 (1)	2.676 (2)	2.682 (3)	2.386 (av)	2.626 (1)
		2.663 (2)	2.663 (3)		
M–As′	2.452 (1)	2.569 (2)	2.573 (3)		
		2.567 (2)	2.571 (3)		
M–M′–As	55.4 (1)	53.0 (1)	53.2 (1)		
		53.0 (1)	53.4 (1)		
M′–M–As	51.0 (1)	56.3 (1)	56.5 (1)	57.1 (av)	
		56.0 (1)	56.3 (1)		
M–As–M′	73.6 (1)	70.8 (1)	70.3 (1)	65.8 (av)	
		71.0 (1)	70.3 (1)		
M–As–As′	66.5 (1)	61.5 (1)	61.3 (1)		
	60.0 (1)	61.6 (1)	61.7 (1)		
M′–As–As′	73.6 (1)	66.3 (1)	66.2 (1)	61.5 (av)	
		65.9 (1)	65.8 (1)		
As–M–As′	53.5 (1)	52.2 (1)	52.5 (1)	56.9 (av)	
		52.4 (1)	52.6 (1)		

[a] This work. [b] No esd was given in ref 84.

thereby decreasing electron-pair repulsion between the As atoms.[19] The Cr - Cr distance of 3.026 Å is close to that expected of a single bond.[67]

In the presence of a single metal-metal bond and on the assumption that the μ-η^2-As_2 ligand serves as a 4 e donor, the noble-gas configuration at each Cr atom is achieved. The marginally shorter M-As and M-As' distances in **2** could result from the smaller size of Cr when compared to those of Mo and W.

$CpCr(CO)_2(\eta^3$-$As_3)$ (3)

The molecular structure of the compound **3** is illustrated in Figure 32. The molecule has similar geometry to those of $[(C_5Me_5)Mo(CO)_2As_3]$[20] and $[(C_5Me_5)Cr(CO)_2As_3]$.[87]

The Cr atom is situated at the apex of a tetrahedron with an essentially equilateral basal As_3 triangle. The As-As bond lengths [2.331 (2)- 2.346 (2) Å] fall between those of the single As-As bond (2.44 Å), as in As_4[74] and the As=As double bond (2.24Å).[88, 89] There is good agreement with the values of As-As bond lengths in the (η^3-As_3) complexes known to date, as illustrated in Table 11. Foust *et al.*[19] had attributed the shortening of the As-As bond length from that of the single-bond value in As_4 to a reduction in interarsenic repulsions by the introduction of the more electronegative organometallic fragment. The molecular structure is also similar to that of its (η^3-P_3) analogue,[15] with differences in E-E and M-E bond lengths (E = P, As) commensurate with the covalent radii of P and As.

Figure 32. Molecular Structure of $CpCr(CO)_2As_3$ (**3**).

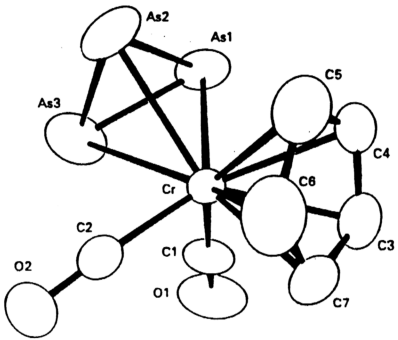

Table 11. A Comparison of As-As and M-As Bond Lengths (Å) in (η^3- As_3) Complexes.

	As—As	M—As
$[Co(CO)_3(\eta^3\text{-}As_3)]$ [a]	2.372 (5)	2.439 (5)
$[(C_5Me_5)Mo(CO)_2(\eta^3\text{-}As_3)]$ [b]	2.372 (1)-2.377 (2)	2.639 (1)-2.706 (2)
$[(C_5Me_5)Cr(CO)_2(\eta^3\text{-}As_3)]$ [c]	2.347 (2)-2.361 (2)	2.542 (1)-2.635 (2)
$[(C_5H_5)Cr(CO)_3(\eta^3\text{-}As_3)]$ [d]	2.331 (2)-2.356 (2)	2.555 (2)-2.619 (2)
$[\{(C_5Me_4Et)Ru\}_3Ru(\eta^3\text{-}As_3)\text{-}\mu_3\text{-}(\eta^3\text{-}As_3)(\mu_3\text{-}As_3)]$ [e]	2.310 (7)-2.329 (1)*	2.521 (5)-2.536 (5)†

[a] - Ref. 19.

[b] - Ref. 20.

[c] - Ref. 87.

[d] - This work.

[e] - Ref. 90.

* - In (η^3-As_3) ligand.

† - For Ru to (η^3-As_3) ligand.

2.3 Studies with Tetraphosphorus Trisulfide

2.3.1 The reaction of $[CpCr(CO)_3]_2$ with Tetraphosphorus Trisulfide

The reaction of a suspension of yellow P_4S_3 in a deep green toluene solution of 1 mole equivalent of $[CpCr(CO)_3]_2$ (**1**) for 13 days at ambient temperature, resulted in a yellowish brown mixture. Column chromatography of the product mixture on silica gel led to the isolation of unreacted P_4S_3 (33%), $Cp_4Cr_4(CO)_9(P_4S_3)$ (**9**) as dark brown crystals (49.6%), $[CpCr(CO)_2]_2S$ (**10**) as deep green crystals (12.8%), and an inseparable mixture of $CpCr(CO)_2(\eta^3\text{-}P_3)$ (**14**) as brownish yellow crystals (3%), $CpCr(CO)_3H$ (**11**) as lemon yellow crystals (27.9%) and P_4S_3 as yellow crystals (20%).

In the presence of isoprene as "scavenger" for the hydride **11**, converting it to **1**,[91] this reaction at ambient temperature for 9 days yielded **9** (59%), **10** (5.3%), **14** (2%), $[CpCr(CO)_2]_2P_2$ (**15**) (2.5%) and $[CpCr(CO)_2]_2$ (**4**) (4.4%) with recovered P_4S_3 (41%), but none of the hydride **11**.

A similar reaction at 60°C for 3h gave a substantially lower yield of **9** (30%) with increased yields of **10** (36%) and $Cp_4Cr_4S_4$ (**18**) as dark green solids (6.7%), together with **14** (0.4%), **11** (3%) and **15** as magenta crystals (*ca.* 1%) and unreacted P_4S_3 (13%). The formation of **10**, **14**, **15** and **18** apparently at the expense of **9** is substantiated in a thermolysis study described below.

Although the elemental analysis of **11** is not attainable, its identity was unambiguously established via a crystal structure analysis, as well as a match of its spectral characteristics with those of a synthesised authentic sample as discussed below. In addition, thin-layer chromatography on Kieselgel $^{60}F_{254}$ showed that compound **11** and the authentic $CpCr(CO)_3H$ complex were identical species (R_f = 0.69 with 3:2 *n*-hexane-toluene as eluent). The isolation of the hydride **11** is unexpected. It is significant that hydride formation was not observed in a reaction in the presence of isoprene, the reagent used for the synthesis of the dimer **1** from the hydride **11**.[91] One may envisage that its appreciable yield from the present reaction is

a consequence of the effect of the P_4S_3 cage molecule on the $[CpCr(CO)_3\cdot]$ radical, rendering its reverse dimerisation unfavourable versus hydrogen atom abstraction from a hydrogen source. Slight formation of the hydride had also occurred before in the reaction of **1** with Ph_2S_2,[92] though its identity was not recognised then, owing to the variability of the chemical shift of the Cp resonance.[93c] In this context, we note that atom transfer reactions constitute a common feature of transition metal-centered radicals.[94] Indeed, Baird has recently established the facile halogen atom abstraction from organic halides by $CpCr(CO)_3$.[93]

2.3.2 The reaction of $[CpCr(CO)_2]_2$ with Tetraphosphorus Trisulfide

No reaction was observed at ambient temperature. At 60°C , the reaction with one mole equivalent of P_4S_3 almost reached completion (92%) in *ca.* 18 h, giving $CpCr(CO)_3H$ (**11**) in significant yield (34%), together with $Cp_4Cr_4S_4$ (**18**) (30%) as the second major product. The formation of **11** in such substantial yield does indeed constitute a novel feature of this reaction. The occurrence of intramolecular carbonyl scrambling in $[(CO)_2CpCr{\equiv}CrCp(CO)_2]$ is implicated, either prior to or concurrent with M≡M bond dissociation to form $CpCr(CO)_3$. It seems that again the cage of the P_4S_3 molecule plays a role in assisting the formation of the hydride, as suggested above.

There are two possible pathways to **18** (14%) and the (η^3-P_3) complex **14** (10%). They may be formed directly from the fragmentation of the P_4S_3 cage by the Cr≡Cr bonded complex **4** or they may be derived from the thermal degradation of a primary product such as $Cp_4Cr_4(CO)_9(P_4S_3)$ (**9**). The latter route would lead to the formation of $[CpCr(CO)_2]_2S$ (**10**), as demonstrated in the thermolytic studies described below. However, neither **9**nor**10** was observed despite careful monitoring of NMR tube experiments (see Table 14), suggesting that **9** is an unlikely primary product in this reaction. On a comparative note, we observe that the reaction of the Mo≡Mo complex $[(C_5Me_5)Mo(CO)_2]_2$ with P_4S_3 for 5 h in boiling toluene produced Mo

complexes containing P_2S_3 and P_4S ligands, in addition to the Mo analogues of **14** and **15**.[57]

2.3.3 NMR spectral studies

It was observed in NMR tube reactions of **1** with 0.5 to 2 mole equivalents of P_4S_3 at 60°C for 3 h, that the yield (*ca.* 14%) of the hydride complex **11** was independent of the amount of P_4S_3. A time-dependent variation of the product composition from the reaction of **1** with 0.5 mole equivalent of P_4S_3 at 60°C is given in Table 12. The reaction was complete within 4 h, giving as main products **9** (24%), **10** (14%), **11** (18%) and **18** (12%) with small amounts of **14** (6%) and **15** (7%). Subsequently, **9** was observed to degrade to **10**, **14**, **15** and predominantly the cubane complex $Cp_4Cr_4S_4$ (**18**). The yield of **11** peaks at 3-4 h, *ca.* the time of completion of the reaction of **1**.

At 80°C, the reaction was completed within 1 h, yielding **9** (19%), **10** (21%), **14** (18%), **15** (16%) and **18** (18%) as shown in Table 13. Within the next hour, all of **9** had degraded leading to slightly increased yields of **10** and **14**, and a much higher yield of **18** (41%). At the end of 8 h, only **14** (23%) and **18** (68%) remained. As distinct from the reaction at 60°C, there was no sign of the formation of the hydride **11**, throughout the reaction. It may be envisaged that the enhanced rate of reaction of $CpCr(CO)_3\cdot$ with P_4S_3 is now competitive with that of its hydrogen atom abstraction and the small amount of the hydride that may be formed would react with P_4S_3. Indeed $CpCr(CO)_3H$ was found to react with P_4S_3 with a half-life of *ca.* 12 h at 60°C (*ca.* 5 h at 80°C) to give predominantly $CpCr(CO)_2P_3$ (**14**) (*ca.* 3%) and **18** (*ca.* 10%) with small amounts of $[CpCr(CO)_2]_2$ and $[CpCr(CO)_2]_2P_2$, as intermediate products.

The proton NMR spectral observation of the reaction of $[CpCr(CO)_2]_2$ with P_4S_3 at 60°C is summarised in Table 14. The reaction rate is approximately doubled on increasing the amount of P_4S_3 from 0.5 to 1.0 mole equivalent ($t_{½} \cong 2$ h and 1 h, respectively). After 18 h, the spectra showed the presence of $CpCr(CO)_3H$ in 28 and

Table 12. Time-dependent variation of product composition# from the reaction of $[CpCr(CO)_3]_2$ (**1**) with 0.5 mole equivalent of P_4S_3 at 60°C.

Time (h) \ Complexes†	**1**	**9**	**10**	**14**	**11**	**15**	**18**
1	75	9	3	1	8	0	0
2	13	28	9	5	12	5	6
3	8	30	12	6	14	6	10
4	0	24	14	6	18	7	12
5	0	18	16	6	24	8	15
18	0	0	12	9	12	8	17*

Yields (%), based on **1**

*An additional 30% was obtained as precipitated solids

† **9** - $Cp_4Cr_4(CO)_9(P_4S_3)$

10 - $[CpCr(CO)_2]_2S$

11 - $CpCr(CO)_3H$

14 - $CpCr(CO)_2P_3$

15 - $[CpCr(CO)_2]_2P_2$

18 - $Cp_4Cr_4S_4$

Table 13. Time-dependent variation of product composition[a] from the reaction of $[CpCr(CO)_3]_2$ with an equivalent of P_4S_3 at 80 °C

Time (h) \ Products	$Cp_4Cr_4(CO)_9(P_4S_3)$ (**9**)	$[CpCr(CO)_2]_2S$ (**10**)	$CpCr(CO)_2P_3$ (**14**)	$[CpCr(CO)_2]_2P_2$ (**15**)	$Cp_4Cr_4S_4$ (**18**)
1[a]	19	21	18	16	18
2	0	19	19	14	41
3	0	17	21	6	43
8	0	0	23	0	68

[a] - Product yields obtained by integration of Cp resonances in ^1H NMR spectrum of product mixture.

Table 14. Time-dependent variation of product composition[a] from the reaction of $[CpCr(CO)_2]_2$ (4) with n equivalents of P_4S_3 at 60 °C

Complexes *	4		14		11		15		18		unknown δ 5.13	
n / Time (h)	0.5	1	0.5	1	0.5	1	0.5	1	0.5	1	0.5	1
1	87	52	0	0	9	5	0	0	4	2	0	0
2	50	23	4	2	19	15	5	6	4	3	2	1
4	45	21	4	2	22	18	5	6	4	3	2	1
6	30	17	4	3	23	18	8	8	4	4	2	1
18	4	5	11	4	28	36	10	5	7[b]	6[c]	3	2

[a]% yield estimated from NMR integrals and based on **4**
[b]An additional 26% as precipitated solids.
[c]An additional 29% as precipitated solids.
* **11** - $CpCr(CO)_3H$
14 - $CpCr(CO)_2P_3$
15 - $Cp_2Cr_2(CO)_4P_2$
18 - $Cp_4Cr_4S_4$

36% yields, respectively, in close agreement to the isolated yield given earlier. The complexes **14**, **15** and an unknown possessing a proton resonance at δ 5.13, are formed in much lower yields, whilst **9** and **10** were not observed at all throughout the reaction.

2.3.4 Thermolysis of $Cp_4Cr_4(CO)_9(P_4S_3)$

Thermolysis of a toluene solution of $Cp_4Cr_4(CO)_9(P_4S_3)$ (**9**) for 3.5 h at 80°C led to complete degradation to $[CpCr(CO)_2]_2S$ (**10**), $[CpCr(CO)_2]_2P_2$ (**15**), $CpCr(CO)_2P_3$ (**14**) and $Cp_4Cr_4S_4$ (**18**) in 23.3, 10.1, 9.9 and 54.9% yields, respectively. This finding indicates that the reaction of **1** with P_4S_3 produces primarily the complex **9**, which degrades to the triply bonded Cr≡S≡Cr complex **10**,[13] the (μ-η^2-P_2) complex **15** together with the *cyclo*-P_3 complex **14**.[15] Based on previous observations on the facile thermal transformation of **10** to the cubane complex **18** at room temperature[13] and 60°C,[95] it is more likely that in this reaction **18** is derived from **10**, rather than directly from **9**.

The rate of thermal degradation of **9** is enhanced in the presence of excess P_4S_3 ($t_{½}$ = 1 h), compared to that in the absence of P_4S_3 ($t_{½}$ = 3-4 h) is illustrated in Table 15. Primary products include **10**, **14** and **15** which at the end of 4 h reached *ca.* 10, 7 and 4%, respectively, together with the secondary product **18** (24%). In the presence of excess P_4S_3, the formation of the hydride **11** was observed, comprising 3-4% of the total product composition throughout the reaction. This seems to support the above-mentioned hypothesis that P_4S_3 assists the formation of **11** from $CpCr(CO)_3$· formed from homolysis of Cr-P and Cr-S bonds in **9**. After 18 h, the predominant product was **18** (*ca.* 60%), with minor amounts of **14** (4%) and **15** (2%).

Table 15. Time-dependent variation of product composition from (a) the thermolysis of $Cp_4Cr_4(CO)_9(P_4S_3)$ at 60°C* and (b) its cothermolysis with an equimolar equivalent of P_4S_3 at 60°C.

Time (h)	$Cp_4Cr_4(CO)_9(P_4S_3)$ (**9**)	Products				
		$[CpCr(CO)_2]_2S$ (**10**)	$CpCr(CO)_3H$ (**11**)	$CpCr(CO)_2P_3$ (**14**)	$[CpCr(CO)_2]_2P_2$ (**15**)	$Cp_4Cr_4S_4$ (**18**)
1	48 [86]	7 [0]	3 [0]	2 [0]	5 [1]	3 [0]
3	11 [69]	9 [5]	3 [0]	3 [1]	4 [4]	8 [8]
4	0 [18]	0 [10]	0 [0]	0 [7]	0 [4]	0 [24]
5	0 [0]	8 [10]	4 [0]	3 [11]	5 [7]	13 [60]
18	0 [0]	4 [0]	3 [0]	4 [16]	2 [0]	63 [72]

*- Results given in parentheses [ ].

2.3.5 Mechanistic pathways : Formation of $Cp_4Cr_4(CO)_9(P_4S_3)$

Consonant with the established facile thermal dissociation of the Cr-Cr bond in **1**[65-69, 96] and the accumulating evidence suggesting reaction of **1** generally proceed *via* its 17e monomeric derivative,[65, 66, 91] the role of $CpCr(CO)_3\cdot$ is again implicated in this reaction as observed in our previous studies with Groups 15 and 16 nonmetals.[13,14b,15,16,97] The reaction of $[CpCr(CO)_3]_2$ (**1**) with P_4S_3 can be represented in Scheme III.

It is conceivable that the initial step involves a radical attack of $CpCr(CO)_2\cdot$ and/ or $CpCr(CO)_3\cdot$ on the P_4S_3 cage resulting in the P-P and P-S bond cleavages with concomitant bond formation. The radical cleavage of the P2-S1, P4-S2 and P3-P4 bonds of the P_4S_3 cage, with subsequent cage rearrangement and concomitant coordination of $CpCr(CO)_n$ (n = 2, 3) fragments (Figure 33) will generate the molecular structure of **9** (Figure 42) described below.

The variation of product composition with reaction conditions (section **2.3.1**) and the results of thermolytic studies (section **2.3.4**), as summarised in Table 16, together with NMR spectral studies (section **2.3.3** including Table 15) show that **9** together with the hydride **11** are the primary products of the reaction with subsequent degradation of **9** leading to the complexes **10**, **14** and **15** and ultimately the cubane **18**.

2.3.6 Physical properties

$Cp_4Cr_4(CO)_9(P_4S_3)$ (9)

The complex exists as dark brown crystals which remain unchanged after several days in air at ambient temperature. It is not soluble in *n*-hexane but soluble in most organic solvents to give a reddish brown solution. The solution is slightly air-sensitive but fairly stable at room temperature under an inert atmosphere for a few days.

Scheme III

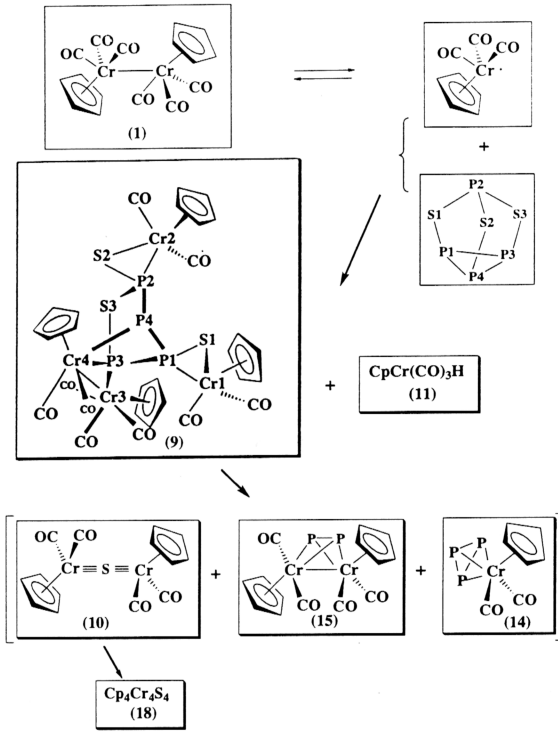

Figure 33. Bond-breaking and Bond-making (·····) in the P_4S_3 cage.

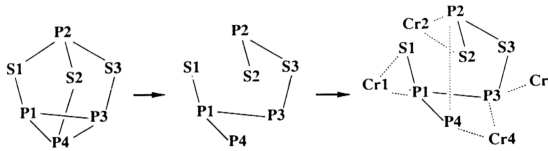

Table 16. Product composition[a] from the reaction of $[CpCr(CO)_3]_2$ with P_4S_3 at R.T and 60°C, and thermolysis of $Cp_4Cr_4(CO)_9(P_4S_3)$ (**9**) at 80°C.

Reactions \ Complexes	$Cp_4Cr_4(CO)_9(P_4S_3)$ (**9**)	$[CpCr(CO)_2]_2S$ (**10**)	$CpCr(CO)_3H$ (**11**)	$CpCr(CO)_2P_3$ (**14**)	$[CpCr(CO)_2]_2P_2$ (**15**)	$Cp_4Cr_4S_4$ (**18**)
13 days / R.T.[b]	49.6	12.8	27.9	3	0	0
3 h/ 60°C[b]	29.9	36.2	3	0.4	1	6.7
Thermolysis of **9**	0	23.3	0	9.9	10.1	54.9

[a] - % isolated yields.

[b] - Reaction of $[CpCr(CO)_3]_2$ with an equimolar equivalent of P_4S_3.

$CpCr(CO)_3H$ (11)

The complex exists as lemon yellow platelets which is soluble in most organic solvents to give a yellow solution. It is extremely air-sensitive in both the solid and solution state and converts readily to the dimer complex, $[CpCr(CO)_3]_2$ (**1**).

2.3.7 Spectral characteristics

2.3.7.1 I.R. spectra

$Cp_4Cr_4(CO)_9(P_4S_3)$ (9)

A sample of **9** showed the ν_{CO} stretching frequencies at 2028 vs, 1983 vs, 1969 vs, 1950 vs, 1942 vs, 1899 s, 1882 s,sh, 1874 vs cm^{-1} in nujol as shown in Figure 34.

$CpCr(CO)_3H$ (11)

The complex **11** in solution exhibits ν_{CO} at 2008 s, 1922 vs cm^{-1} (THF) and 2018 s, 1946 s, 1936 vs cm^{-1} (*n*-hexane) [cf. ν_{CO} at 2010 s, 1922 vs, br cm^{-1} (THF) and 2018 s, 1946 s, 1936 vs cm^{-1} (*n*-hexane)].[91] The spectra of **11** and a synthesized authentic sample of $CpCr(CO)_3H$ are compared in Figure 35.

2.3.7.2 NMR spectra

$Cp_4Cr_4(CO)_9(P_4S_3)$ (9)

The proton NMR of **9** indicates an approximately 3:1 molar mixture of two isomers. Isomer A: δ(Cp) = 4.58(s), 4.61(s), 4.76(s), 4.77 (*d*, *J* = 1.5 Hz) and isomer B: δ(Cp) = 4.61(s), 4.70(s), 4.79 (*d*, *J* = 1.5 Hz) and 4.86(s) (Figure 36). A variable-temperature ^1H NMR study in toluene-d_8 shows that isomer A is the predominant species below -30°C [δ(Cp) 4.39, 4.53, 4.63 and 4.71], and that rapid exchange of the four Cp rings at 90°C gives rise to a singlet at δ 4.77 (Figure 37). The ^{13}C NMR of the isomeric mixture shows Cp resonances at δ 90.39, 91.71 (the most intense peak, unresolved with δ 91.58 and 91.45), 92.07, 92.72 and 93.15.

The ^{31}P NMR spectrum is complex and is illustrated in Figure 38. Analysis shows that the signals belong to two ABCD spin systems (**I** and **II**) with an intensity

Figure 34. CO stretching frequencies of $Cp_4Cr_4(CO)_9(P_4S_3)$ (**9**) in nujol.

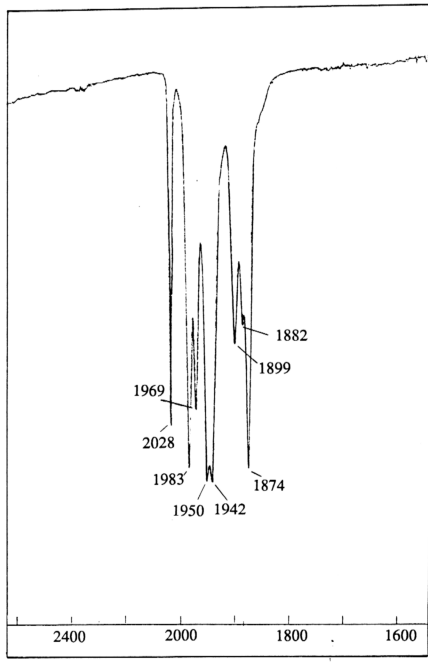

Figure 35. Comparison of CO stretching frequencies of $CpCr(CO)_3H$ (**11**) with synthesized authentic sample of $CpCr(CO)_3H$ in THF.

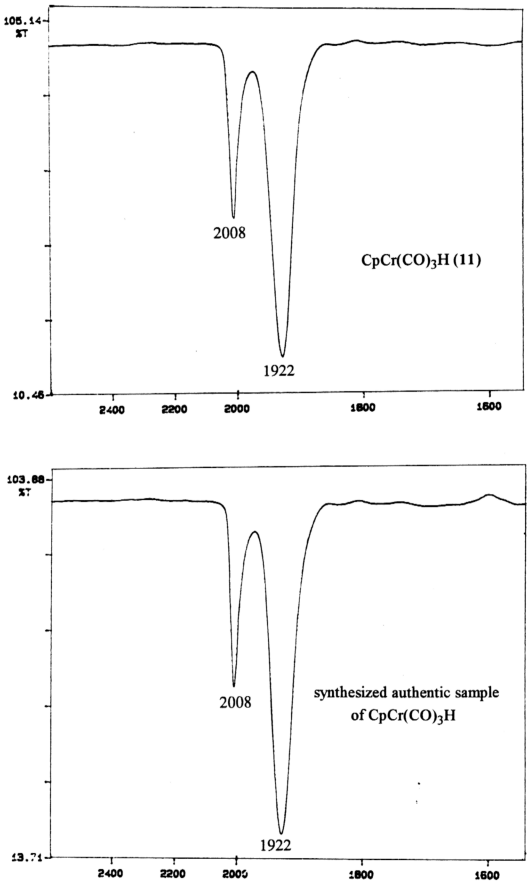

Figure 36. ^1H NMR spectrum of $Cp_4Cr_4(CO)_9(P_4S_3)$ in C_6D_6

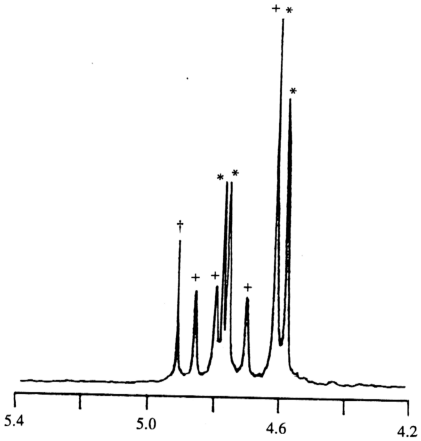

*Isomer A : δ 4.58, 4.61, 4.76 and 4.77.

+Isomer B : δ 4.61, 4.70, 4.79 and 4.86

† - impurity peak

Figure 37. Temperature-dependent ^1H NMR spectra of a 2mM solution of $Cp_4Cr_4(CO)_6(P_4S_3)$ in d_8-toluene.

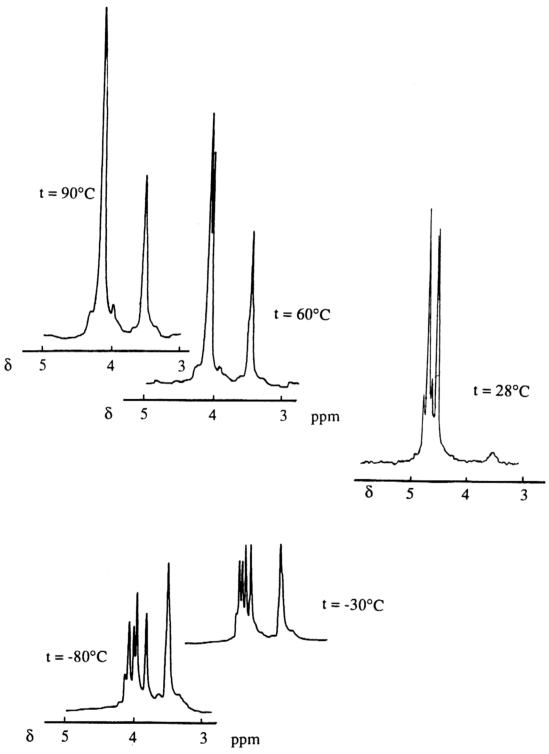

Figure 38. ^{31}P NMR spectrum of $Cp_4Cr_4(CO)_6(P_4S_3)$

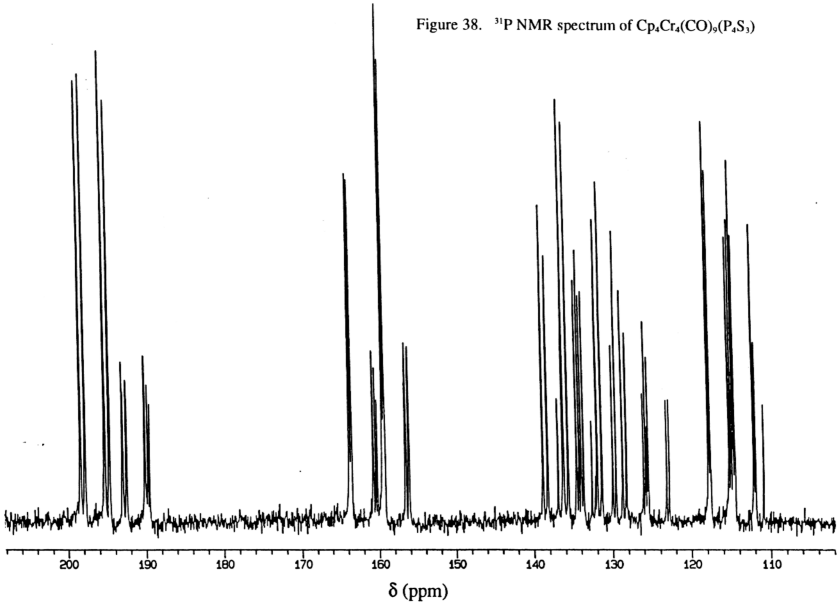

ratio of approximately 3:1. Both spin systems have been successfully analysed using the LAOCN-5 computer program,[98] and their respective calculated spectra are shown in Figure 39a and 39b. The combined simulated spectrum for a 3:1 mixture, shown in Figure 40 agrees remarkably well with the experimental spectrum (Figure 38), with the exception of δ 110.87, which pertains to $[CpCr(CO)_2]_2P_2$.[15] The matching of experimental and calculated frequencies is given in Table 17. The spectrum of spin system **I** is nearly first-order. In the case of spin system **II**, however, the signals of P_1 and P_3 get closer as compared to **I**, leading to a large value for $J(P_1, P_3)/\nu_o \cdot \delta(P_1, P_3)$ and thus to a spectrum of higher order. This affects also the signals of P_2 and P_4, causing additional splittings.

The NMR parameters of **I** and **II** (Table 18) are quite similar. The large coupling constants indicate for both cases a P_4-chain with the connectivity P_3-P_1-P_4-P_2 in agreement with the result of the X-ray structure determination of **9**. Thus most probably the two spin systems correspond to isomers having the same skeleton and differing only with respect to the configuration at P_1 or, more likely, P_2 (e.g. **9a** and **9b** in Figure 41). The assignment of the ^{31}P NMR signals to the individual phosphorus atoms is based on the assumption that $\delta^{31}P$ of the P atom with two Cr-neighbours appears at lower field than that of the P atom having one Cr- and one S-neighbour.

$CpCr(CO)_3H$ (11)

The spectral data of **11** were found to match closely those of a synthesised authentic sample of $CpCr(CO)_3H$, *viz.* ^1H NMR (benzene-d_6): δ(Cp) 4.06, δ(Cr-H) -5.62; (toluene-d_8): δ(Cp) 4.10, δ(Cr-H) -5.63. (cf. δ 3.84 and δ -5.70).[91] ^{13}C NMR (benzene-d_6): δ(Cp) 86.16; (toluene-d_8): δ(Cp) 86.06. The slight discrepancy in the δ(Cp) values is congruent with Baird's observation of a hydrogen atom exchange between the hydride and the $CpCr(CO)_3\cdot$ radical species, which results in coalescence of the Cp resonance of the dimer **1** with that of the hydride.[93a,c]. In fact, we have observed that different samples of the product complex **11** possessed δ(Cp) values in the range δ 4.02 to 4.26, with a corresponding increase in line-width. This

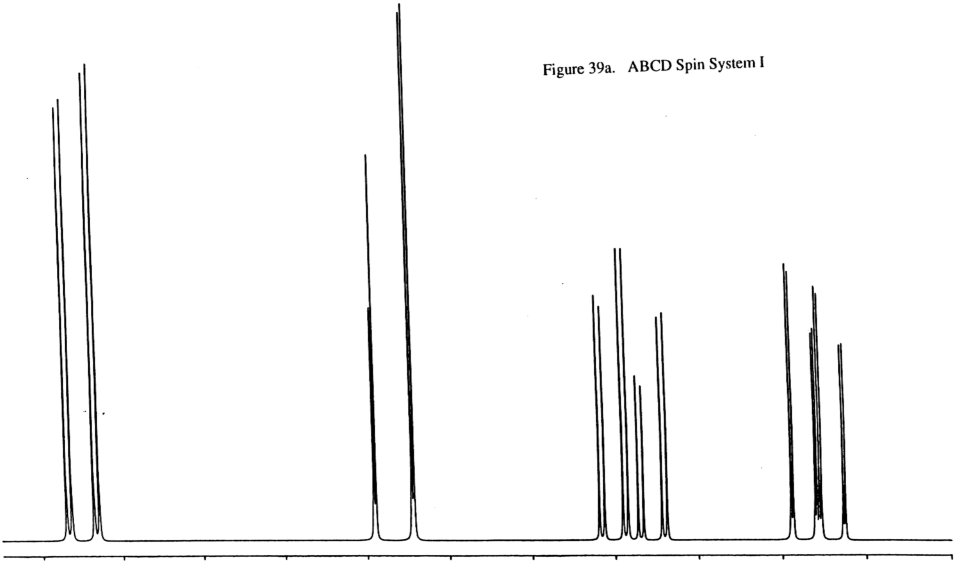

Figure 39a. ABCD Spin System I

Figure 39b. ABCD Spin System II

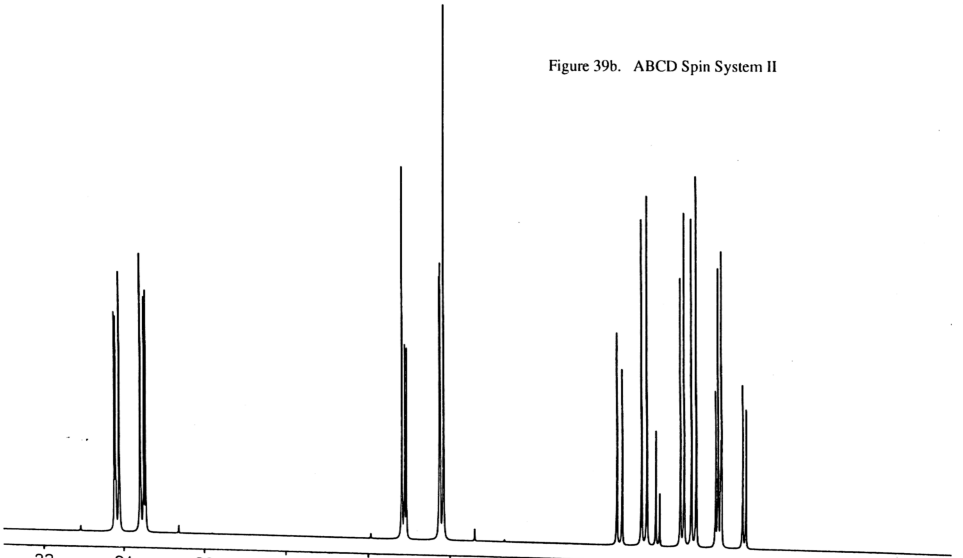

Figure 40. Calculated Sum of System I and System II

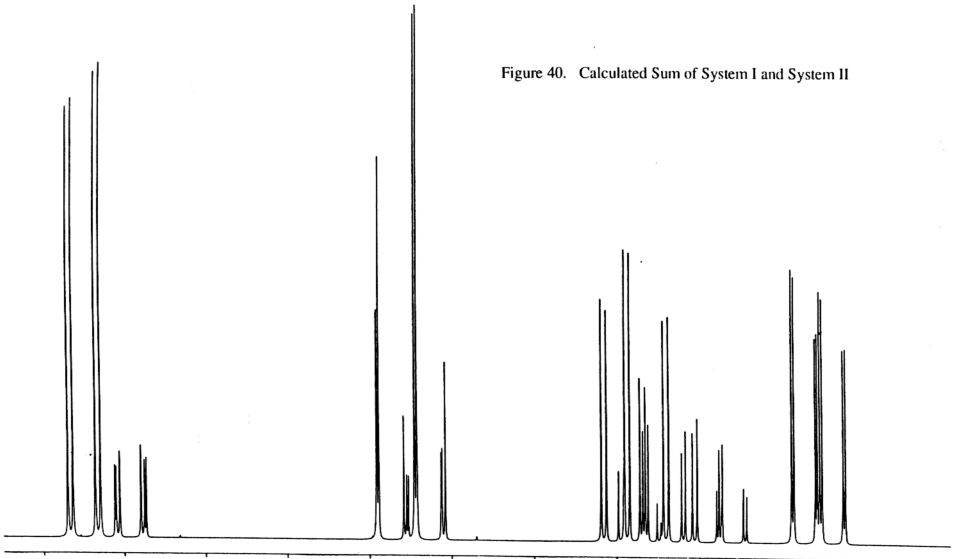

Table 17. ^{31}P NMR Chemical Shifts[a] and Peak Frequencies of $Cp_4Cr_4(CO)_6(P_4S_3)$ (**9**)

Observed resonance peaks δ (PPM)	Frequency (Hz) Exptl.	Calc.	Assignment to ABCD Spin System
198.34	21691.00	21693.98	
	21691.00	21693.23	
197.80	21632.30	21630.57	
	21632.30	21630.53	
195.28	21356.40	21355.32	I
	21356.40	21355.28	
194.69	21291.90	21292.53	
	21291.90	21291.78	
193.02	21109.90	21111.46	
192.92	21098.20	21097.51	
192.49	21051.30	21052.60	
	21051.30	21048.31	II
190.13	20793.00	20793.63	
		20789.44	
189.75	20752.00	20748.61	
189.48	20722.60	20726.18	
163.78	17911.50	17912.87	
	17911.50	17912.13	I
163.56	17888.00	17885.52	
	17888.00	17885.48	
160.77	17582.80	17584.36	
	17582.80	17580.06	II
160.45	17547.60	17545.90	
160.24	17524.10	17523.46	
159.54	17447.80	17447.42	
	17447.80	17447.38	I
159.27	17418.50	17420.78	
	17418.50	17420.03	
156.53	17119.20	17116.08	
156.10	17072.20	17077.62	II
	17072.20	17073.42	
138.82	15182.50	15183.10	I
138.23	15117.90	15119.65	
136.95	14977.10	14976.76	II
136.25	14900.80	14900.60	
135.66	14836.20	14837.06	I
134.58	14718.90	14717.60	
134.26	14683.70	14684.98	II
133.99	14654.30	14654.95	I
133.67	14619.10	14621.72	
132.65	14507.60	14508.48	II
132.22	14460.60	14463.57	
132.01	14437.20	14435.10	I
131.42	14372.60	14372.35	
130.02	14220.00	14216.70	
129.59	14173.10	14171.68	
128.79	14085.00	14084.95	
128.25	14026.30	14028.35	II
126.11	13791.60	13793.07	
125.84	13762.30	13762.82	
125.62	13738.80	13736.47	
125.52	13727.00	13724.37	
123.15	13468.80	13471.05	
122.83	13433.60	13432.59	
117.84	12887.80	12886.74	
117.57	12859.50	12860.09	
115.27	12606.10	12604.15	
115.00	12576.80	12577.50	I
114.73	12547.40	12548.70	
114.52	12523.90	12521.35	
112.15	12265.70	12266.20	
111.89	12236.40	12238.85	
110.87	12124.90*		

* Pertains to $[CpCr(CO)_2]_2P_2$ (**15**)

[a] In C_6D_6, referenced to external 85% H_3PO_4

Table 18. Summary of NMR parameters of spin systems I and II

ABCD Spin system I	ABCD Spin system II
$\delta^{31}P$: P_3 196.5	$\delta^{31}P$: P_3 191.3
P_2 161.5	P_2 158.3
P_4 135.2	P_4 133.1
P_1 115.0	P_1 126.1
$^1J(P_3,P_1)$ = -339.9 Hz	$^1J(P_3,P_1)$ = -330.5 Hz
$^1J(P_4,P_1)$ = -284.9 Hz	$^1J(P_4,P_1)$ = -293.9 Hz
$^1J(P_2,P_4)$ = -467.4 Hz	$^1J(P_2,P_4)$ = -478.3 Hz
$^2J(P_3,P_2)$ < 1 Hz	$^2J(P_3,P_2)$ = 3.8 Hz
$^2J(P_3,P_4)$ = 65.3 Hz	$^2J(P_3,P_4)$ = 72.3 Hz
$^2J(P_2,P_1)$ = 31.6 Hz	$^2J(P_2,P_1)$ = -26.6 Hz

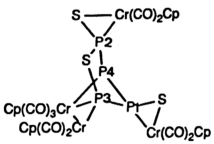

Isomer **9a**

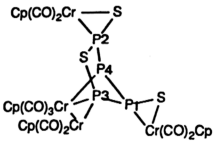

Isomer **9b**

Figure 41 Proposed isomers for **9a** and **9b**

undoubtedly arose from some contamination with **1**, into which $CpCr(CO)_3H$ readily converts in the presence of trace of air. It has been pointed out that the observed chemical shift and line-width of the coalesced resonance of **1** and its hydride is a weighted average of those of **1**, its monomer and hydride.[93c]

2.3.7.3 Mass spectra

$Cp_4Cr_4(CO)_9(P_4S_3)$ (9)

The fast atom bombardment (FAB) mass spectra of **9** are given in Table 19.

$CpCr(CO)_3H$ (11)

The fragmentation pattern in the E.I. mass spectrum of **11** is given in Table 20.

2.3.8 Molecular structures

$Cp_4Cr_4(CO)_9(P_4S_3)$ (9)

The molecular structure of **9** is shown in Figure 42 and the packing diagram in Figure 43. It is apparent from a comparison of Figure 33 and the structure of **9** (Figure 42) that bond cleavages of the P_4S_3 cage as mentioned above, coupled with bond formation between P2 and P4, have led to the formation of a five membered P_4S ring, namely P3P1P4P2S3, with two external S atoms as substituents at P1 and P2. Together with Cr4, this five-membered ring forms a bicyclo[2.1.1] system, possessing common vertices at P3 and P4. In fact the P_4S ring bridges four $[CpCr(CO)_n]$ (n = 2 or 3) *via* its four P atoms; the S atom of the five-membered ring is not coordinated to any metal. With the exception of Cr3, the other three Cr atoms are coordinated to two members of the P_4S_3 system. It will be noted that P3 is the only P atom that links two Cr atoms, *viz.* Cr3 and Cr4, and is closer to the latter by 0.084 Å. Cr1 and Cr2 have similar ligand environments, both possessing a pseudo η^2-PS ligand. An earlier example of η^2-PS coordination was established for the $Cr(CO)_5$ adduct of $Cp^*_2Mo_2P_4S$[57] (refer to Section **1.2.2 (c)**). Each of the five-coordinate Cr atoms assumes a

Table 19. Fast atom bombardment and Electron impact mass spectrum of $Cp_4Cr_4(CO)_9(P_4S_3)$(**9**)

m/e	Assignments
940	$[Cp_4Cr_4(CO)_9P_4S_3]$
884	$[Cp_4Cr_4(CO)_7P_4S_3]$
856	$[Cp_4Cr_4(CO)_6P_4S_3]$
482	$[Cp_4Cr_4(CO)P_4S_3]$
391	$[Cp_2Cr_2P_3S_2]$
266	$[CpCr(CO)_2P_3]$ or $[Cp_2Cr_2P_3]$
238	$[CpCr(CO)P_3]$
327	$[Cp_2Cr_2P_3]$
296	$[CpCr_2P_2]$
266	$[CpCr(CO)_2P_3]$
262	$[CpCr_2P_3]$
238	$[CpCr(CO)P_3]$
213	$[Cp_2CrP]$
210	$[CpCrP_3]$
200	$[CpCr_2P]$
182	$[Cp_2Cr]$
169	$[CpCr_2]$

Table 20. Electron impact mass spectrum of $CpCr(CO)_3H$ (**11**)

m/e	Assignments
202	$[CpCr(CO)_3H]$
174	$[CpCr(CO)_2H]$
173	$[CpCr(CO)_2]$
146	[CpCr(CO)H]
145	[CpCr(CO)]
118	[CpCrH]
117	[CpCr]

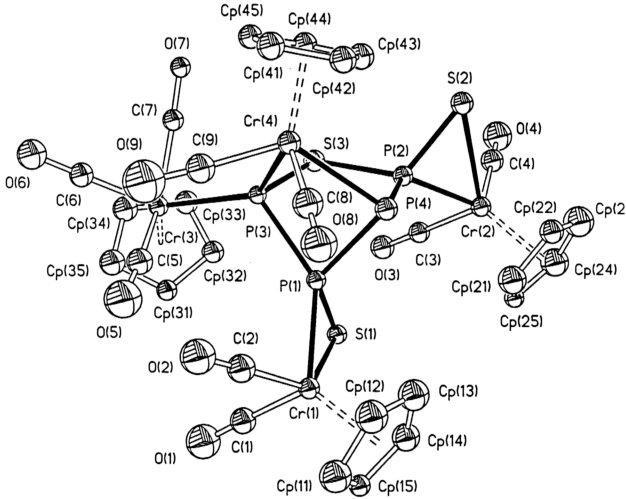

Figure 42. Molecular structure of $Cp_4Cr_4(CO)_9(P_4S_3)$ (**9**).

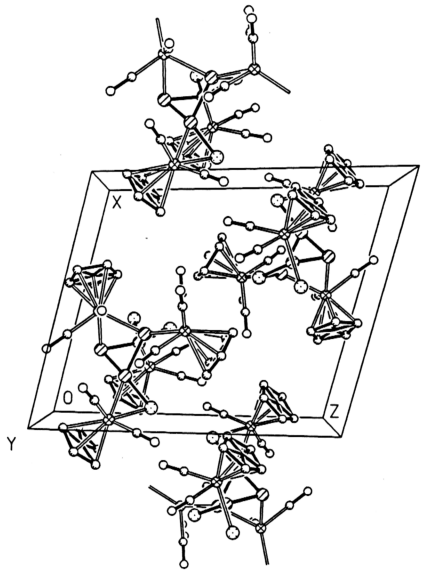

Figure 43. Molecular packing of $Cp_4Cr_4(CO)_9(P_4S_3)$ (**9**) in the unit cell.

four-legged piano-stool geometry. This is the first example of multiple bond-cleavage without fragmentation of the P_4S_3 cage molecule by a transition-metal complex.

Atomic coordinates and their equivalent displacement parameters are listed in Table 21. Selected bond lengths and bond angles are given in Table 22. The P-P bonds lengths (av. 2.201 Å), significantly shorter than those in the P_4S_3 cage (av. 2.235 Å),[46] are very close to the value for the single bond (2.21 Å) in P_4 vapor.[74] The P-S distances (av. 2.0067 Å) are also shorter than the intact cage (av. 2.090 Å).[46] The Cr-P distances (av. 2.282 Å) in the CrPS rings for Cr1 and Cr2 are significantly shorter than the other three Cr-P bonds (av. 2.440 Å), which fall within the range 2.341-2.494 Å observed for other CpCr-phosphorus complexes [15, 16] The Cr-S distances (2.486 and 2.517 Å) are longer than those observed in $Cr(\mu\text{-}\eta^2\text{-}S_2)$ and $Cr(\mu\text{-}\eta^1, \eta^2\text{-}S_2)$ complexes (range 2.348-2.466 Å).[13]

$CpCr(CO)_3H$ (11)

The molecular structure of complex **11** is shown in Figure 44 and the packing diagram in Figure 45. Atomic coordinates and their equivalent isotropic displacement parameters are given in Table 23. Bond lengths and bond angles are presented in Table 24. The CO ligands form the three legs of a piano stool configuration. Unlike the tungsten analogue, where there was a large CO-W-CO angle which can accomodate a hydrogen atom, this hydride has two CO-Cr-CO angles obtuse and the remaining one acute. The hydrogen atoms are disordered at the two sites above the two obtuse angles making H-Cr-Cp centre angles of 107(4)°. The thermal parameters of all the atoms are quite high consistent with the instability of the crystal. The Cr-H distances of 1.24(5) and 1.22(8) Å are within the sum of the covalent radii of Cr (1.18 Å) and hydrogen (0.2 Å).[99]

Table 21. Atomic Coordinates and their Equivalent Displacement Parameters for $Cp_4Cr_4(CO)_9(P_4S_3)$ (9).

Atom	x	y	z	$B_{eq}(A^2)$
Cr1	0.9669(1)	0.1427(1)	0.7459(1)	3.51(4)
Cr2	0.7739(1)	0.6350(1)	0.6664(1)	3.27(4)
Cr3	0.6101(1)	0.1827(1)	0.5715(1)	3.43(4)
Cr4	0.5347(1)	0.2363(1)	0.8763(1)	3.98(4)
S1	0.9265(2)	0.3135(2)	0.6192(2)	3.53(6)
S2	0.5665(2)	0.6216(2)	0.7671(2)	4.45(7)
S3	0.6059(2)	0.4341(2)	0.6271(2)	3.31(6)
P1	0.7961(2)	0.2554(2)	0.7332(2)	2.90(6)
P2	0.6668(2)	0.4930(2)	0.7225(2)	3.09(6)
P3	0.6257(2)	0.2624(2)	0.7025(2)	2.83(5)
P4	0.6938(2)	0.3469(2)	0.8428(2)	3.40(6)
O1	1.0422(8)	0.0423(7)	0.5732(6)	8.5(3)
O2	0.8308(7)	-0.0472(6)	0.8483(7)	7.6(3)
O3	0.8287(6)	0.5748(6)	0.4722(5)	5.2(2)
O4	0.6748(7)	0.8390(6)	0.5411(7	7.5(3)
O5	0.7339(8)	-0.0154(6)	0.6870(6	7.5(3)
O6	0.4526(6)	0.0115(6)	0.6186(6)	6.5(2)
O7	0.3714(6)	0.2997(7)	0.6402(6)	6.6(2)
O8	0.6860(7)	0.1018(8)	1.0123(6)	7.8(3)
O9	0.5310(9)	0.0148(6)	0.8545(7)	8.4(3)
C1	1.0117(9)	0.0817(9)	0.6401(8)	5.3(3)
C2	0.8822(9)	0.0273(8)	0.8052(8)	5.0(3)
C3	0.8080(8)	0.5971(8)	0.5480(7)	4.0(3)
C4	0.7099(9)	0.7619(8)	0.5913(8)	4.6(3)
C5	0.6861(9)	0.0614(7)	0.6489(8)	4.5(3)
C6	0.5134(9)	0.0775(8)	0.5995(8)	4.6(3)
C7	0.4624(8)	0.2558(8)	0.6157(8)	4.2(3)
C8	0.6282(9)	0.1560(9)	0.9581(8)	5.3(3)
C9	0.536(1)	0.1009(9)	0.8588(8)	5.1(3)
Cp11	1.0917(9)	0.056(1)	0.8322(9)	6.5(3)
Cp12	1.002(1)	0.116(1)	0.8914(8)	6.0(3)
Cp13	1.0071(9)	0.2235(9)	0.8457(8)	5.5(3)
Cp14	1.0964(9)	0.2345(9)	0.7609(8)	5.5(3)
Cp15	1.1485(9)	0.132(1)	0.7518(9)	6.6(4)
Cp21	0.9019(9)	0.5464(9)	0.7519(8)	5.7(3)
Cp22	0.8291(9)	0.615(1)	0.8029(8)	5.6(3)
Cp23	0.840(1)	0.7184(8)	0.7462(8)	6.1(3)
Cp24	0.9209(9)	0.713(1)	0.6554(9)	7.1(3)
Cp25	0.9581(9)	0.604(1)	0.6614(8)	6.3(3)
Cp31	0.7825(9)	0.1816(8)	0.4635(8)	4.8(3)
Cp32	0.7389(8)	0.2912(8)	0.4637(7)	4.3(3)
Cp33	0.6352(9)	0.3138(9)	0.4337(8)	5.2(3)
Cp34	0.6156(9)	0.2187(9)	0.4151(8)	5.5(3)
Cp35	0.7060(9)	0.1380(9)	0.4330(8)	5.3(3)
Cp41	0.368(1)	0.214(1)	0.9834(9)	6.6(4)
Cp42	0.419(1)	0.288(1)	1.0053(9)	7.4(4)

(continued)

Cp43	0.426(1)	0.379(1)	0.925(1)	7.2(4)
Cp44	0.385(1)	0.360(1)	0.8532(9)	6.3(4)
Cp45	0.3466(9)	0.260(1)	0.890(1)	6.6(4)
C101	0.123	0.777	0.887	19(1)*
C102	0.233	0.726	0.871	22(1)*
C103	0.038	0.703	0.907	21(1)*
C104	0.115	0.603	0.878	26(2)*
C105	0.219	0.629	0.862	26(2)*

Starred atoms were refined isotropically.
Anisotropically refined atoms are given in the form of the isotropic equivalent displacement parameter defined as:
$(4/3) * [a^2*B(1,1) + b^2*B(2,2) + c^2*B(3,3) + ab(\cos \text{gamma})*B(1,2) + ac(\cos \text{beta})*B(1,3) + bc(\cos \text{alpha})*B(2,3)]$

Table 22. Bond Lengths (Å) and Angles (°) for $Cp_4Cr_4(CO)_9P_4S_3$ (**9**).

Cr1	S1	2.486(3)	Cr3	Cp31	2.21(1)
Cr1	P1	2.298(3)	Cr3	Cp32	2.23(1)
Cr1	C1	1.82(1)	Cr3	Cp33	2.19(1)
Cr1	C2	1.83(1)	Cr3	Cp34	2.15(1)
Cr1	Cp11	2.17(1)	Cr3	Cp35	2.18(1)
Cr1	Cp12	2.18(1)	Cr4	P3	2.384(3)
Cr1	Cp13	2.21(1)	Cr4	P4	2.467(3)
Cr1	Cp14	2.23(1)	Cr4	C8	1.83(1)
Cr1	Cp15	2.20(1)	Cr4	C9	1.83(1)
Cr2	S2	2.517(3)	Cr4	Cp41	2.17(1)
Cr2	P2	2.266(3)	Cr4	Cp42	2.17(1)
Cr2	C3	1.83(1)	Cr4	Cp43	2.21(1)
Cr2	C4	1.84(1)	Cr4	Cp44	2.20(1)
Cr2	Cp21	2.19(1)	Cr4	Cp45	2.19(1)
Cr2	Cp22	2.19(1)	S1	P1	2.000(4)
Cr2	Cp23	2.17(1)	S2	P2	2.002(4)
Cr2	Cp24	2.15(1)	S3	P2	2.105(4)
Cr2	Cp25	2.16(1)	S3	P3	2.162(3)
Cr3	P3	2.468(3)	P1	P3	2.206(4)
Cr3	C5	1.88(1)	P1	P4	2.193(4)
Cr3	C6	1.84(1)	P2	P4	2.203(4)
Cr3	C7	1.87(1)	Cp23	Cp24	1.40(2)
O1	C1	1.16(1)	Cp24	Cp25	1.37(2)
O2	C2	1.16(1)	Cp31	Cp32	1.41(1)
O3	C3	1.16(1)	Cp31	Cp35	1.40(2)
O4	C4	1.13(1)	Cp32	Cp33	1.39(2)
O5	C5	1.12(1)	Cp33	Cp34	1.40(2)
O6	C6	1.15(1)	Cp34	Cp35	1.38(2)
O7	C7	1.14(1)	Cp41	Cp42	1.38(2)
O8	C8	1.18(1)	Cp41	Cp45	1.38(2)
O9	C9	1.14(1)	Cp42	Cp43	1.38(2)
Cp11	Cp12	1.42(2)	Cp43	Cp44	1.37(2)
Cp11	Cp15	1.39(2)	Cp44	Cp45	1.36(2)
Cp12	Cp13	1.36(2)	C101	C102	1.351
Cp13	Cp14	1.37(2)	C101	C103	1.444
Cp14	Cp15	1.37(2)	C102	C105	1.334
Cp21	Cp22	1.34(2)	C103	C104	1.522
Cp21	Cp25	1.36(2)	C104	C105	1.306
Cp22	Cp23	1.35(2)			

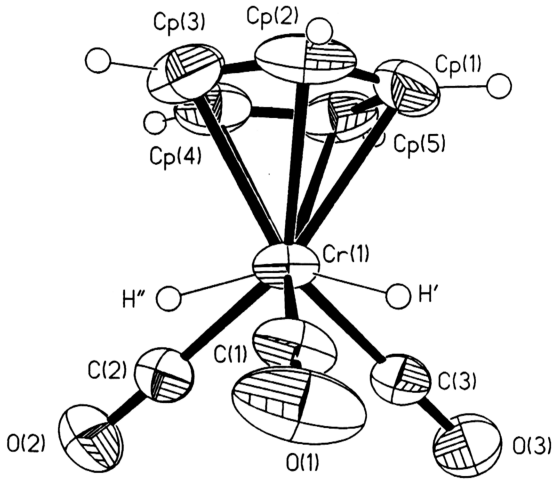

Figure 44. Molecular Structure of $CpCr(CO)_3H$ (**11**)

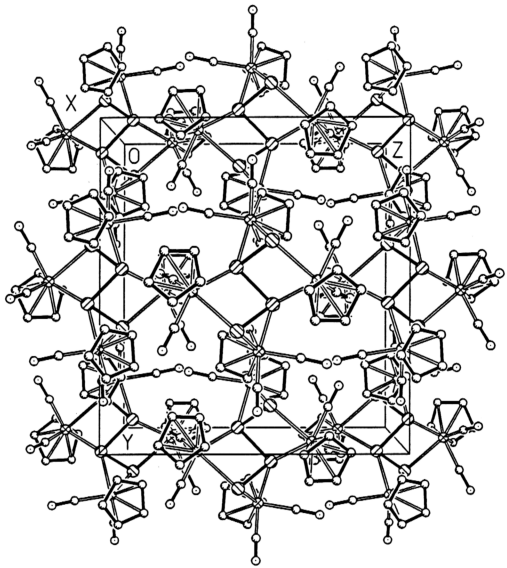

Figure 45. Molecular packing of $CpCr(CO)_3H$ (**11**) in the unit cell

Table 23. Atomic coordinates ($x_{,}10^4$) and equivalent isotropic displacement parameters ($Å^2$ x 10^3) for $CpCr(CO)_3H$. U(eq) is defined as one third of the trace of the orthogonalize Uij tensor.

	x	y	z	U(eq)
Cr	4830(1)	-102(1)	2171(1)	63(1)
O1	7576(4)	317(6)	2339(7)	145(2)
O2	5534(4)	-3082(6)	4072(4)	114(1)
O3	4006(6)	-3179(5)	320(4)	138(2)
C1	6519(5)	148(6)	2265(6)	83(1)
C2	5266(5)	-1946(7)	3334(5)	74(1)
C3	4332(6)	-1998(6)	1032(5)	83(1)
Cp1	3431(7)	1963(9)	967(6)	104(2)
Cp2	4501(6)	2826(6)	2005(8)	101(2)
Cp3	4441(6)	2255(8)	3061(6)	100(2)
Cp4	3379(6)	1062(7)	2749(7)	94(2)
Cp5	2751(5)	872(7)	1479(7)	92(2)

Table 24. Bond Lengths (Å) and Angles (°) for $CpCr(CO)_3H$ (**11**).

Cr-C(1)	1.816(5)
Cr-C(2)	1.826(5)
Cr-C(3)	1.833(5)
Cr-Cp3	2.156(5)
Cr-Cp2	2.157(4)
Cr-Cp1	2.163(5)
Cr-Cp5	2.167(5)
Cr-Cp4	2.171(4)
Cr-H'	1.24(5)
Cr-H"	1.22(8)
O(1)-C(1)	1.131(6)
O(2)-C(2)	1.141(5)
O(3)-C(3)	1.143(6)
Cp1-Cp5	1.402(8)
Cp1-Cp2	1.408(8)
Cp2-Cp3	1.347(8)
Cp3-Cp4	1.365(8)
Cp4-Cp	1.349(7)
C(1)-Cr-C(2)	96.6(2)
C(1)-Cr-C(3)	94.5(2)
C(2)-Cr-C(3)	83.7(2)
C(1)-Cr-Cp3	108.2(2)
C(2)-Cr-Cp3	105.1(3)
C(3)-Cr-Cp3	154.2(2)
C(1)-Cr-Cp2	91.8(2)
C(2)-Cr-Cp2	140.6(3)
C(3)-Cr-Cp2	134.1(3)
Cp3-Cr-Cp2	36.4(2)
C(1)-Cr-Cp1	111.9(2)
C(2)-Cr-Cp1	151.0(2)
C(3)-Cr-Cp1	98.7(2)
Cp3-Cr-Cp1	62.0(2)
Cp2-Cr-Cp1	38.0(2)
C(1)-Cr-Cp5	149.6(2)
C(2)-Cr-Cp5	113.5(2)
C(3)-Cr-Cp5	93.2(2)
Cp3-Cr-Cp5	61.1(2)
Cp2-Cr-Cp5	62.4(2)
Cp1-Cr-Cp5	37.8(2)
C(1)-Cr-Cp4	144.7(2)
C(2)-Cr-Cp4	91.7(2)
C(3)-Cr-Cp4	120.6(2)
Cp3-Cr-Cp4	36.8(2)
Cp2-Cr-Cp4	61.7(2)
Cp1-Cr-Cp4	62.1(2)
Cp5-Cr-Cp4	36.2(2)
C(1)-Cr-H'	59(3)
C(2)-Cr-H'	128(2)
C(3)-Cr-H'	57(2)
Cp3-Cr-H'	126(2)

2.4 Studies with Tetraphosphorus Triselenide

2.4.1 The reaction of $[CpCr(CO)_3]_2$ with Tetraphosphorus Triselenide

The reaction of a deep green suspension of $[CpCr(CO)_3]_2$ (**1**) with one mole equivalent of P_4Se_3 in toluene for 6 days at ambient temperature produced a dark brown mixture from which was isolated $CpCr(CO)_3H$ (**11**), $Cp_4Cr_4(CO)_9(P_4Se_3)$ (**12**), $Cp_4Cr_4(CO)_8(P_2Se_2)$ (**13**), $CpCr(CO)_2P_3$ (**14**) and $Cp_2Cr_2(CO)_4P_2$ (**15**) in 7, 48.3, 13.2, 2.3 and 16.3% yields, respectively. A prolonged reaction for 12 days yielded the complexes **11** (6.9%), **12** (27.0%), **13** (33.5%) and **14** (8.4%). The same reaction at 60°C for 2 h produced the complexes **11** (2%), **12** (36.6%), **13** (15.9%), **14** (8.2%), **15** (8.7%), $Cp_2Cr_2(CO)_4Se$ (**17**) (19.4%) and $Cp_4Cr_4Se_4$ (**19**) (3.5%) yields. These product compositions and yields are summarised in Table 26 and the above observation is represented in Scheme IV.

The reaction of **1** with P_4Se_3 was completed in 6 days compared to 13 days for completion with P_4S_3 at ambient temperature, and 2 h versus 3 h, respectively, at 60°C. The relative reaction rate is consistent with relative P-X bond strengths (X = S : 444 ± 8 $kJmol^{-1}$) and (X = Se : 363.6 ± 10 $kJmol^{-1}$).[100]

As in the reaction with P_4S_3, $CpCr(CO)_3H$ (**11**) was also isolated in this reaction. The main products isolated are **12**, the Se analogue of $Cp_4Cr_4(CO)_9P_4S_3$ and **13**, a new tetrachromium complex for which there is no S analogue. It is significant that the yields of **12** (48.3%) and **13** (13.2%) after 6 days have changed to 27.0 and 33.5%, respectively, after 12 days of reaction. This indicates the formation of **13** from **12**, since all of **1** has completely reacted after 6 days. Although the amount of **11** remained unchanged (*ca.* 7%), **15** seem to have subsequently degraded to **14**, a process which has been observed before in studies of **1** with P_4.[15]

Scheme IV

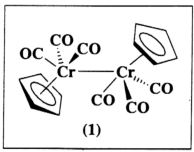

(1)

+

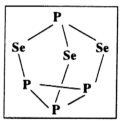

$Cp_4Cr_4(CO)_9(P_4Se_3)$
(12)

$CpCr(CO)_3H$
(11)

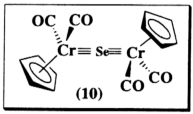

(10)

$Cp_4Cr_4(CO)_8(P_2Se_2)$
(13)

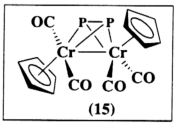

(15)

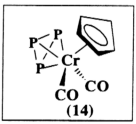

(14)

2.4.2 The reaction of $[CpCr(CO)_2]_2$ with Tetraphosphorus Triselenide

No reaction was observed in a mixture of $[CpCr(CO)_2]_2$ (**4**) with one mole equivalent of P_4Se_3 after 24 h at ambient temperature. At 60°C, the reaction took *ca.* 18 h to reach completion giving $CpCr(CO)_3H$ (**11**), $CpCr(CO)_2P_3$ (**14**), $Cp_2Cr_2(CO)_4P_2$ (**15**) and $Cp_4Cr_4Se_4$ (**19**) in 28.9, 6.8, 12.8 and 37.9%, respectively.

The reaction yielded a similar mixture of products as in the case of P_4S_3, and again the yield of **11** is significant. Here again intramolecular carbonyl scrambling in **4** must have occured to form $CpCr(CO)_3$.

There are two possible pathways to **19** (37.9%), **14** (6.8%) and **15** (12.8%). They may be formed directly from the fragmentation of the P_4Se_3 cage by the Cr≡Cr bonded complex **4** or they may be derived from the thermal degradation of a primary product such as $Cp_4Cr_4(CO)_9(P_4Se_3)$ (**12**) and/or $Cp_4Cr_4(CO)_8(P_2Se_2)$ (**13**). The latter route would lead to the formation of $Cp_2Cr_2(CO)_4Se$ (**17**), as demonstrated in the thermolytic studies below. However, neither **12**, **13** or **17** were detected suggesting that **12** or **13** is an unlikely primary product in this reaction.

2.4.3 The reaction of $Cp_2Cr_2(CO)_4Se$ with Tetraphosphorus Triselenide

An orange brown mixture of $Cp_2Cr_2(CO)_4Se$ (**17**) and P_4Se_3 in toluene for 6 days at ambient temperature produced $CpCr(CO)_3H$ (**11**), $CpCr(CO)_2P_3$ (**14**), $Cp_4Cr_4(CO)_9(P_4Se_3)$ (**12**) and $Cp_4Cr_4(CO)_8(P_2Se_2)$ (**13**) in 6, 2, 3.5 and 76.4% yields, respectively (refer to Scheme V).

2.4.4 The reaction of $Cp_2Cr_2(CO)_4Se$ with Tetraphosphorus Trisulfide

An orange brown mixture of $Cp_2Cr_2(CO)_4Se$ (**17**) and P_4S_3 in toluene for 6 days at ambient temperature produced $Cp_2Cr_2(CO)_4S$ (**10**), $CpCr(CO)_3H$ (**11**), $CpCr(CO)_2P_3$ (**14**), $Cp_4Cr_4(CO)_9(P_4Se_3)$ (**12**) and $Cp_4Cr_4(CO)_8(P_2Se_2)$ (**13**) in 15.5, 5, 1, 6.9 and 50.1% yields, respectively, together with a yellow precipitate containing a mixture of P_7 and $CpCr(CO)_2P_3$ (refer to Scheme VI).

2.4.5 NMR spectral studies

(a) Reaction of $[CpCr(CO)_3]_2$ with P_4Se_3 at ambient temperature

The reaction of $[CpCr(CO)_3]_2$ (**1**) with one molar equivalent of P_4Se_3 under ultrasonication at ambient temperature has been monitored *via* ^1H NMR at intervals for which the product compositions are given in Table 25. After 3 h, the spectrum showed the presence of $Cp_2Cr_2(CO)_4Se$ (**17**), $Cp_4Cr_4(CO)_9(P_4Se_3)$ (**12**), $[CpCr(CO)_2]_2$ (**4**) and a cluster of unidentified Cp-containing complexes (δ 5.00, 4.88, 4.72) in 13, 4, 3 and 9% yields, respectively, together with unreacted **1** (63% recovery). **1** has completely reacted within *ca.* 5 h, giving as main products **17** (31%) and **12** (27%), together with the above-mentioned cluster of unidentified complexes (8%), $CpCr(CO)_2P_3$ (**14**) (1%) and $[CpCr(CO)_2]_2P_2$ (**15**) (4%). Subsequently, after 9 h, the relative yield of **17** has decreased to 8%, while there are increases in **12** (41%), **14** (3%), **15** (8%) and $Cp_4Cr_4(CO)_8(P_2Se_2)$ (**13**) (8%).

It is significant to note that the absence of $CpCr(CO)_3H$ (**11**) in this reaction agrees with earlier findings from the reaction with P_4S_3 at 80°C, suggesting that the enhanced rate of reaction of $CpCr(CO)_3$· with P_4Se_3 is now competitive with that of its hydrogen atom abstraction.

(b) Reaction of $Cp_2Cr_2(CO)_4Se$ with P_4Se_3 at ambient temperature

A time-dependent variation of the product composition from the reaction of $Cp_2Cr_2(CO)_4Se$ (**17**) with one molar equivalent of P_4Se_3 at ambient temperature has been studied via ^1H NMR spectral scans which are illustrated in Figure 46. After 1 day of reaction, the main product formed is $Cp_4Cr_4(CO)_9(P_4Se_3)$ (**12**) together with a small amount of $Cp_4Cr_4(CO)_8(P_2Se_2)$ (**13**), $CpCr(CO)_3H$ (**11**) and $Cp_4Cr_4Se_4$ (**19**). Over 2 to 3 days, a gradual increase of the products **11**, **12**, **13** and **19** was observed. Finally, after 4 days of reaction, most of **12** has been degraded to **13**, accompanied by formation of **19**. The above observation is represented in Scheme V:

Table 25. Variation of product composition[a] from the reaction of $[CpCr(CO)_3]_2$ with equimolar equivalent of P_4Se_3 under ultrasonication at ambient temperature.

Time (h) \ Complexes	$[CpCr(CO)_2]_3$ (1)	$[CpCr(CO)_2]_2Se$ (17)	$[CpCr(CO)_2]_2$ (4)	$Cp_4Cr_4(CO)_9P_4Se_3$ (12)	$Cp_4Cr_4(CO)_8P_2Se_2$ (13)	$CpCr(CO)_2P_3$ (14)	$[CpCr(CO)_2]P_2$ (15)	Unidentified complexes[b]
3	63	13	3	4	0	0	0	9
5	0	31	7	27	6	1	4	8
7	0	16	10	39	8	2	6	12
9	0	8	9	41	8	3	8	11

[a] - Product yields by integration of Cp resonances in ^1H NMR spectrum of product mixture.

[b] - Cluster of unidentified Cp resonances at δ 5.00, 5.22, 4.99, 4.86 and 4.76.

Figure 46. Time-dependent ^1H NMR spectra for an NMR tube reaction of a 2 mM solution of $Cp_2Cr_2(CO)_4Se$ (**17**) with one molar equivalent of P_4Se_3 at ambient temperature under argon.

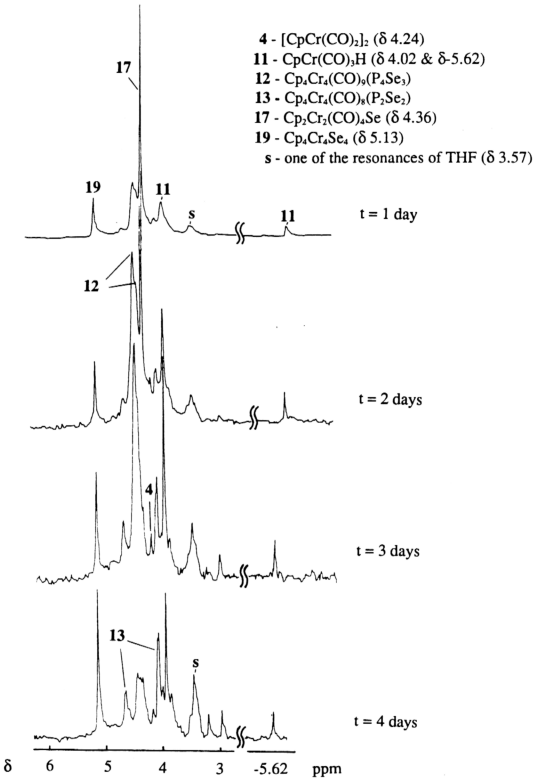

Scheme V

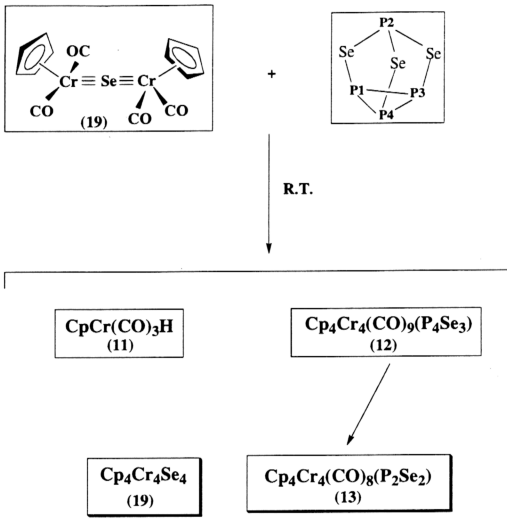
OC
Cr ≡ Se ≡ Cr
CO
CO
CO
CO
(19)
+
P2
Se
Se
Se
P1
P3
P4
R.T.
CpCr(CO)3H
(11)
Cp4Cr4(CO)9(P4Se3)
(12)
Cp4Cr4Se4
(19)
Cp4Cr4(CO)8(P2Se2)
(13)

Reaction of $[CpCr(CO)_2]_2Se$ with P_4S_3 at ambient temperature

A similar ^1H NMR spectral study of the reaction of $[CpCr(CO)_2]_2Se$ (**17**) with one molar equivalent of P_4S_3 is illustrated in Figure 47. As in the reaction with P_4Se_3 described above, **12** was the predominant product after 1 day, with a substantial amount of the hydride **11**. The reaction of **17** was complete after 3 days when **12** and **11** were estimated to constitute 44 and 31%, respectively, of the products. After an additional day, **12** was found to have degraded to **13** and **19**. It is noted that the quantity of hydride had persisted unchanged. Also it is noted that the proton resonance of $Cp_2Cr_2(CO)_4S$ (**10**) isolated in substantial yield (Section **2.4.4**) , cannot be differentiated from that of **17**. The above observation is represented in Scheme VI.

(c) **Variable temperature NMR measurement of $Cp_4Cr_4(CO)_8(P_2Se_2)$**

The thermolytic degradation of $Cp_4Cr_4(CO)_8(P_2Se_2)$ (**13**) in C_6D_6 at 50°C was followed via its ^1H NMR spectral changes as shown in Figure 48. The initial spectrum indicates the presence of isomers **A** (δ 4.69 and 4.14) and **B** (δ 4.52 and 4.45) in the ratio of 4 : 1. After 2 h, the amount of isomer **B** has been reduced to approximately 50% (*ie.* $t_{1/2} \approx 2$ h), resulting in an ratio of **A** : **B** ratio of 3 : 1. At the same time, the formation of $[CpCr(CO)_2]_2Se$ (**17**) (*ca.* 5%) and $Cp_4Cr_4Se_4$ (**19**) (*ca.* 5%) was also observed. By 6 h, the presence of isomer **B** was not detected and **A** has been reduced to approximately 50% (*ie.* $t_{1/2} \approx 6$ h) together with **17** (*ca.* 4%) and **19** (*ca.* 15%). After *ca.* 36 h, **13** has completely degraded to mainly **19** and a small amount of $[CpCr(CO)_2]P_2$ (**15**).

2.4.6 Thermolysis of $Cp_4Cr_4(CO)_9(P_4Se_3)$ and $Cp_4Cr_4(CO)_8(P_2Se_2)$

The thermolysis of a brown solution of $Cp_4Cr_4(CO)_9(P_4Se_3)$ (**12**) in toluene at 60°C for 4 h led to the isolation of $Cp_4Cr_4(CO)_8(P_2Se_2)$ (**13**), $CpCr(CO)_2P_3$ (**14**), $[CpCr(CO)_2]P_2$ (**15**) and $Cp_4Cr_4Se_4$ (**19**) in 51.9, 6.3, 28.2 and 12.1% yields, respectively. A similar thermolysis of a reddish brown solution of **13** at 80°C for 3 h gave **14** (4.3%), **15** (55.9%) and **19** (36.8%) as isolated complexes. The degradation

Figure 47. Time-dependent ^1H NMR spectra for an NMR tube reaction of a 2 mM solution of $Cp_2Cr_2(CO)_4Se$ (**17**) with one molar equivalent of P_4S_3 at ambient temperature under argon.

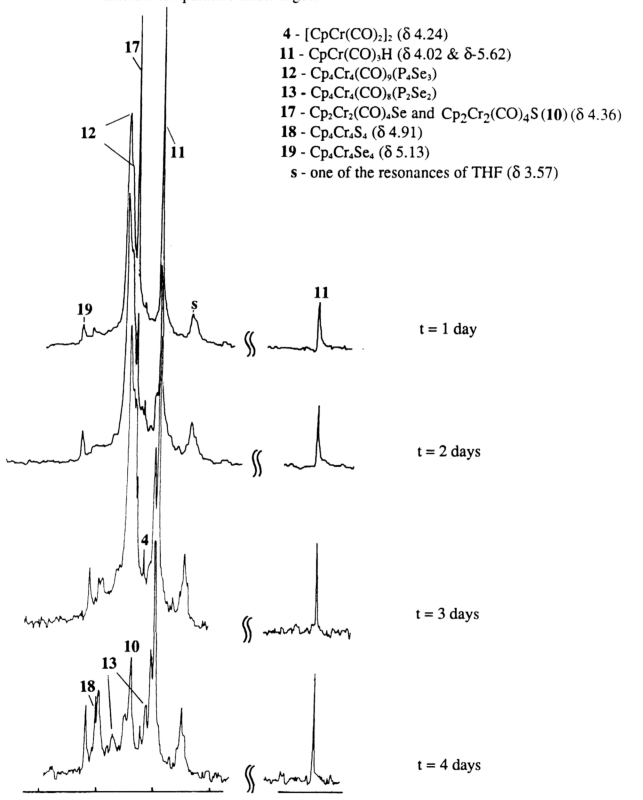

Scheme VI

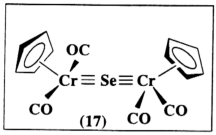

(17)

+

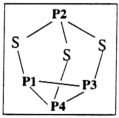

R.T.

$Cp_4Cr_4(CO)_9(P_4Se_3)$ (12) + P_7 ? ≡  + $Cp_2Cr_2(CO)_4S$ (10) + $CpCr(CO)_3H$ (11)

$Cp_4Cr_4(CO)_8(P_2Se_2)$ (13)

$Cp_4Cr_4S_4$ (18)

$Cp_4Cr_4Se_4$ (19)

Figure 48 The time-dependent ^1H NMR spectral changes of a 2 mM solution of $Cp_4Cr_4(CO)_8(P_2Se_2)$ C_6D_6 at 50°C.

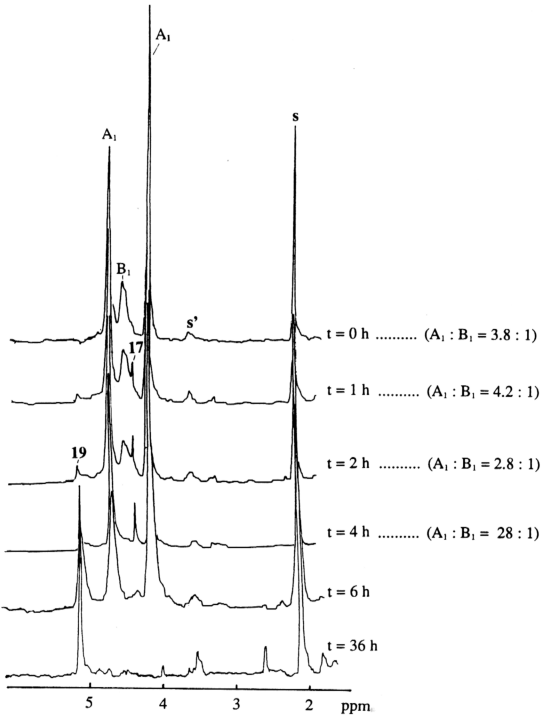

A_1 - isomer corresponding to δ 4.69 and 4.14.
B_1 - isomer corresponding to δ 4.52 and 4.45.
17 - $Cp_2Cr_2(CO)_4Se$ (δ 4.36)
19 - $Cp_4Cr_4Se_4$ (δ 5.13)
s'- one of the resonances of toluene (δ 2.11).
s - one of the resonances of THF (δ 3.57)

of **12** to **13** indicates that the former is the primary product in the reaction of **1** with P_4Se_3. Further degradation of **13** subsequently gave **14**, **15** and **19** as secondary products. These product compositions and yields are summarised in Table 26 and the above observations are represented in Schemes VII and VIII.

2.4.7 Mechanistic pathways for the formation of $Cp_4Cr_4(CO)_9(P_4Se_3)$ and $Cp_4Cr_4(CO)_8(P_2Se_2)$

The results presented in the preceding sections seem to indicate that the complex $Cp_4Cr_4(CO)_9(P_4Se_3)$ (**12**) is formed *via* two different pathways. The first route involves the same radical mechanism as proposed for the analogous $Cp_4Cr_4(CO)_9(P_4S_3)$ (**9**), as illustrated in Scheme IV. As in the formation of **9**, the P_4Se_3 cage underwent radical cleavage resulting in the same cage rearrangement and concomitant coordination of $CpCr(CO)_n$ (n = 2, 3) fragments.

The secondary products of $CpCr(CO)_2P_3$ (**14**) and $[CpCr(CO)_2]P_2$ (**15**) are common in both the reactions of **1** with P_4S_3 and P_4Se_3. Conspicuously absent was the Se analogue of $Cp_2Cr_2(CO)_4S$ in the ambient temperature reaction of P_4Se_3. The reason for this is obvious from the discussion below.

Indeed, the NMR spectral studies (Section **2.4.6 (a)** including Table 25) show that $Cp_2Cr_2(CO)_4Se$ (**17**) is an intermediate complex in the reaction of $[CpCr(CO)_3]_2$ (**1**) with P_4Se_3. Thus a relatively high concentration of **17** is formed in the early stages of the reaction at ambient temperature, followed by its subsequent decrease as the concentration of the main product **12** increases. Indeed, an independent experiment shows that **17** does react with P_4Se_3 (Figure 46) to give **12** which has been isolated. Figure 46 also shows that the hydride **11** is formed alongside **12**, while **13** and **19** are formed as secondary products. In fact, the initial formation of **17** in the reaction of **1** with P_4Se_3 is consistent with the faster rate of reaction of **17** with one mole equivalent P_4Se_3 (complete in *ca.* 4 days), compared to that of the reaction of **1** with P_4Se_3 (complete in *ca.* 6 days).

Table 26. Product composition from the reactions of $[CpCr(CO)_3]_2$ with P_4Se_3 at R.T and 60°C and thermolysis of $Cp_4Cr_4(CO)_9(P_4Se_3)$ (**12**) and $Cp_4Cr_4(CO)_8(P_2Se_2)$ (**13**).

Reactions \ Complexes	$CpCr(CO)_3H$ (**11**)	$Cp_4Cr_4(CO)_9(P_4Se_3)$ (**12**)	$Cp_4Cr_4(CO)_8(P_2Se_2)$ (**13**)	$CpCr(CO)_2P_3$ (**14**)	$[CpCr(CO)_2]_2P_2$ (**15**)	$[CpCr(CO)_2]_2Se$ (**17**)	$Cp_4Cr_4Se_4$ (**19**)
6 days / R.T.[b]	7	48.3	13.2	2.3	16.3	0	0
12 days / R.T.[b]	6.9	43.8	33.5	8.4	0	0	0
2 h/ 60°C[b]	2	36.6	15.9	8.2	8.7	21.7	3.5
Thermolysis of **12**	0	0	51.9	6.3	28.2	0	12.1
Thermolysis of **13**	0	0	0	3.3	55.9	0	36.8

[a] - % isolated yields.

[b] - Reaction of $[CpCr(CO)_3]_2$ with an equimolar equivalent of P_4Se_3.

Scheme VII

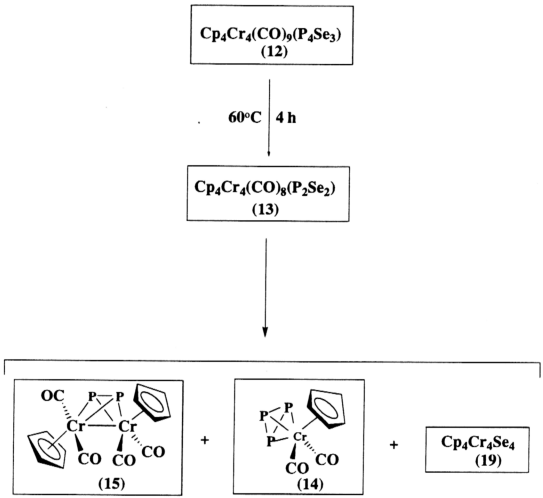
Cp4Cr4(CO)9(P4Se3)
(12)
60°C
4 h
Cp4Cr4(CO)8(P2Se2)
(13)
OC
P
P
Cr
Cr
CO
CO
CO
CO
(15)
+
P
P
P
Cr
CO
CO
(14)
+
Cp4Cr4Se4
(19)

Scheme VIII

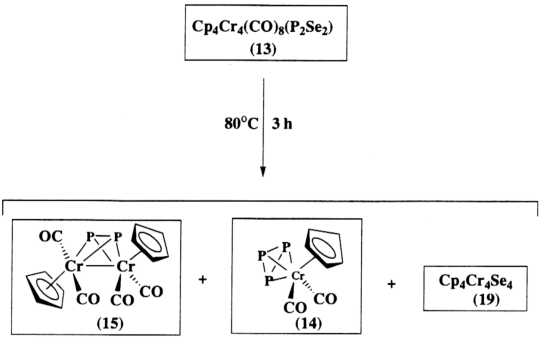
Cp4Cr4(CO)8(P2Se2)
(13)
80°C
3 h
OC
P
P
Cr
Cr
CO
CO
CO
(15)
+
P
P
P
Cr
CO
CO
(14)
+
Cp4Cr4Se4
(19)

As a follow-up to the reaction of $Cp_2Cr_2(CO)_4Se$ (**17**) with P_4Se_3, the reaction of **17** with P_4S_3 was investigated, both *via* NMR spectral studies (Figure 47) and for purposes of product isolation. Substantial yields of **12** and the hydride **11** were obtained. There was no evidence of any *mixed* S/Se analogue of **9** or **12**. The mechanism is difficult to ascertain. However, in view of the well-documented ability of **17** to insert Se[14b], S[101] and $Fe_2(CO)_9$[10] as shown in Equations (xxiii), (xxiv) and (xxv), it may be envisaged that **17** undergoes insertion reactions with the P_4Se_3 and P_4S_3 cage molecules, forming $Cp_2Cr_2(CO)_4Se_2$ and $Cp_2Cr_2(CO)_4SeS$ in the process.

. . . (xxiii)

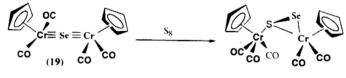

. . . (xxiv)

. . . (xxv)

Subsequent degradation of the latter would lead to the formation of $Cp_2Cr_2(CO)_4S$, one of the products from the reaction with P_4S_3. The formation of **12** must have involved a complex series of multiple bond cleavages and linkages in the intra- and intermolecular rearrangement of the P_4X_3 cages. The NMR spectral studies together with the isolation of products show that **13** is derived from the degradation of **12**. This is supported by the thermolysis of the latter at 60°C, which has resulted in

decarbonylation together with loss of P and Se atoms followed by rearrangement to yield **13**.

2.4.8 Physical properties

$Cp_4Cr_4(CO)_9(P_4Se_3)$ (12)

The complex exists as dark brown crystals stable for several days in air at ambient temperature. It is not soluble in *n*-hexane but soluble in most organic solvents to give a yellowish brown solution. The solution is slightly sensitive to air but fairly stable at -28°C under inert atmosphere for a few weeks.

$Cp_4Cr_4(CO)_8(P_2Se_2)$ (13)

The complex exists as dark brown crystals stable for several days in air at ambient temperature. It is not soluble in *n*-hexane but soluble in most organic solvents to give a reddish brown solution. The solution is slightly air-sensitive but fairly stable at room temperature under inert atmosphere for a few days.

2.4.9 Spectral characteristics

2.4.9.1 I.R. spectra

$Cp_4Cr_4(CO)_9(P_4Se_3)$ (12)

The I.R. spectrum in nujol shows ν_{CO} stretching frequencies at 2019 vs, 1971 vs, 1947 vs, 1923 vs, 1886 vs, 1848 s, ν(others) 1063 w, 1011w, 828 s, 728 w, 634 s, 580 s, 554 s, 525 w cm^{-1} (Figure 49).

$Cp_4Cr_4(CO)_8(P_2Se_2)$ (13)

The I.R spectrum in nujol shows ν_{CO} stretching frequencies at 1943 vs, 1889 s cm^{-1} (toluene) and 1967 s, sh, 1929 vs, 1892 vs, 1869 vs cm^{-1}(nujol) (Figure 50).

2.4.9.2 NMR spectra

$Cp_4Cr_4(CO)_9(P_4Se_3)$ (12)

The complex is diamagnetic showing δ(Cp) resonances at 4.78, 4.56, 4.47, 4.26 in the ^1H NMR spectrum in benzene-d_6, at 93.91, 92.42, 91.97, 91.32, 90.66,

Figure 49. CO stretching frequencies of $Cp_4Cr_4(CO)_9(P_4Se_3)$ (**12**) in nujol

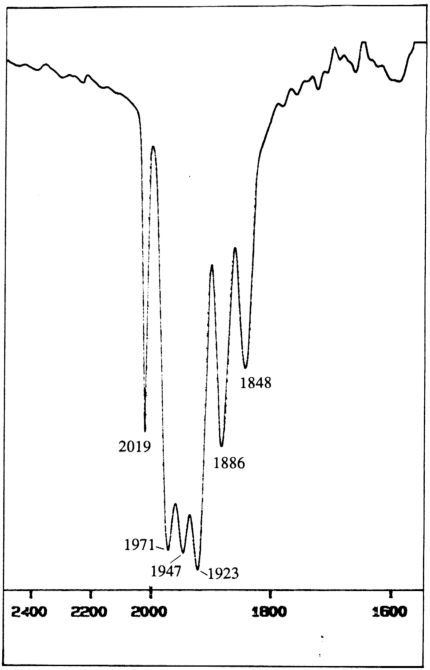

Figure 50. CO stretching frequencies of $Cp_4Cr_4(CO)_8(P_2Se_2)$ (**13**) in nujol

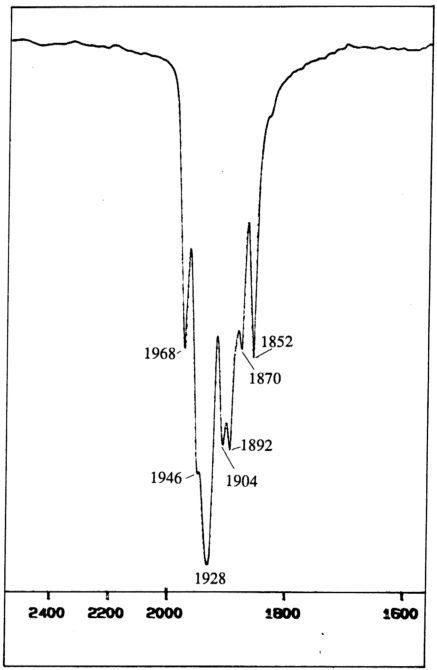

90.40 in the ^{13}C spectrum and δ 301.04, 91.23 with a relative intensity of 10:1 in the ^{31}P NMR spectrum in benzene-d_6.

$Cp_4Cr_4(CO)_8(P_2Se_2)$ (13)

The proton NMR spectra of various samples of **13** indicate the presence of 2 isomers A_1 (δ 4.69 and 4.14) and B_1 (δ 4.52 and 4.45). Thus different samples have been observed to consist of mixtures of A_1:B_1 the molar ratios of 5:1, 4:1, 1:1.6 and 1:1.7, respectively. The relative amount of isomer B_1 seems to increase with further recrystallisations. A sample containing a 5:1 with molar mixture of A_1:B_1 as indicated by its ^1H NMR shows δ 333.24, 351.17, with a relative intensity of 5:1 in ^{31}P NMR and at δ(Cp) 93.10 and 89.91 (weak peak) in the ^{13}C NMR spectra in benzene-d_6. A temperature-dependent ^1H NMR spectral study of a sample of **13** which consists of a 3:5 molar mixture of A_1:B_1 is illustrated in Figure 51. The spectra at 28°C and 50°C remain basically unchanged. At 70°C, decomposition began to set in, giving $Cp_2Cr_2(CO)_4P_2$ (**15**) and $Cp_4Cr_4Se_4$ (**18**) and was very pronounced when the sample was scanned at 90°C, as seen by the intensity of the two relevant resonances at δ 4.28 and δ 5.52, respectively. At 70°C, the resonances of B_1 (δ 4.54 and 4.47) reverse in relative intensity when compared to those at 28°C and 50°C, and finally was a singlet (δ 4.51) at 90°C. At the same time, B_1 becomes the less dominant component of the mixture with A_1:B_1 equal to 1: 0.9 at 70°C and 1: 0.4 at 90°C. This same relative intensity of A_1:B_1 was obtained upon a reversal of temperature to 28°C. Further it was observed that after *ca.* 18 h at ambient temperature, isomer B_1 had totally disappeared though *ca.* 30% of the initial concentration of isomer A_1 still persisted. The presence of $Cp_2Cr_2(CO)_4Se$, was also detected as a minor decomposition product. Thus the changes observed in this study most likely arise from the easier and faster decomposition of isomer B_1.

In the present circumstances in which it has not been found feasible to separate these isomers, it is not possible to ascertain which of these isomers conform to the

Figure 51. Temperature-dependent ^1H NMR spectra of a 2mM solution of $Cp_4Cr_4(CO)_8(P_2Se_2)$ in d_8-toluene.

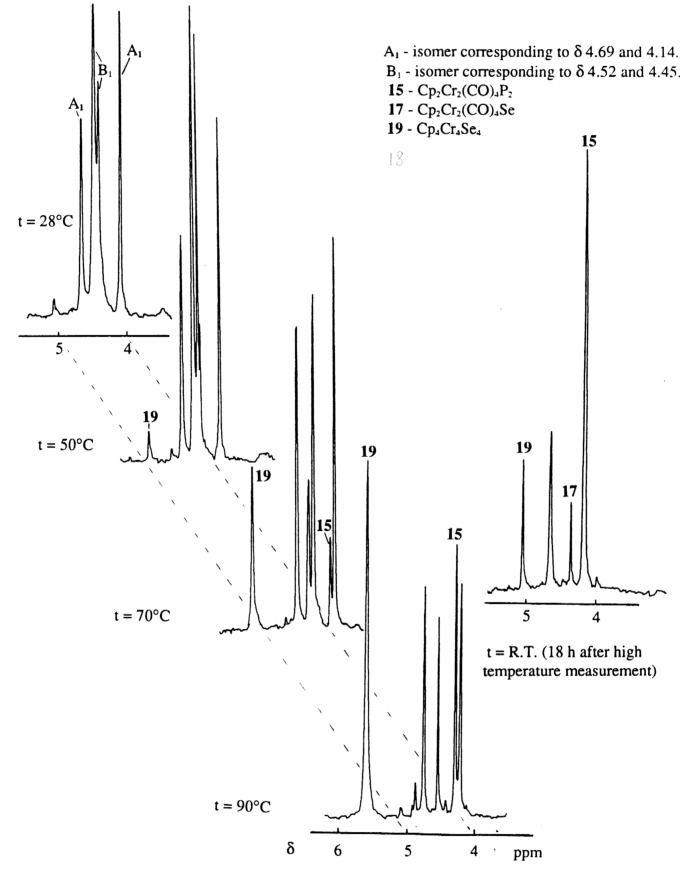

molecular structure described below, though it is likely to be isomer B_1, the sligthly more predominantly species in recrystallised batches.

2.4.9.3 Mass spectra

$Cp_4Cr_4(CO)_9(P_4Se_3)$ (12)

The electron impact mass spectrum of **12** is given in Table 27.

$Cp_4Cr_4(CO)_8(P_2Se_2)$ (13)

The electron impact mass spectrum of **13** is given in Table 28.

2.4.10 Molecular structures

$Cp_4Cr_4(CO)_9(P_4Se_3)$ (12)

The molecular structures of $Cp_4Cr_4(CO)_9P_4Se_3$ (**12**) shown in Figure 52 and the packing diagram in Figure 53. Bond lengths and bond angles are given in Table 29 and 30. The molecular structure of **12** and its S analogue are similar. The only difference in bond distances corresponds to the difference in the covalent radii of Se and S (0.14 Å). The P-Se bonds fall in the range observed for P_4Se_3 except for an obvious shortening in the Se-Cr bond (2.565 Å vs 2.63 Å). The Se atoms are 2-coordinate in this complex, but 3-coordinate in complex **13** described below.

$Cp_4Cr_4(CO)_8(P_2Se_2)$ (13)

The compound crystallised in the chiral space group $C222_1$; its absolute molecular structure is shown in Figure 54 and the packing diagram in Figure 55. The molecule possessses two-fold symmetry with the symmetry axis passing through the mid-point of the P-P bond. This bond forms the backbone of an unusual "open-book" framework and joins two CrP_2Se trapezoidal planes separated by a dihedral angle of 119.4°. The PSe edges of the trapezoids are each η^2-bonded to a $CpCr(CO)_2$ fragment. Thus each of the Cr atoms assumes a four-legged piano stool configuration. Each of the P atoms is four-coordinate while the Se atoms are each three-coordinate. The approximately Z-shaped conformation of the Se-P-P-Se aggregate and its manner

Table 27. Electron impact mass spectrum of $Cp_4Cr_4(CO)_9P_4Se_3$ (**12**)

m/e	Assignments
626	$[Cp_4Cr_4Se_2]$
597	$[Cp_2Cr_2(CO)_4P_3Se_2]$
573	$[Cp_3Cr_3(CO)_4PSe]$
508	$[Cp_2Cr_3(CO)_4PSe]$
456	$[Cp_2Cr_2(CO)_4PSe]$
425	$[Cp_2Cr_2(CO)_4Se]$
408	$[Cp_2Cr_2(CO)_4P_2]$
389	$[Cp_2Cr_2P_5]$
380	$[Cp_2Cr_2(CO)_3P_2]$
352	$[Cp_2Cr_2(CO)_2P_2]$
324	$[Cp_2Cr_2(CO)P_2]$
296	$[Cp_2Cr_2P_2]$
266	$[CpCr(CO)_2P_3]$
238	$[CpCr(CO)P_3]$
210	$[CpCrP_3]$
182	$[Cp_2Cr]$
117	$[CpCr]$

Table 28. Electron impact mass spectrum of $Cp_4Cr_4(CO)_8(P_2Se_2)$ (**13**)

m/e	Assignments
626	$[Cp_4Cr_4Se_2]$
597	$[Cp_2Cr_2(CO)_4P_3Se_2]$
573	$[Cp_3Cr_3(CO)_4PSe]$
540	$[Cp_2Cr_2(CO)_7PSe]$
521	$[Cp_3Cr_2(CO)_4PSe]$
508	$[Cp_2Cr_3(CO)_4PSe]$
493	$[Cp_3Cr_2(CO)_3PSe]$
480	$[Cp_2Cr_3(CO)_3PSe]$
456	$[Cp_2Cr_2(CO)_4PSe]$
425	$[Cp_2Cr_2(CO)_4Se]$
408	$[Cp_2Cr_2(CO)_4P_2]$
389	$[Cp_2Cr_2P_5]$
380	$[Cp_2Cr_2(CO)_3P_2]$
352	$[Cp_2Cr_2(CO)_2P_2]$
324	$[Cp_2Cr_2(CO)P_2]$
296	$[Cp_2Cr_2P_2]$
266	$[CpCr(CO)_2P_3]$
238	$[CpCr(CO)P_3]$
210	$[CpCrP_3]$
182	$[Cp_2Cr]$
117	$[CpCr]$

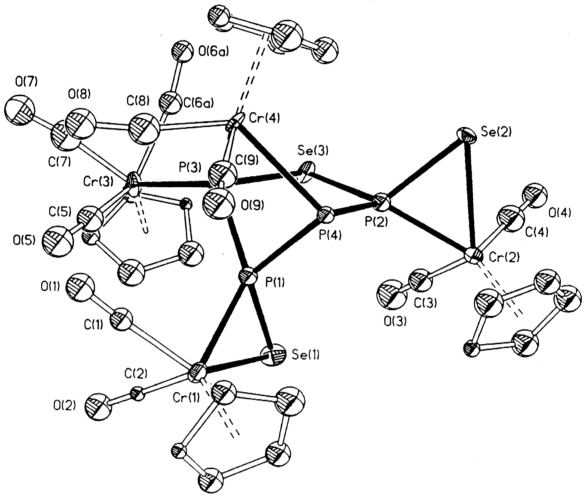

Figure 52. Molecular Structure of $[Cp_4Cr_4(CO)_9](P_4Se_3)$ (**12**)

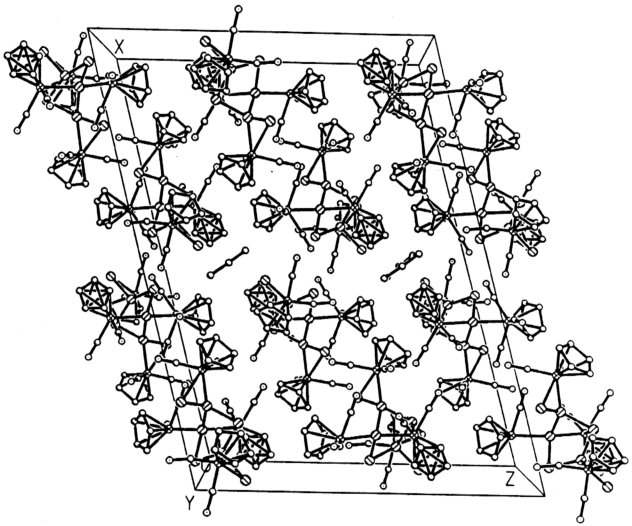

Figure 53. Molecular packing of $[Cp_4Cr_4(CO)_8](P_4Se_3)$ (**12**) in the unit cell

Table 29. Bond Lengths (Å) for $[Cp_4Cr_4(CO)_9](P_4Se_3)$ (**12**)

Se1	Cr1	2.630(9)
Se1	P1	2.16(1)
Se2	Cr2	2.630(9)
Se2	P2	2.18(1)
Se3	P2	2.26(1)
Se3	P3	2.32(1)
Cr1	P1	2.31(1)
Cr1	C1	1.89(6)
Cr1	C2	1.82(5)
Cr1	C11	2.09(4)
Cr1	C12	2.27(5)
Cr1	C13	2.19(4)
Cr1	C14	2.15(5)
Cr1	C15	2.10(4)
Cr2	P2	2.28(2)
Cr2	C3	1.78(6)
Cr2	C4	1.82(6)
Cr2	C21	2.16(5)
Cr2	C22	2.19(5)
Cr2	C23	2.25(5)
Cr2	C24	2.16(6)
Cr2	C25	2.10(5)
Cr3	P3	2.51(2)
Cr3	C5	1.81(6)
Cr3	C6	1.87(6)
Cr3	C7	1.78(7)
Cr3	C31	2.23(5)
Cr3	C32	2.19(5)
Cr3	C33	2.20(5)
Cr3	C34	2.16(4)
Cr3	C35	2.19(5)
Cr4	P3	2.41(2)
Cr4	P4	2.50(2)
Cr4	C8	1.93(5)
Cr4	C9	1.84(7)
Cr4	C41	2.15(5)
Cr4	C42	2.17(5)
Cr4	C43	2.12(5)
Cr4	C44	2.22(5)
Cr4	C45	2.18(5)
P1	P3	2.20(2)
P1	P4	2.17(2)
P2	P4	2.20(2)
O1	C1	1.09(6)
O2	C2	1.18(5)
O3	C3	1.18(6)
O4	C4	1.16(6)
O5	C5	1.15(6)

(continued)

O6	C6	1.14(6)
O7	C7	1.17(6)
O8	C8	1.11(5)
O9	C9	1.19(6)
C11	C12	1.41(6)
C12	C13	1.42(5)
C13	C14	1.32(6)
C14	C15	1.41(5)
C11	C15	1.33(5)
C21	C22	1.40(6)
C21	C25	1.40(6)
C22	C23	1.44(6)
C23	C24	1.23(7)
C24	C25	1.30(6)
C31	C32	1.37(6)
C33	C34	1.40(5)
C34	C35	1.50(6)
C31	C35	1.36(6)
C32	C33	1.42(6)
C41	C42	1.37(5)
C42	C43	1.51(5)
C43	C44	1.34(6)
C44	C45	1.33(6)
C45	C41	1.36(6)
C101	C102	1.40(6)
C102	C103	1.42(6)
C103	C104	1.48(7)

Table 30. Bond Angles for (°) $Cp_4Cr_4(CO)_9(P_4Se_3)$ (**12**)

Cr1	Se1	P1	56.5(4)
Cr2	Se2	P2	55.7(4)
P2	Se3	P3	93.7(5)
Se1	Cr1	P1	51.4(4)
Se1	Cr1	C1	133.(2)
Se1	Cr1	C2	84.(2)
P1	Cr1	C1	91.(2)
P1	Cr1	C2	105.(2)
C1	Cr1	C2	81.(2)
Se2	Cr2	P2	52.2(4)
Se2	Cr2	C3	118.(2)
Se2	Cr2	C4	82.(2)
P2	Cr2	C3	82.(2)
P2	Cr2	C4	112.(2)
C3	Cr2	C4	80.(2)
P3	Cr3	C5	74.(2)
P3	Cr3	C6	71.(2)
P3	Cr3	C7	127.(2)
C5	Cr3	C6	118.(2)
C5	Cr3	C7	82.(3)
C6	Cr3	C7	80.(3)
P3	Cr4	P4	74.3(5)
P3	Cr4	C8	113.(2)
P3	Cr4	C9	80.(2)
P4	Cr4	C8	71.(2)
P4	Cr4	C9	128.(2)
C8	Cr4	C9	79.(2)
Se1	P1	Cr1	72.1(5)
Se1	P1	P3	118.3(6)
Se1	P1	P4	124.6(7)
Cr1	P1	P3	137.9(8)
Cr1	P1	P4	123.9(7)
P3	P1	P4	85.5(7)
Se2	P2	Cr2	72.1(5)
Se2	P2	P4	112.1(6)
Se3	P2	Cr2	123.3(6)
Se3	P2	P4	104.2(7)
Cr2	P2	P4	125.8(7)
Se2	P2	Se3	115.0(6)
Se3	P3	Cr3	100.3(5)
Se3	P3	Cr4	108.7(6)
Se3	P3	P1	98.8(6)
Cr3	P3	Cr4	132.9(6)
Cr3	P3	P1	122.4(7)
Cr4	P3	P1	89.4(6)

(continued)

Cr4	P4	P1	87.8(6)
Cr4	P4	P2	108.2(7)
P1	P4	P2	93.3(7)
Cr1	C1	O1	174.(5)
Cr1	C2	O2	173.(4)
Cr2	C3	O3	173.(5)
Cr2	C4	O4	170.(5)
Cr3	C5	O5	167.(5)
Cr3	C6	O6	170.(5)
Cr3	C7	O7	176.(6)
Cr4	C8	O8	171.(5)
Cr4	C9	O9	169.(5)
C12	C11	C15	113.(5)
C11	C12	C13	99.(5)
C12	C13	C14	115.(5)
C13	C14	C15	104.(5)
C11	C15	C14	108.(4)
C22	C21	C25	102.(5)
C21	C22	C23	107.(5)
C22	C23	C24	108.(6)
C23	C24	C25	112.(7)
C24	C25	C21	111.(6)
C31	C32	C33	110.(5)
C32	C33	C34	105.(5)
C33	C34	C35	110.(5)
C31	C35	C34	103.(5)
C45	C41	C42	118.(5)
C41	C42	C43	97.(5)
C42	C43	C44	109.(5)
C43	C44	C45	112.(5)
C44	C45	C41	104.(5)
C101	C102	C103	120.(6)
C102	C103	C104	125.(7)
C102	C101	C102'	119.(7)
C103	C104	C103'	110.(7)

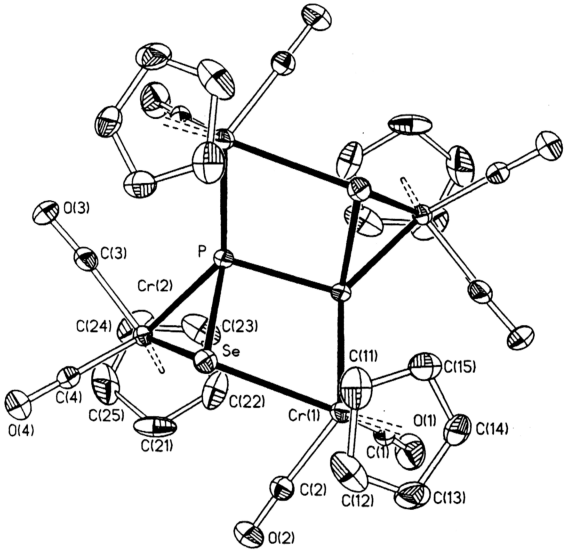

Figure 54. Molecular Structure of $[Cp_4Cr_4(CO)_8](P_2Se_2)$ (**13**)

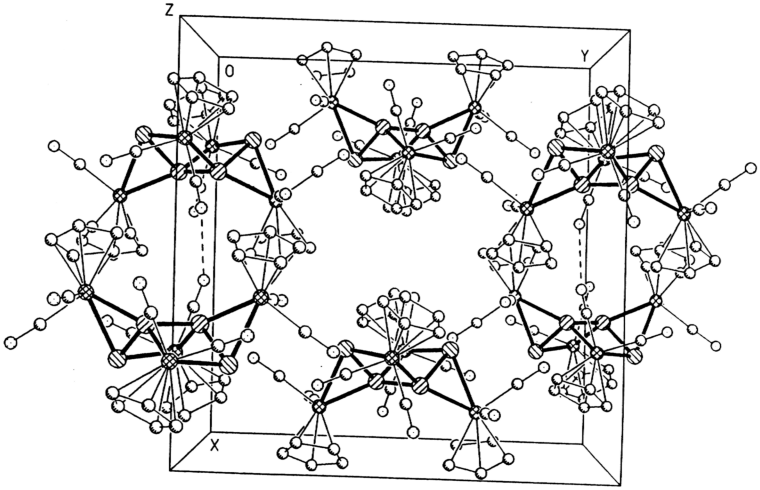

Figure 55. Molecular packing of $[Cp_4Cr_4(CO)_8](P_2Se_2)$ (**13**) in the unit cell

of bonding to the CpCr fragments is an unusual feature not observed before in complexes arising from reactions of transition-metal compounds with the P_4X_3 (X = S, Se) molecules.

Bond lengths and bond angles are given in Table 31. The P-P bond distance of 2.237(5) Å is very close to those in the P_4Se_3 cage (mean 2.25 Å).[102] Known values of P-P bond lengths average 2.22 Å in the P_{10} core of $[CpCr(CO)_2]_5P_{10}$[16] and 2.21 Å in P_4 vapour.[74] The P-Se distance of 2.250(3) Å is very close to that in the intact P_4Se_3 cage (mean 2.24 Å). The Cr-P distances (2.340(3) and 2.393(3) Å) fall within the range of 2.341-2.494 Å observed for other CpCr complexes with phosphorus ligands.[15a, 16] The Cr-Se distances (2.566(2) Å and 2.575(2) Å) are longer than those observed in the (μ, η-Se_2) complex $Cp_2Cr_2(CO)_4Se_2$ (2.538- 2.551 Å)[14] or in the cubanes $Cp_4Cr_4Se_2(CO)_2$ (2.317- 2.400 Å) and $Cp_4Cr_4Se_2O_2$ (2.441- 2.462 Å).[103]

Table 31. Bond Lengths (Å) and Angles (°) for $Cp_4Cr_4(CO)_8(P_2Se_2)$ (**13**).

Se-P	2.250(2)
Se-Cr(2)	2.565(1)
Se-Cr(1)	2.565(1)
Cr(1)-C(1)	1.823(8)
Cr(1)-C(2)	1.854(7)
Cr(1)-CP12	2.151(8)
Cr(1)-CP13	2.172(8)
Cr(1)-CP14	2.194(7)
Cr(1)-CP15	2.209(7)
Cr(1)-CP11	2.222(8)
Cr(1)-P#1	2.386(2)
Cr(2)-C(3)	1.824(8)
Cr(2)-C(4)	1.843(8)
Cr(2)-CP25	2.154(8)
Cr(2)-CP21	2.167(8)
Cr(2)-CP24	2.174(9)
Cr(2)-CP22	2.190(8)
Cr(2)-CP23	2.203(8)
Cr(2)-P	2.346(2)
P-P#1	2.233(3)
P-Cr(1)#1	2.386(2)
O(1)-C(1)	1.146(9)
O(2)-C(2)	1.139(8)
O(3)-C(3)	1.154(8)
O(4)-C(4)	1.142(8)
CP11-CP15	1.39(1)
CP11-CP12	1.42(1)
CP12-CP13	1.38(1)
CP13-CP14	1.38(1)
CP14-CP15	1.36(1)
CP21-CP22	1.37(1)
CP21-CP25	1.39(1)
CP22-CP23	1.36(1)
CP23-CP24	1.34(1)
CP24-CP25	1.35(1)
P-Se-Cr(2)	57.88(5)
P-Se-Cr(1)	97.98(5)
Cr(2)-Se-Cr(1)	117.09(4)
C(1)-Cr(1)-C(2)	78.0(3)
C(1)-Cr(1)-CP12	130.7(4)
C(2)-Cr(1)-CP12	90.0(3)
C(1)-Cr(1)-CP13	94.8(4)
C(2)-Cr(1)-CP13	91.1(3)
CP12-Cr(1)-CP13	37.2(4)
C(1)-Cr(1)-CP14	86.2(4)
C(2)-Cr(1)-CP14	124.1(3)
CP12-Cr(1)-CP14	61.5(4)
CP13-Cr(1)-CP14	37.0(3)
C(1)-Cr(1)-CP15	113.3(3)
C(2)-Cr(1)-CP15	149.9(3)

(continued)

CP12-Cr(1)-CP15	61.1(3)
CP13-Cr(1)-CP15	61.1(3)
CP14-Cr(1)-CP15	36.1(3)
C(1)-Cr(1)-CP11	147.6(3)
C(2)-Cr(1)-CP11	122.4(3)
CP12-Cr(1)-CP11	37.8(4)
CP13-Cr(1)-CP11	62.6(4)
CP14-Cr(1)-CP11	61.6(3)
CP15-Cr(1)-CP11	36.5(3)
C(1)-Cr(1)-P#1	82.3(2)
C(2)-Cr(1)-P#1	123.8(2)
CP12-Cr(1)-P#1	139.4(3)
CP13-Cr(1)-P#1	143.0(3)
CP14-Cr(1)-P#1	106.1(2)
CP15-Cr(1)-P#1	86.1(2)
CP11-Cr(1)-P#1	101.6(3)
C(1)-Cr(1)-Se	126.1(2)
C(2)-Cr(1)-Se	76.5(2)
CP12-Cr(1)-Se	96.0(3)
CP13-Cr(1)-Se	132.1(3)
CP14-Cr(1)-Se	146.6(3)
CP15-Cr(1)-Se	112.6(2)
CP11-Cr(1)-Se	85.4(2)
P#1-Cr(1)-Se	74.03(5)
C(3)-Cr(2)-C(4)	82.6(3)
C(3)-Cr(2)-CP25	101.1(4)
C(4)-Cr(2)-CP25	89.0(4)
C(3)-Cr(2)-CP21	138.6(4)
C(4)-Cr(2)-CP21	91.6(3)
CP25-Cr(2)-CP21	37.6(4)
C(3)-Cr(2)-CP24	86.6(4)
C(4)-Cr(2)-CP24	120.1(4)
CP25-Cr(2)-CP24	36.3(4)
CP21-Cr(2)-CP24	61.2(4)
C(3)-Cr(2)-CP22	143.5(4)
C(4)-Cr(2)-CP22	125.3(4)
CP25-Cr(2)-CP22	61.2(4)
CP21-Cr(2)-CP22	36.7(3)
CP24-Cr(2)-CP22	60.0(3)
C(3)-Cr(2)-CP23	107.8(4)
C(4)-Cr(2)-CP23	148.8(3)
CP25-Cr(2)-CP23	60.4(4)
CP21-Cr(2)-CP23	60.9(3)
CP24-Cr(2)-CP23	35.5(4)
CP22-Cr(2)-CP23	36.0(4)
C(3)-Cr(2)-P	81.8(2)
C(4)-Cr(2)-P	118.3(2)
CP25-Cr(2)-P	152.6(3)
CP21-Cr(2)-P	134.8(3)
CP24-Cr(2)-P	118.1(4)
CP22-Cr(2)-P	100.4(3)
CP23-Cr(2)-P	92.6(3)
C(3)-Cr(2)-Se	110.9(3)
C(4)-Cr(2)-Se	77.3(2)
CP25-Cr(2)-Se	142.9(4)

(continued)

CP21-Cr(2)-Se	107.6(3)
CP24-Cr(2)-Se	157.7(3)
CP22-Cr(2)-Se	99.1(2)
CP23-Cr(2)-Se	122.7(3)
P-Cr(2)-Se	54.31(5)
P#1-P-Se	83.48(8)
P#1-P-Cr(2)	117.13(10)
Se-P-Cr(2)	67.81(5)
P#1-P-Cr(1)#1	103.93(9)
Se-P-Cr(1)#1	119.56(7)
Cr(2)-P-Cr(1)#1	138.94(8)
O(1)-C(1)-Cr(1)	173.6(7)
O(2)-C(2)-Cr(1)	177.4(6)
O(3)-C(3)-Cr(2)	175.5(6)
O(4)-C(4)-Cr(2)	177.1(7)
CP15-CP11-CP12	104.5(8)
CP15-CP11-Cr(1)	71.3(4)
CP12-CP11-Cr(1)	68.4(5)
CP13-CP12-CP11	109.6(8)
CP13-CP12-Cr(1)	72.3(5)
CP11-CP12-Cr(1)	73.8(5)
CP12-CP13-CP14	107.2(8)
CP12-CP13-Cr(1)	70.6(5)
CP14-CP13-Cr(1)	72.4(4)
CP15-CP14-CP13	108.2(9)
CP15-CP14-Cr(1)	72.6(5)
CP13-CP14-Cr(1)	70.6(5)
CP14-CP15-CP11	110.5(8)
CP14-CP15-Cr(1)	71.3(5)
CP11-CP15-Cr(1)	72.3(4)
CP22-CP21-CP25	106.2(9)
CP22-CP21-Cr(2)	72.6(5)
CP25-CP21-Cr(2)	70.7(5)
CP23-CP22-CP21	108.5(9)
CP23-CP22-Cr(2)	72.5(5)
CP21-CP22-Cr(2)	70.7(5)
CP24-CP23-CP22	108.2(9)
CP24-CP23-Cr(2)	71.0(6)
CP22-CP23-Cr(2)	71.5(5)
CP25-CP24-CP23	109.6(9)
CP25-CP24-Cr(2)	71.1(5)
CP23-CP24-Cr(2)	73.4(5)
CP24-CP25-CP21	107.4(8)
CP24-CP25-Cr(2)	72.7(5)
CP21-CP25-Cr(2)	71.7(5)

Symmetry transformations used to generate equivalent atoms:
#1 x,-y,-z

2.5 Studies with Realgar

2.5.1 The reaction of $[CpCr(CO)_3]_2$ with Realgar, As_4S_4

The reaction of an orange green suspension of $[CpCr(CO)_3]_2$ (**1**) with excess As_4S_4 in toluene under ultrasonication at ambient temperature was *ca.* 80% complete after 25 h, leading to the isolation of $[CpCr(CO)_2]_2As_2S_2$ (**20**) and $[CpCr(CO)_2]_2S$ (**10**) in 20.5 and 36.5% yields, respectively, and precipitated solids consisting of a mixture of the $[CpCr(CO)_2]_2As_2$ (**2**) (1%), $[CpCr(CO)_2]_2$ (**4**) (3.8%), (**10**) (3.5%), $Cp_4Cr_4S_4$ (**18**) (6.7%) and a trace amount of species with δ(Cp) 5.13 in the ^1H NMR spectrum.

A similar reaction at 60°C for 8 h led to the isolation of $[CpCr(CO)_2]_2As_2S_2$ (**20**) and $[CpCr(CO)_2]_2S$ (**10**) in 12.6 and 18.6% yields, respectively, and precipitated solids consisting of a mixture of $[CpCr(CO)_2]_2As_2$ (**2**) (5.7%), $CpCr(CO)_2As_3$ (**3**) (1.8%), $[CpCr(CO)_2]_2$ (**4**) (16.3%), (**10**) (7.4%), $Cp_4Cr_4S_4$ (**18**) (22.9%) and (**20**) (2.5%) and a trace amount of species with δ(Cp) 5.13.

From these observations, it can be deduced that **20** is the primary product of the reaction of **1** with As_4S_4. This is substantiated by thermolysis studies which showed degradation of $[CpCr(CO)_2]_2As_2S_2$ (**20**) at 50°C for 7 h to **3** (14.1%), **10** (59.3%) and **18** (18.8%) together with a small amount of the species with δ(Cp) 5.13. It would be desirable to obtain the structure of **20** but unfortunately all attempts to grow a single crystal of **20** have failed so far, owing to its poor solubility as well as low stability in solution.

2.5.2 The reaction of $[CpCr(CO)_2]_2$ with Realgar, As_4S_4

The reaction of $[CpCr(CO)_2]_2$ (**4**) with excess As_4S_4 in toluene at 60°C for 7 h gave $CpCr(CO)_2As_3$ (**3**), $[CpCr(CO)_2]_2S$ (**10**) and $Cp_4Cr_4S_4$ (**18**) in 15.2, 13.7 and 38.3% yields, respectively, together with a small amount of an unidentified species possessing δ(Cp) 5.13. The above products are similar to those isolated in the thermolysis of $[CpCr(CO)_2]_2As_2S_2$ (**20**). This indicates that there may be two possible

pathways to these products *viz.* direct fragmentation of the As_4S_4 cage by the Cr≡Cr bonded complex **4** or derived from the initial formation of **20** followed by its thermal degradation. However, **20** was not observed during the reaction, suggesting that **20** is an unlikely primary product in this reaction. By comparison, the reaction of the Mo≡Mo complex $[(C_5Me_5)Mo(CO)_2]_2$ with As_4S_4 for 17 h at 100°C yielded $[(C_5Me_5)Mo]_2As_2S_3$ (the structure of which is shown in Section 1.3), in addition to the Mo analogues of $[CpCr(CO)_2]_2As_2$ (**2**) and $CpCr(CO)_2As_3$ (**3**).[20]

2.5.3 Mechanistic pathways : Formation of $[CpCr(CO)_2]_2As_2S_2$

The reaction of $[CpCr(CO)_3]_2$ (**1**) with As_4S_4 under heterogeneous conditions has proceeded in a facile manner, in contrast to that of the analogous Mo complex which required more drastic conditions (17 h in refluxing toluene). The ease of reaction is most probably due to the same radical mechanism as discussed in the earlier sections. Here, the radical attack of $CpCr(CO)_3$· on the As_4S_4 cage would generate the complex $[CpCr(CO)_2]_2As_2S_2$ (**20**).

In the much less facile reaction of $[CpCr(CO)_2]_2$ (**4**) with As_4S_4, which required 7 h at 60°C, only $CpCr(CO)_2As_3$ (**3**), $[CpCr(CO)_2]_2S$ (**10**) and $Cp_4Cr_4S_4$ (**18**) in predominantly amounts, were isolated. However, this does not preclude the formation of **20** as a primary product. Independent thermolysis studies of **20** showed that under the conditions of the reaction, any of **20** formed would have degraded to **3**, **10** and **18**.

2.5.4 Physical properties

$[CpCr(CO)_2]_2As_2S_2$

The complex exists as fine reddish orange solids which are not very stable except under inert atmosphere. It is not soluble in *n*-hexane but partially soluble in toluene and THF to give an orange solution. The solution is very air-sensitive but fairly stable under inert atmosphere at -28°C for a few days. At room temperature

under inert atmosphere an orange solution of the complex slowly decomposed to yield a brownish green solution of $[CpCr(CO)_2]S$ (**10**).

2.5.5 Spectral characteristics

2.5.5.1 I.R. spectrum

$[CpCr(CO)_2]_2As_2S_2$ (20)

The I.R. spectrum shows ν_{CO} at 1997 vs; 1938 vs, sh; 1917 vs; 1903 vs, sh cm^{-1} (nujol) (Figure 56).

2.5.5.2 NMR spectra

$[CpCr(CO)_2]_2As_2S_2$ (20)

The complex is diamagnetic showing δ(Cp) resonances at 4.26 in the ^1H NMR spectrum and at 96.53 in the ^{13}C spectrum in benzene-d_6.

2.5.5.3 Mass spectrum

$[CpCr(CO)_2]_2As_2S_2$ (20)

The E.I mass spectrum is given in Table 32.

Figure 56. CO stretching frequencies of $[CpCr(CO)_2]_2As_2S_2$ (**20**) in nujol

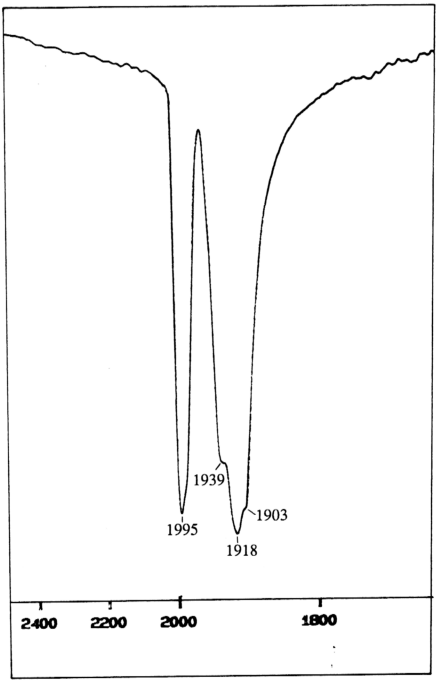

Table 32. Electron impact mass spectrum of $[CpCr(CO)_2]_2As_2S_2$ (**20**)

m/e	Assignments
596	$[Cp_4Cr_4S_4]$
531	$[Cp_3Cr_4S_4]$
466	$[Cp_2Cr_4S_4]$
428	$[Cp_2CrAs_2S_3]$
396	$[Cp_2CrAs_2S_2]$
321	$[Cp_2CrAsS_2]$
289	$[Cp_2CrAsS]$
257	$[Cp_2CrAs]$
201	$[CpCr(CO)_3]$
150	$[As_2]$
117	[CpCr]
75	[As]
52	[Cr]

2.6 Conclusion

The reaction pathways involved in the reaction of $[CpCr(CO)_3]_2$ **(1)** with P_4S_3 and P_4Se_3 are illustrated in Scheme (III) and (IV), respectively. Both reactions proceed *via* a radical route to give $Cp_4Cr_4(CO)_9(P_4X_3)$ [**(9)** : X = S; **(12)** : X = Se] as a primary product. The reaction with P_4Se_3 also proceeds *via* the initial formation of $Cp_2Cr_2(CO)_4Se$ **(17)** which subsequently undergoes insertion reactions with P_4Se_3 or P_4S_3 to give $Cp_4Cr_4(CO)_9(P_4Se_3)$ **(12)**. Thermolysis of **9** led to $CpCr(CO)_2P_3$ **(14)**, $Cp_2Cr_2(CO)_4P_2$ **(15)** and $Cp_2Cr_2(CO)_4S$ **(10)** which further degrades to $Cp_4Cr_4S_4$ **(18)** as the final product. The Se analogue, **12** is first transformed to $Cp_4Cr_4(CO)_8(P_2Se_2)$ **(13)**, before further degradation to yield $CpCr(CO)_2P_3$ **(14)** and $Cp_2Cr_2(CO)_4P_2$ **(15)** and $Cp_4Cr_4Se_4$ **(19)**.

In these reactions, P_4X_3 (X = S, Se) have undergone both non-disruptive and disruptive processes to yield complexes **9** and **12** containing opened-up rearranged aggregates. Previous reported reactions of transition metal complexes with P_4X_3 have led to fragmentation of P_4X_3 giving products with X, P_2X_2, P_2 and P_3 ligands. The observations from the reactions of $[CpCr(CO)_3]_2$ are unprecedented and may be attributed to the unusual reactivity of the radical-like $[CpCr(CO)_n]$ (n = 2 or 3) fragments, as was observed in the formation of the polycyclophosphido-chromium cluster $[CpCr(CO)_2]_5P_{10}$ from elemental P_4.[16]

The reaction pathways involved in the reaction of $[CpCr(CO)_3]_2$ **(1)** with As_4S_4 are presented schematically as in Scheme IX, showing a radical route to give $[CpCr(CO)_2]_2As_2S_2$ **(20)** as a primary product. Thermolysis of **20** led to $CpCr(CO)_2As_3$ **(3)**, $Cp_2Cr_2(CO)_4S$ **(10)** and $Cp_4Cr_4S_4$ **(18)**. In this reaction, As_4S_4 has undergone an extensive fragmentation process which is reminiscent of those observed in its reactions with $[Cp^*M(CO)_2]_2$ (M = Fe, Co, or Mo) systems,[20, 59] as discussed in Section **1.1.3** and **1.3**.

As a concluding remark, it may be noted that the scope of the work can be expanded to include reactions with other polynuclear molecules of the non-metals, as well as other radical-like organometallic complexes.

Scheme IX

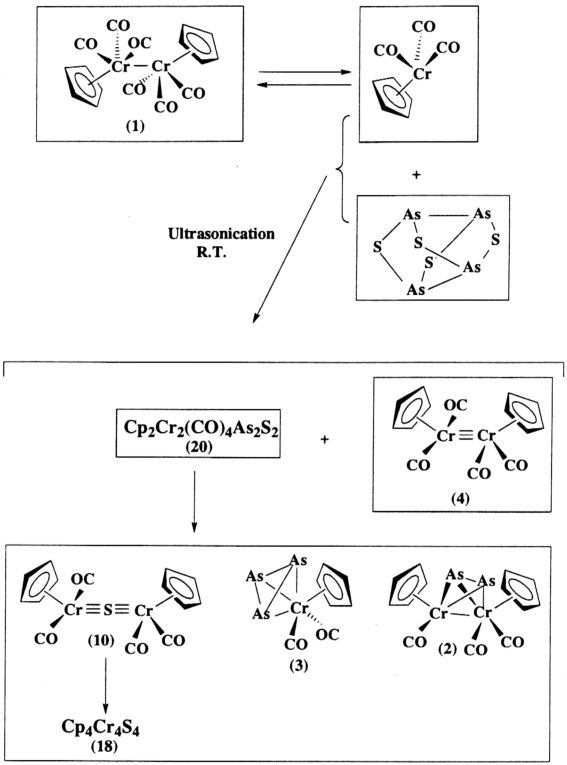
CO
CO
OC
Cr
Cr
CO
CO
CO
(1)
CO
CO
CO
Cr
+
As
As
S
S
S
S
As
As
Ultrasonication
R.T.
Cp2Cr2(CO)4As2S2
(20)
+
OC
Cr
Cr
CO
CO
CO
(4)
OC
Cr
S
Cr
CO
(10)
CO
CO
As
As
Cr
CO
OC
(3)
As
As
Cr
Cr
CO
(2)
CO
CO
Cp4Cr4S4
(18)

2.7 Coordination of the (μ-η^2-As_2) ligand to Group 6 transition-metal carbonyl fragments, $M(CO)_5(THF)$ [M = Cr, W].

2.7.1 The reaction of $[CpCr(CO)_2]_2As_2$ with $M(CO)_5(THF)$ (M =Cr, W)

The reaction of $[CpCr(CO)_2]_2As_2$ (**2**) with two molar equivalents of $M(CO)_5(THF)$ (M = Cr, W) at ambient temperature led to the isolation of the complexes $[CpCr(CO)_2]_2As_2[M(CO)_5]_2$ [M = Cr (**21**); W (**22**)] in 59.6 and 55.2% yields, respectively, as shown in Scheme X.

It appears that the facile coordination of the ligated μ-η^2-As_2 unit to additional transition metal carbonyl fragments is a common feature of Group VI dinuclear $Cp_2M_2(CO)_4E_2$ (E = P, As) complexes. The first example of such coordination was reported by Scherer for the reactions of $[CpMo(CO)_2]_2P_2$ with $Cr(CO)_5(THF)$ and $Re(CO)_6(\mu\text{-}Br)_2(THF)_2$.[37]

Coordination of these complexes to transition metal carbonyl fragments are possible due to the presence of the lone electron pairs of the As_2 unit, capable of acting as electron donors. Here the μ-η^2-As_2 unit of the dinuclear $Cp_2M_2(CO)_4As_2$ complexes acts as an 8-electron donor in the dimetallated derivatives of **21** and **22**.

2.7.2 Physical properties

$[CpCr(CO)_2]_2As_2[M(CO)_5]_2$ [M = Cr (21); W (22)]

The complexes are air-stable in the solid state and both are obtained as dark crystals. They are not soluble in *n*-hexane but soluble in most organic solvents giving a purplish brown solutions which are fairly stable at room temperature under an inert atmosphere.

Scheme X

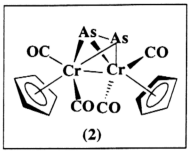

THF

$M(CO)_5THF$
[M = Cr, W]

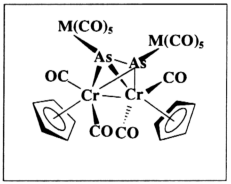

[M = Cr(21), W(22)]

2.7.3 Spectral characteristics

2.7.3.1 I.R. spectra

$[CpCr(CO)_2]_2As_2[M(CO)_5]_2$ [M = Cr (21); W (22)]

The I.R. spectra of **21** and **22** in nujol showed stretching frequencies at ν_{CO} 2071 s, 2059 s, 1979 vs, 1945 vs, 1920 vs and 2077 s, 2066 s, 1980 vs, 1941 vs, 1907 vs cm^{-1}, respectively. Both spectra are presented in Figure 57 and 58.

2.7.3.2 NMR spectra

$[CpCr(CO)_2]_2As_2[M(CO)_5]_2$ [M = Cr (21); W (22)]

Both complexes **21** and **22** are diamagnetic. It is observed that the Cp rings all appeared as singlets in the ^1H [(benzene-d_6): δ(Cp) 4.03 in **21**; 4.01in **22**] and ^{13}C [(benzene-d_6): δ(Cp)87.28 in **21**; 87.46 in **22**]. Attempts to measure the ^{13}C resonances of the CO ligands of both the complexes at 30°C failed to detect any signals.

2.7.3.3 Mass spectra

$[CpCr(CO)_2]_2As_2[M(CO)_5]_2$ [M = Cr (21); W (22)]

Their Electron Impact mass spectra are presented in Table 33 and 34, respectively.

2.7.4 Molecular structures

The molecules are isostructural. A perspective view of **21** is presented in Figure 59. Bond lengths and bond angles for **21** and **22** are given in Table 35 and 36. Selected bond parameters of the Cr_2As_2 core of the molecules are compared with those of the parent compound $[CpCr(CO)_2]_2As_2$ (**2**) in Table 37. Table 38 gives significant bond parameters of **21** compared with those of its Mo analogue **32a**[18] and parent **30a**[84] (refer to Section **1.1.2**). The Cr_2As_2 cores in these analogous molecules all possess a similar geometry, with the crystallographic C_2 axis passing through the

Figure 57. CO stretching frequencies of $[CpCr(CO)_2]_2As_2[Cr(CO)_5]_2$ (**21**) in nujol

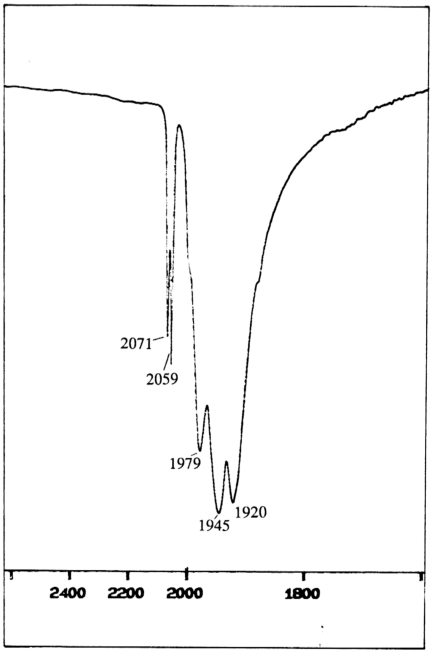

Figure 58. CO stretching frequencies of $[CpCr(CO)_2]_2As_2[W(CO)_5]_2$ (**22**) in nujol

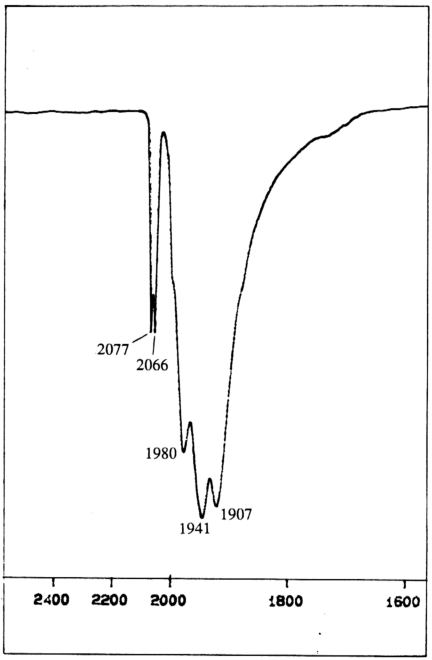

Table 33. Electron impact mass spectrum of $[CpCr(CO)_2]_2As_2[Cr(CO)_5]_2$ (**21**)

m/e	Assignments
496	$[Cp_2Cr_2(CO)_4As_2]$
468	$[Cp_2Cr_2(CO)_3As_2]$
440	$[Cp_2Cr_2(CO)_2As_2]$
384	$[Cp_2Cr_2As_2]$
182	$[Cp_2Cr]$
169	$[CpCr_2]$
117	[CpCr]

Table 34. Electron impact mass spectrum of $[CpCr(CO)_2]_2As_2[W(CO)_5]_2$ (**22**)

m/e	Assignments
496	$[Cp_2Cr_2(CO)_4As_2]$
440	$[Cp_2Cr_2(CO)_3As_2]$
412	$[Cp_2Cr_2(CO)_2As_2]$
384	$[Cp_2Cr_2As_2]$
201	$[CpCr(CO)_3]$
182	$[Cp_2Cr]$
173	$[CpCr(CO)_2]$
169	$[CpCr_2]$
117	[CpCr]

Figure 59. Molecular Structure of $[CpCr(CO)_2]_2As_2[Cr(CO)_5]_2$ (**21**)

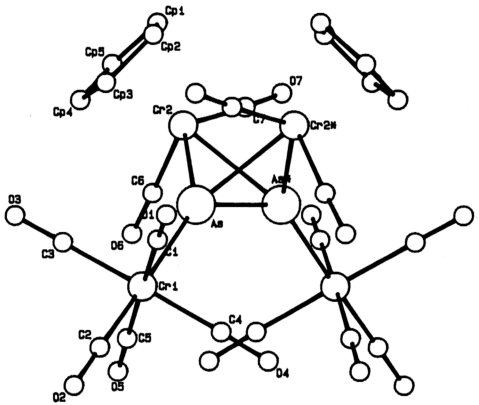

Table 35. Bond lengths (Å) and angles (°) for $[CpCr(CO)_2]_2As_2[Cr(CO)_5]_2$ (**21**)

As	As'	2.284(1)	As	Cr2'	2.610(1)
As	Cr1	2.479(1)	Cr2	C7	1.859(7)
As	Cr2	2.431(1)	O1	C1	1.130(9)
Cr1	C1	1.895(9)	O2	C2	1.154(8)
Cr1	C2	1.846(8)	O3	C3	1.145(9)
Cr1	C3	1.890(9)	O4	C4	1.143(9)
Cr1	C4	1.888(9)	O5	C5	1.128(8)
Cr1	C5	1.895(8)	O6	C6	1.144(8)
Cr2	Cp1	2.204(7)	O7	C7	1.150(8)
Cr2	Cp2	2.243(7)	Cp1	Cp2	1.39(1)
Cr2	Cp3	2.225(8)	Cp1	Cp5	1.41(1)
Cr2	Cp4	2.178(8)	Cp2	Cp3	1.40(1)
Cr2	Cp5	2.158(7)	Cp3	Cp4	1.41(1)
Cr2	C6	1.871(8)	Cp4	Cp5	1.40(1)
Cr2	Cr2'	3.070(2)	Cp1	H1	0.96(5)
Cp4	H4	0.95(6)	Cp2	H2	0.96(6)
Cp5	H5	0.84(8)	Cp3	H3	0.96(6)

Cr1	As	Cr2	146.75(4)	As	Cr2	C7	125.0(2)
As	Cr1	C1	94.1(2)	As'	As	Cr1	135.57(3)
As	Cr1	C2	177.9(2)	As'	As	Cr2'	67.13(3)
As	Cr1	C3	88.2(3)	As'	As	Cr2	59.14(3)
As	Cr1	C4	92.3(2)	Cr2'	As	Cr2	74.94(5)
As	Cr1	C5	89.5(2)	Cr2'	As	Cr1	134.85(4)
C1	Cr1	C2	87.4(3)	Cr2'	Cr2	As	55.17(3)
C1	Cr1	C3	91.1(4)	Cr2'	Cr2	As'	49.88(3)
C1	Cr1	C4	90.0(4)	Cr2'	Cr2	C6	129.1(2)
C1	Cr1	C5	176.0(3)	Cr2'	Cr2	C7	87.9(2)
C2	Cr1	C3	90.1(4)	As'	Cr2	C6	81.3(2)
C2	Cr1	C4	89.3(3)	As'	Cr2	C7	71.4(2)
C2	Cr1	C5	89.1(3)	As	Cr2	C6	86.8(2)
C3	Cr1	C4	178.8(4)	C6	Cr2	C7	89.2(3)
C3	Cr1	C5	90.9(4)	Cr1	C3	O3	180.(0)
C4	Cr1	C5	88.1(4)	Cr1	C4	O4	178.3(8)
Cp2	Cp1	Cp5	108.2(8)	Cp3	Cp4	Cp5	108.5(8)
Cr1	C1	O1	176.7(8)	Cr1	C5	O5	177.4(7)
Cp1	Cp2	Cp3	108.3(8)	Cp1	Cp5	Cp4	107.4(8)
Cr1	C2	O2	179.0(7)	Cr2	C6	O6	177.8(6)
Cp2	Cp3	Cp4	107.5(8)	Cr2	C7	O7	176.5(6)
Cp4	Cp3	H3	124.(4)	Cp2	Cp1	H1	128.(3)
Cp5	Cp1	H1	124.(3)	Cp3	Cp4	H4	122.(4)
Cp1	Cp2	H2	124.(4)	Cp5	Cp4	H4	130.(4)
Cp3	Cp2	H2	128.(4)	Cp1	Cp5	H5	131.(6)
Cp2	Cp3	H3	128.(4)	Cp4	Cp5	H5	122.(6)
As	Cr2	As'	53.73(3)				

Table 36. Bond lengths (Å) and angles (°) for $[CpCr(CO)_2]_2As_2[W(CO)_5]_2$ (**22**)

As	As'	2.285(2)	As	Cr	2.426(2)
Cr	Cr'	3.071(3)			
W	As	2.6003(9)	Cr	C7	1.85(1)
W	C1	2.00(1)	O1	C1	1.16(1)
W	C2	1.96(1)	O2	C2	1.16(1)
W	C3	2.04(1)	O3	C3	1.15(1)
W	C4	2.01(1)	O4	C4	1.14(1)
W	C5	2.02(1)	O5	C5	1.14(1)
As	Cr'	2.606(2)	O6	C6	1.13(1)
Cr	Cp1	2.20(1)	O7	C7	1.16(1)
Cr	Cp2	2.23(1)	Cp1	Cp2	1.38(2)
Cr	Cp3	2.23(1)	Cp1	Cp5	1.44(2)
Cr	Cp4	2.18(1)	Cp2	Cp3	1.38(2)
Cr	Cp5	2.15(1)	Cp3	Cp4	1.41(2)
Cr	C6	1.87(1)	Cp4	Cp5	1.39(2)

As	W	C1	94.4(3)	As'	As	Cr	67.12(4)
As	W	C2	178.1(3)	Cr'	As	Cr	75.13(6)
As	W	C3	87.8(3)	As'	Cr	As	53.86(5)
As	W	C4	91.6(3)	As	Cr'	Cr	49.76(4)
As	W	C5	89.8(3)	W	As	Cr	147.40(5)
C1	W	C2	86.7(5)	As	Cr'	C6'	81.4(4)
C1	W	C3	92.5(5)	As	Cr'	C7'	71.5(4)
C1	W	C4	88.5(5)	As	Cr	Cr'	55.11(4)
C1	W	C5	175.0(5)	As	Cr	C6	85.9(4)
C2	W	C3	90.7(5)	W	C1	O1	177.(1)
C2	W	C4	89.9(5)	Cr'	Cr	C7	88.8(4)
C2	W	C5	89.1(4)	W	C2	O2	179.(1)
C3	W	C4	178.9(4)	W	C3	O3	178.(1)
C3	W	C5	90.4(5)	C4	W	C5	88.7(5)
W	As	As'	134.67(2)	W	As	Cr'	134.52(4)
As'	As	Cr'	59.03(4)	As	Cr	C7	125.3(4)
Cr'	Cr	C6	128.8(4)	C6	Cr	C7	89.2(5)
W	C5	O5	177.(1)	W	C4	O4	176.5(9)
Cr	C6	O6	177.(1)	Cr	C7	O7	178(1)
Cp2	Cp1	Cp5	108(1)	Cp1	Cp2	Cp3	110(1)
Cp2	Cp3	Cp4	107(1)	Cp3	Cp4	Cp5	109(1)
Cp1	Cp5	Cp4	107(1)				

Table 37. A Comparison of Selected Bond Parameters of the Cr_2As_2 Core of $[CpCr(CO)_2]_2As_2[Cr(CO)_5]_2$ (**21**) and $[CpCr(CO)_2]_2As_2[W(CO)_5]_2$ (**22**) with those of $[CpCr(CO)_2]_2As_2$ (**2**)

	(**2**)	(**21**)	(**22**)
As-As'	2.276(1)	2.284(1)	2.285(2)
Cr-Cr'	3.026(1)	3.070(2)	3.071(3)
As-Cr'	2.597(1)	2.610(1)	2.606(2)
As-Cr	2.452(1)	2.431(1)	2.426(2)
Cr-C6	1.859(6)	1.871(8)	1.87(1)
Cr-C7	1.829(7)	1.859(7)	1.85(1)
As'-As-Cr	60.0(1)	59.14(3)	59.03(4)
As'-As-Cr'	66.5(1)	67.13(3)	67.12(4)
Cr'-As-Cr	73.6(1)	74.94(5)	75.13(6)
As-Cr-As'	53.5(1)	53.73(3)	53.86(5)
Cr'-Cr-As'	51.0(1)	49.88(3)	49.76(4)
As'-Cr-C7	71.8(2)	71.4(2)	71.5(4)
As'-Cr-C6	79.4(2)	81.3(2)	81.4(4)
Cr'-Cr-As	55.4(1)	55.17(3)	55.11(4)
As-Cr-C7	125.2(2)	125.0(2)	125.3(4)
As-Cr-C6	85.6(2)	86.8(2)	85.9(4)
Cr'-Cr-C7	89.3(2)	87.9(2)	88.8(4)
Cr'-Cr-C6	128.3(2)	129.1(2)	128.8(4)
C6-Cr-C7	87.8(3)	89.2(3)	89.2(5)

Table 38.

Some Selected Bond Parameters of $[CpM(CO)_2]_2As_2[Cr(CO)_5]_2$ (M = Cr (**21**), Mo(**32a**)) and $[CpMo(CO)_2]_2As_2$ (**30a**)

	(**21**)	(**32a**)	(**30a***)
As-As'	2.284(1)	2.310(3)	2.312(3)
Cr1-As	2.479(1)	2.471(3)	
Mo/Cr2-Mo'/Cr2'	3.070(2)	3.064(3)	3.038(2)
Mo/Cr2-As	2.431(1)	2.531(3)	2.568(2)
Mo/Cr2-Mo'/Cr2'	3.070(2)	3.064(3)	3.038(2)
Mo/Cr2-As'	2.610(1)	2.645(3)	2.670(2)
Mo/Cr2-CO	1.859-1.871(8)	1.96-1.98(1)	
Mo/Cr2-Cp	2.158-2.243(8)	2.28-2.37(1)	
Cr1-CO_{ax}	1.846(8)	1.81(1)	
Cr1-CO_{eq}	1.888-1.895(9)	1.84-1.88(1)	
Mo/Cr2-As'-As	67.13(3)	66.1(1)	66.1(1)
Mo/Cr2-As-As'	59.14(3)		61.6(1)
Mo/Cr2-As-Mo'/Cr2'	74.94(5)		70.9(1)
As-Mo/Cr2-As'	53.73(3)	53.0(1)	52.3(1)
As-Mo/Cr2-Mo'/Cr2'	55.17(3)	55.5(1)	56.2(0)
As'-Mo/Cr2-Mo'/Cr2'	49.88(3)		53.0(0)
Cr1-As-Mo/Cr2	146.75(4)	147.2(1)	
Cr1-As-As'	135.57(3)	135.4(1)	

*Average for two crystallographically independent molecules.

midpoints of the As-As and M-M bonds. The As-As' distances in **21** and **22** (2.284(2) Å), though lying between the observed range for such complexes, *ie.* 2.273 Å in $Co_2(CO)_5(PPh_3)As_2$,[19] and 2.312(3) in **30a** are in that they are contrary to expectation, slightly longer than in the parent As_2 complex **2** (2.276(1) Å).[18] The shortening of the As-As distances in these complexes, as compared to that in gaseous As_4 (2.44 Å),[74] has been ascribed to a partial charge transfer from the As_2 moiety to the metal fragment " electron sink ", thereby decreasing electron-pair repulsion between the As atoms.[19] In view of this, the coordination of the As_2 ligand to two electron-attracting $M(CO)_5$ groups would be expected to cause a further reduction in the As-As distance. However, this effect was not observed here, nor in **32a**,[18] and the $(\mu,\eta^2\text{-}P_2)$ analogue of **21**.[104]

The M-M' bond distances are distinctly longer in the adducts than in the parent **2** (3.070 Å versus 3.026 Å[18]). It would appear that the Cr_2As_2 core in **21** and **22** experience some steric effects, as well as in **32a** (3.064 Å versus 3.038 Å) the Mo analogue of **21**.[18] While both the Mo-As and Mo-As' distances are sligthly shortened in **32a** (2.53 and 2.65 Å[18]) when compared to those in the parent complex **30a** (2.57 and 2.67 Å,[104] respectively) in the case of **2** the Cr-As distances in its adducts are shortened (2.45 Å to 2.43 Å), whereas the Cr-As' distance are slightly lengthened (2.60 Å to 2.61 Å), making the AsAs'Cr triangle even more distorted. Likewise, as shown in Table 37, the Cr-CO distances have been increased from 1.86 Å to 1.87 Å, and 1.83 to 1.86 Å in **21** and 1.85 Å in **22**.

2.8 Coordination of the (μ-η^2-P_2) ligand to $Fe(CO)_4$ fragments from $Fe_2(CO)_9$

2.8.1 The reaction of $[CpCr(CO)_2]_2P_2$ with $Fe_2(CO)_9$

A heterogeneous 1:1 molar mixture of $[CpCr(CO)_2]_2P_2$ **(15)** and $Fe_2(CO)_9$ underwent a facile reaction in THF under an atmosphere of CO at 0 C within *ca.* 15 mins to give a homogeneous brownish magenta solution from which were isolated dark magenta brown crystals of $[CpCr(CO)_2]_2P_2[Fe(CO)_4]$**(23)** (68.5% yield) and greenish brown crystal of $[CpCr(CO)_2]_2P_2[Fe(CO)_4]_2$ **(24)** (16.5% yield), as represented in Scheme XI, together with some unreacted substrate $[CpCr(CO)_2]_2P_2$ **(15)** and a trace of an unidentifiable compound. The reaction is reminiscent of the coordination of the lone electron pairs of the P_2 unit of **15** to $M(CO)_5(THF)$ (M = Cr[104], Mo and W[105]), and earlier similar reaction of $Cp_2Mo_2(CO)_4P_2$ studied by Scherer[37] and of $Co_2(CO)_5LP_2$ (L=CO, PBu_3, PPh_3) studied by Marko.[106] Therein was described the first instance of the coordination of the (μ-η^2-P_2) unit to a $Fe(CO)_4$ fragment. Similar coordination to two $Fe(CO)_3$ uints was achieved in $[Fe(CO)_3]_2(\mu\text{-}CO)(P_2)[Cr(CO)_5]_2$, obtained from the reaction of $Fe_2(CO)_9$ with $(CO)_5CrPBr_3$.[107] However, (μ-η^2-P_2) complexes containing $Fe(CO)_m$ (m = 3 or 4) fragments are still of rare occurence, though the coordination of the phosphene unit (-P=P-) to $Fe(CO)_4$ is rather common.[108]

2.8.2 Physical properties

$[CpCr(CO)_2]_2P_2[Fe(CO)_4]$ (23)

The complex is air-stable in the solid state and obtained as dark crystalline solids. It is sparingly soluble in *n*-hexane but soluble in most organic solvents giving a magenta brown solution which slowly decompose back to its parent complex, $[CpCr(CO)_2]_2P_2$ **(15)**, at room temperature under inert atmosphere.

$[CpCr(CO)_2]_2P_2[Fe(CO)_4]_2$ (24)

The complex is air-stable in the solid state and obtained as dark crystalline solids. It is not soluble in *n*-hexane but soluble in most organic solvents giving a dirty

Scheme XI

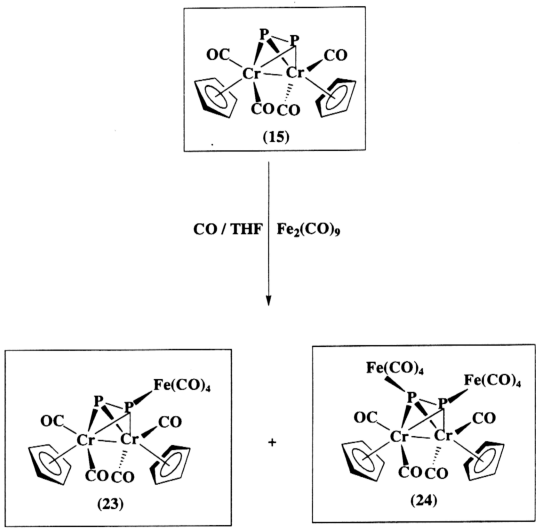

green solution which slowly decompose to **15** and **23** at room temperature under inert atmosphere.

2.8.3 Spectral characteristics

2.8.3.1 I.R. spectra

$[CpCr(CO)_2]_2P_2[Fe(CO)_4]$ (23)

The CO stretching frequencies of **23** are 2045 vs, 1978 vs, 1935 s,sh, 1920 s,sh (nujol) (Figure 60).

$[CpCr(CO)_2]_2P_2[Fe(CO)_4]_2$ (24)

The CO stretching frequencies of **24** are 2060 s, 2050 s, 1970 vs, br, 1949 s,sh, 1927 s cm^{-1} (nujol) (Figure 61).

2.8.3.2 NMR spectra

$[CpCr(CO)_2]_2P_2[Fe(CO)_4]$ (23)

Complex **24** is diamagnetic and the Cp rings appeared as singlets in the ^1H NMR (benzene-d_6) : δ (Cp) 4.14 and ^{13}C NMR (benzene-d_6) : δ (Cp) 87.32, δ (CO) unresolved cluster of peaks with main resonances at 215.48 and 214.87. ^{31}P NMR (benzene-d_6) : δ 28.20 (*d, J* 499Hz) and 151.25 (*d, J* 499Hz).

$[CpCr(CO)_2]_2P_2[Fe(CO)_4]_2$ (24)

^1H NMR (benzene-d_6) : δ (Cp) 4.16. ^{31}P NMR (benzene-d_6) : δ -33.22 (*d, J* 505Hz) and 51.09 (*d, J* 505Hz).

2.8.3.3 Mass spectrum

$[CpCr(CO)_2]_2P_2[Fe(CO)_4]$ (23)

The Electron Impact mass spectrum of **23** is tabulated in Table 39.

Figure 60. CO stretching frequencies of $[CpCr(CO)_2]_2P_2[Fe(CO)_4]$ (**23**) in nujol

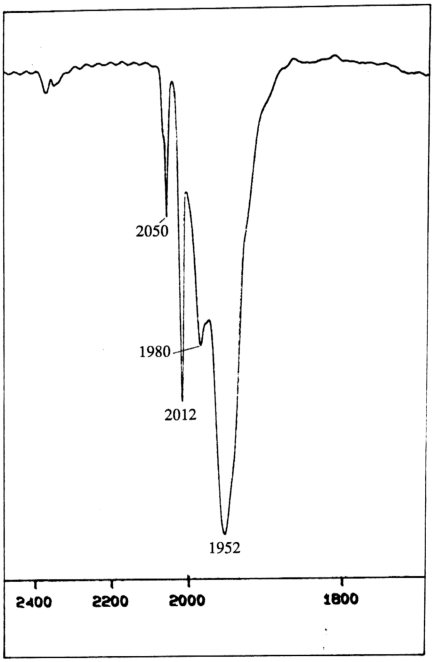

Figure 61. CO stretching frequencies of $[CpCr(CO)_2]_2P_2[Fe(CO)_4]_2$ (**24**) in nujol

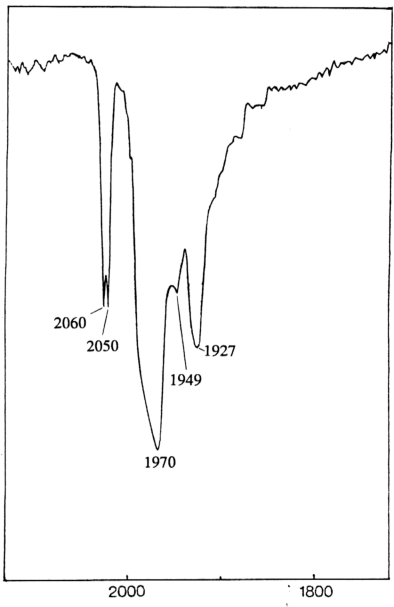

Table 39. Electron impact mass spectrum of $[CpCr(CO)_2]_2P_2[Fe(CO)_4]$ (**23**)

m/e	Assignments
576	$[Cp_2Cr_2(CO)_4P_2Fe(CO)_4]$
492	$[Cp_2Cr_2(CO)_4P_2Fe(CO)]$
464	$[Cp_2Cr_2(CO)_4P_2Fe]$
436	$[Cp_2Cr_2(CO)_3P_2Fe]$
408	$[Cp_2Cr_2(CO)_4P_2]$
380	$[Cp_2Cr_2(CO)_3P_2]$
352	$[Cp_2Cr_2(CO)_2P_2]$
324	$[Cp_2Cr_2(CO)P_2]$
296	$[Cp_2Cr_2P_2]$
182	$[Cp_2Cr]$
169	$[CpCr_2]$

2.8.4 Molecular structures

The perspective drawings of **23** and **24** are illustrated in Figure 62 and 63, respectively. Their respective bonding parameters are given in Tables 40 and 41. Some selected bond lengths and bond angles in **23** and **24**, and its parent compound **15** are given in Table 42.

As shown in Table 42, the lengths of the Cr-Cr bonds in **23** and **24** are very close to that of their parent $[CpCr(CO)_2]_2P_2$ (**15**) (3.011(1) Å), for which a single bond has been indicated.[15a, 67] On the basis of this and on the assumption that the μ-η^2-P_2 ligand serves as a 4 e donor, each Cr atom achieves the noble gas configuration. The P-P length in **15** (2.060 Å) is only very slightly shortened by the coordination of one $Fe(CO)_4$ fragment (2.056 Å, av.) or two (2.058 Å). These values lie within the range [2.019(9) - 2.154(4) Å][8] of P-P distances in μ-η^2-P_2 complexes to date. Their significant difference from the single bond P-P distance (2.21Å) in P_4 vapor, probably arises from the ability of the organometallic fragment(s) to act as an " electron sink ", thus causing a reduction in electron-pair repulsions between the P atoms and resulting in P-P bond shortening, as was rationalised by Dahl[19] and Sacconi[109] for similar As and P complexes, respectively.

The bonding parameters of the $Cr_2P_2Fe_m$ (m = 1, 2) core compare favorably with the parent $[CpCr(CO)_2]_2P_2$, especially in the more symmetrical compound **24** as illustrated in Table 42. A larger range observed for ⟨Cr-P-Fe⟩ in **24** is consistent with steric hindrance due to the two $Fe(CO)_4$ groups which are deviated from each other by a torsional angle (Fe1-P1-P2-Fe2) of -25.56 . The significant difference between the structure of the two compounds lies in the geometry about the Fe atoms. In compound **15**, the P is coordinated axially while in compound **24** both P atoms are coordinated equatorially to the trigonal bipyramidal Fe atoms. This change of geometry about Fe will ensure that the two equatorial planes do not intersect with each other, in order to alleviate steric hindrance.

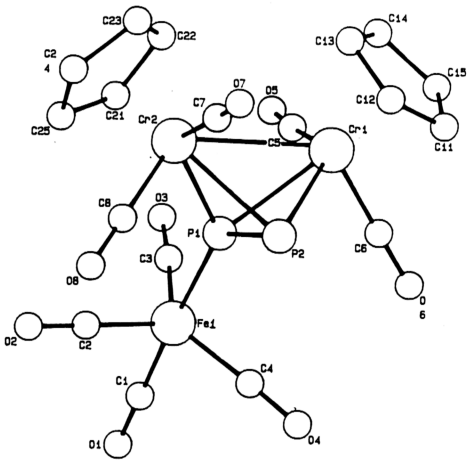

Figure 62. Molecular Structure of $[CpCr(CO)_2]_2P_2[Fe(CO)_4]$ (**23**)

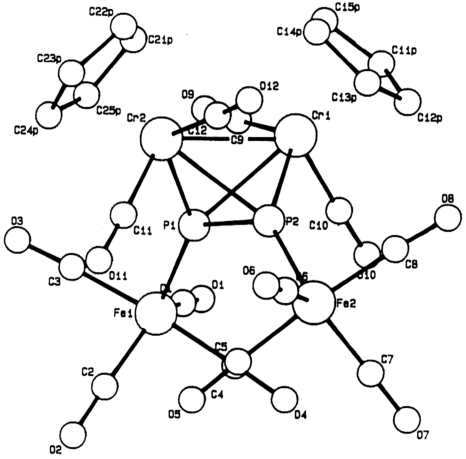

Figure 63. Molecular Structure of $[CpCr(CO)_2]_2P_2[Fe(CO)_4]_2$ (**24**)

Table 40. Bonding Parameters of $[CpCr(CO)_2]_2P_2[Fe(CO)_4]$ (23)[a]

Cr1a	Cr2a	3.006(2)			
Cr1b	Cr2b	3.011(2)			
Fe1a	P1a	2.250(2)	Cr1b	C6b	1.862(9)
Fe1a	C1a	1.752(8)	Cr1b	C11b	2.199(8)
Fe1a	C2a	1.784(9)	Cr1b	C12b	2.212(9)
Fe1a	C3a	1.781(9)	Cr1b	C13b	2.219(9)
Fe1a	C4a	1.782(8)	Cr1b	C14b	2.191(9)
Fe1b	P1b	2.258(2)	Cr1b	C15b	2.188(8)
Fe1b	C1b	1.767(8)	Cr2a	P1a	2.290(2)
Fe1b	C2b	1.787(8)	Cr2a	P2a	2.515(2)
Fe1b	C3b	1.807(9)	Cr2a	C7a	1.862(8)
Fe1b	C4b	1.786(8)	Cr2a	C8a	1.855(8)
Cr1a	P1a	2.430(2)	Cr2a	C21a	2.193(8)
Cr1a	P2a	2.366(2)	Cr2a	C22a	2.250(8)
Cr1a	C5a	1.844(8)	Cr2a	C23a	2.201(8)
Cr1a	C6a	1.829(9)	Cr2a	C24a	2.180(8)
Cr1a	C11a	2.180(9)	Cr2a	C25a	2.180(8)
Cr1a	C12a	2.211(9)	Cr2b	P1b	2.298(2)
Cr1a	C13a	2.248(9)	Cr2b	P2b	2.514(2)
Cr1a	C14a	2.211(8)	Cr2b	C7b	1.866(9)
Cr1a	C15a	2.170(9)	Cr2b	C8b	1.851(9)
Cr1b	P1b	2.434(2)	Cr2b	C21b	2.206(8)
Cr1b	P2b	2.362(2)	Cr2b	C22b	2.238(8)
Cr1b	C5b	1.833(8)	Cr2b	C23b	2.195(8)
Cr2b	C24b	2.159(8)	Cr2b	C25b	2.178(9)
P1a	P2a	2.052(2)	P1b	P2b	2.060(2)
O1a	C1a	1.148(9)	O1b	C1b	1.142(8)
O2a	C2a	1.140(9)	O2b	C2b	1.142(8)
O3b	C3b	1.124(9)	O3a	C3a	1.143(9)
O4b	C4b	1.149(8)	O4a	C4a	1.146(9)
O5a	C5a	1.156(8)	O5b	C5b	1.157(8)
O6a	C6a	1.167(9)	O6b	C6b	1.143(9)
O7a	C7a	1.148(8)	O7b	C7b	1.165(9)
O8a	C8a	1.138(9)	O8b	C8b	1.153(9)
$\langle C-C \rangle_{cp}$		1.40(11)			

[a] Numbers in parentheses are estimated standard deviations in the least significant digits.

P1a	Fe1a	C1a	177.7(3)	P1a	Cr1a	C6a	81.6(3)
P1a	Fe1a	C2a	89.8(2)	P1a	Fe1a	C3a	92.0(2)
P1a	Fe1a	C4a	88.2(2)	C1a	Fe1a	C2a	91.3(4)
C1a	Fe1a	C3a	89.5(4)	C1a	Fe1a	C4a	89.5(4)
P2a	Cr1a	C5a	126.9(2)	C2a	Fe1a	C3a	112.0(4)
P2a	Cr1a	C6a	86.4(3)	C2a	Fe1a	C4a	118.4(4)
C3a	Fe1a	C4a	129.5(4)	P1b	Fe1b	C1b	173.9(3)
P1b	Fe1b	C2b	91.5(2)	P1b	Fe1b	C3b	91.9(2)
P1b	Fe1b	C4b	87.3(2)	C5a	Cr1a	C6a	88.5(4)
C1b	Fe1b	C2b	94.5(4)	C1b	Fe1b	C3b	87.4(4)
C1b	Fe1b	C4b	88.7(3)	C2b	Fe1b	C3b	111.1(4)
C2b	Fe1b	C4b	115.0(4)	C3b	Fe1b	C4b	133.9(4)
P1a	Cr1a	P2a	50.65(6)	P1a	Cr1a	C5a	76.3(2)
C5b	Cr1b	C6b	89.1(3)	P1b	Cr1b	P2b	50.85(6)
P1b	Cr1b	C5b	75.2(2)	P1b	Cr1b	C6b	82.0(3)
P2b	Cr1b	C5b	126.0(2)	P2b	Cr1b	C6b	86.0(3)
P1a	Cr2a	P2a	50.30(6)	P1a	Cr2a	C7a	123.8(3)
P1a	Cr2a	C8a	87.0(2)	P2a	Cr2a	C7a	73.6(3)
P2a	Cr2a	C8a	78.2(2)	P1b	Cr2b	P2b	50.45(6)
C7a	Cr2a	C8a	85.5(3)	P1b	Cr2b	C7b	122.8(3)
P1b	Cr2b	C8b	87.0(2)	P2b	Cr2b	C7b	72.5(3)
P2b	Cr2b	C8b	79.0(3)	Fe1a	P1a	Cr1a	139.04(8)
C7b	Cr2b	C8b	86.1(4)	Fe1a	P1a	Cr2a	138.22(8)
Fe1a	P1a	P2a	134.0(1)	Cr1a	P1a	Cr2a	79.05(6)
Cr1a	P1a	P2a	63.04(8)	Cr2a	P1a	P2a	70.55(8)
Fe1b	P1b	Cr1b	137.86(9)	Fe1b	P1b	Cr2b	140.20(9)
Fe1b	P1b	P2b	132.7(1)	Cr1b	P1b	Cr2b	78.98(7)
Cr1b	P1b	P2b	62.76(8)	Cr2b	P1b	P2b	70.23(8)
Cr1a	P2a	Cr2a	75.97(7)	Fe1a	C2a	O2a	177.2(7)
Cr1a	P2a	P1a	66.30(8)	Cr2a	P2a	P1a	59.15(7)
Cr2b	P2b	Cr2b	76.20(7)	Fe1b	C2b	O2b	177.3(7)
Cr1b	P2b	P1b	66.39(8)	Fe1b	C3b	O3b	174.6(7)
Cr2b	P2b	P1b	59.32(7)	Fe1a	C1a	O1a	179.2(9)
Fe1a	C3a	O3a	176.5(7)	Fe1b	C4b	O4b	176.1(8)
Fe1a	C4a	O4a	177.5(8)	Fe1b	C1b	O1b	179.5(7)
Cr1a	C5a	O5a	175.1(7)	Cr1b	C5b	O5b	176.2(7)
Cr1a	C6a	O6a	178.9(7)	Cr1b	C6b	O6b	178.1(8)
Cr2a	C7a	O7a	176.1(8)	Cr2b	C7b	O7b	176.0(8)
Cr2a	C8a	O8a	180.(1)	Cr2b	C8b	O8b	178.5(7)
$\langle C-C-C \rangle$			108.0(9)				

Table 41. Bonding Parameters of $[CpCr(CO)_2]_2P_2[Fe(CO)_4]_2$ (**24**)[a]

Cr1	Cr2	2.999(1)			
Fe1	P1	2.221(1)	Cr2	C12	1.864(5)
Fe1	C1	1.774(6)	Cr2	C21p	2.241(4)
Fe1	C2	1.767(5)	Cr2	C22p	2.202(5)
Fe1	C3	1.796(6)	Cr2	C23p	2.165(5)
Fe1	C4	1.791(6)	Cr2	C24p	2.171(5)
Fe2	P2	2.221(1)	Cr2	C25p	2.221(5)
Fe2	C5	1.800(6)	P1	P2	2.058(1)
Fe2	C6	1.794(6)	O1	C1	1.138(6)
Fe2	C7	1.764(5)	O2	C2	1.142(6)
Fe2	C8	1.803(6)	O3	C3	1.137(6)
Cr1	P1	2.498(1)	O4	C4	1.139(6)
Cr1	P2	2.322(1)	O5	C5	1.131(6)
Cr1	C9	1.863(5)	O6	C6	1.129(6)
Cr1	C10	1.855(5)	O7	C7	1.141(6)
Cr1	C11p	2.167(5)	O8	C8	1.131(6)
Cr1	C12p	2.174(5)	O9	C9	1.148(5)
Cr1	C13p	2.227(5)	O10	C10	1.139(5)
Cr1	C14p	2.242(4)	O11	C11	1.140(5)
Cr1	C15p	2.198(4)	O12	C12	1.140(5)
Cr2	P1	2.322(1)	Cr2	P2	2.498(1)
Cr2	C11	1.862(5)	C13p	C14p	1.403(7)
C14p	C15p	1.390(8)	C21p	C22p	1.380(7)
C11p	C12p	1.397(9)	C21p	C25p	1.401(7)
C22p	C23p	1.388(8)	C11p	C15p	1.391(8)
C12p	C13p	1.396(8)	C23p	C24p	1.398(9)
C24p	C25p	1.388(8)			

P1	Fe1	C1	114.1(2)	P1	Cr1	C10	81.6(1)
P1	Fe1	C2	121.0(2)	P1	Fe1	C3	91.0(2)
P1	Fe1	C4	89.9(2)	C1	Fe1	C2	124.9(2)
C1	Fe1	C3	93.1(3)	C1	Fe1	C4	91.8(3)
P2	Cr1	C9	123.5(1)	C2	Fe1	C3	87.1(2)
P2	Cr1	C10	86.8(1)	C2	Fe1	C4	87.5(2)
C3	Fe1	C4	174.2(2)	P2	Fe2	C5	90.1(2)
P2	Fe2	C6	114.2(2)	P2	Fe2	C7	121.0(2)
P2	Fe2	C8	91.0(2)	C9	Cr1	C10	87.3(2)
C5	Fe2	C6	91.2(3)	C5	Fe2	C7	87.5(2)
C5	Fe2	C8	174.2(2)	C6	Fe2	C7	124.8(2)
C6	Fe2	C8	93.6(3)	C7	Fe2	C8	87.1(2)
P1	Cr1	P2	50.39(3)	P1	Cr1	C9	73.2(1)
C11	Cr2	C12	87.0(2)	P1	Cr2	P2	50.38(3)
P1	Cr2	C11	86.9(1)	P1	Cr2	C12	123.5(1)
P2	Cr2	C11	81.6(1)	P2	Cr2	C12	73.2(1)
Fe1	C2	O2	177.8(6)	Fe1	P1	Cr1	133.88(5)
Fe1	P1	Cr2	145.88(5)	Fe1	P1	P2	133.75(6)
Fe1	C3	O3	176.5(5)	Cr1	P1	Cr2	76.87(3)
Cr1	P1	P2	60.37(4)	Cr2	P1	P2	69.26(4)
Fe2	P2	Cr1	145.83(5)	Fe2	P2	Cr2	133.95(5)
Fe2	P2	P1	133.77(6)	Fe1	C4	O4	178.4(5)
Cr1	P2	Cr2	76.86(3)	Cr1	P2	P1	69.24(4)
Cr2	P2	P1	60.36(4)	Fe1	C1	O1	177.2(7)
Fe2	C5	O5	178.0(6)	Fe2	C6	O6	177.9(6)
Fe2	C7	O7	177.5(5)	Cr2	C11	O11	177.9(4)
Fe2	C8	O8	177.1(5)	Cr1	C9	O9	177.3(4)
Cr1	C10	O10	177.9(4)	Cr2	C12	O12	177.3(4)
⟨C–C–C⟩			108.0(6)				

[a] Numbers in parentheses are estimated standard deviations in the least significant digits.

Table 42. Some Selected Bond Lengths (Å) and Bond Angles (°) in $[CpCr(CO)_2]_2P_2[Fe(CO)_4]$ (23 and $[CpCr(CO)_2]_2P_2[Fe(CO)_4]_2$ (**24**) and Its Parent Compound (**15**)

	(**23**)	(**24**)	(**15**)
Cr–Cr	3.006(2), 3.011(2)	2.999(1)	3.011(1)
P1–P2	2.052(2), 2.060(2)	2.058(1)	2.060(1)
Fe–P	2.250(2), 2.258(2)	2.221(1), 2.221(1)	—
Cr–P	2.290(2)–2.515(2)	2.322(1)–2.498(1)	2.34(1), 2.474(1)
Cr–P–P	59.15(7)–70.55(8)	60.36(4)–69.26(4)	61.4(1), 68.1(1)
P–Cr–P	50.30(6)–50.85(6)	50.38(3), 50.39(3)	50.5(1), 50.6(1)
Cr–P–Fe	137.86(9) – 140.20(9)	133.88(5) – 145.88(5)	–
Cr–P–Cr	75.97(7) – 79.05(6)	76.86(3), 76.87(3)	77.2(1), 77.5(1)
Fe–P–P	132.7(1), 134.0(1)	133.77(6), 133.75(6)	–
Cr–Cr–P	48.41(5) – 54.27(5)	48.92(3) – 54.22(3)	49.4(1), 53.2(1)
Cr–P–P–Cr	−92.48, −92.66	−86.33	−87.18
Cr–P–P–Fe	131.28, −141.20	124.00 – −149.67	–